GEOPHYSICAL INTERPRETATION OF HIGH RESOLUTION AEROMAGNETIC DATA OF PART OF SOUTHWESTERN NIGERIA FOR SUBSURFACE MAPPING

BY

Zubairu AHMED
B. Tech. (ATBU), M. Sc. (ABU)
P16PSPY9044

A THESIS SUBMITTED TO THE SCHOOL OF POSTGRADUATE STUDIES, AHMADU BELLO UNIVERSITY, ZARIA

IN PARTIAL FULFILLMENT OF THE REQUIREMENTS FOR THE AWARD OF A DOCTORATE DEGREE IN APPLIED GEOPHYSICS

DEPARTMENT OF PHYSICS
FACULTY OF PHYSICAL SCIENCES
AHMADU BELLO UNIVERSITY, ZARIA
NIGERIA

SEPTEMBER, 2018

DECLARATION

I declare that the work in this Project Thesis entitled "GEOPHYSICAL INTERPRETATION OF HIGH RESOLUTION AEROMAGNETIC DATA OF PART OF SOUTHWESTERN NIGERIA FOR SUBSURFACE MAPPING" has been carried out by me in the Department of Physics. The information derived from the literature has been duly acknowledged in the text and a list of references provided. No part of this project thesis was previously presented for another degree or diploma at this or any other Institution.

Zubairu AHMED	_____	_____
Name of Student	Signature	Date

CERTIFICATION

This project thesis entitled "GEOPHYSICAL INTERPRETATION OF HIGH RESOLUTION AEROMAGNETIC DATA OF PART OF SOUTHWESTERN NIGERIA FOR SUBSURFACE MAPPING" by Zubairu AHMED meets the regulations governing the award of the degree of Doctor of Philosophy of the Ahmadu Bello University, Zaria and is approved for its contribution to knowledge and literary presentation.

Prof. K. M. Lawal	_____	_____
Chairman Supervisory Committee	Signature	Date
Dr. A. L. Ahmed	_____	_____
Member Supervisory Committee	Signature	Date
Prof. H. Hamza	_____	_____
Member Supervisory Committee	Signature	Date
Prof. R. Nasiru	_____	_____
Head of Department	Signature	Date
Prof. S. Z. Abubakar	_____	_____
Dean, School of Postgraduate Studies	Signature	Date

ACKNOWLEDGEMENT

I wish to extend my profound gratitude to Prof. K. M. Lawal who supervised this work under strong criticism and advice. Special thanks go to him for information provided during this write up.

I am grateful to Dr. A. L. Ahmed and Prof. H. Hamza my co-supervisors for the assistance given to me during this work and for their comments and suggestions that were of immense help in the write up.

I would like to thank the Head and staff of Physics Department, Ahmadu Bello University, Zaria for their support, advice and patience.

My special thanks go to the Management of Federal College of Education, Zaria for the approval and sponsorship that facilitated my studies.

My unreserved gratitude goes to my family for their patience and supports during this programme.

To all my friends/colleagues at Ahmadu Bello University, Zaria; Federal College of Education, Zaria and elsewhere, I say thank you.

ABSTRACT

High resolution aeromagnetic data of part of southwestern Nigeria (Longitude 2^0 30′ E and 5^0 00′ E and Latitude 6^0 00′ N and 8^0 00′ N) were interpreted qualitatively and quantitatively. First and second vertical derivatives, total horizontal derivative, analytic signal, theta angle and tilt derivatives were employed in the qualitative interpretation with the aim of delineating geological structures (anomalies) and their trends. Euler deconvolution and Werner deconvolution as well as forward modelling and inversion were employed in the quantitative interpretation which was aimed at determining depths to magnetic sources. The results of qualitative interpretation show high amplitude of the magnetic field intensity in the Basement Complex region and low amplitude in the Sedimentary Basin and some part of the Basement Complex associated with the schist. The directions of linear features delineated correlate with the geology of the study area. The trending patterns of the linear features are NE-SW, NW-SE, NNE-SSW and E-W. The NE-SW trending structures coincide with the structures from the Atlantic Ocean, the NNE-SSW structures provide a possible link to the Ifewara-Kalangai fault axis and the NW-SE trends could probably be due to the separation of the South American continent from Africa to accommodate the emerging Atlantic Ocean. The windowed Euler solution points coincide with regions having anomalies whose depths (<100 m - >9000 m) gave useful information about topography of the basement. The estimated depths range from Werner deconvolution was from 1.4 to 5.0 km. Modelling of anomalies using Geosoft GM-SYS have shown that Ifewara fault is about 3.2 km deep.

TABLE OF CONTENTS

Title Page- - - - - - - - - - - -i

Declaration- - - - - - - - - - - -ii

Certification- - - - - - - - - - - -iii

Acknowledgement- - - - - - - - - - -iv

Abstract- - - - - - - - - - - -v

Table of Contents- - - - - - - - - - -vi

List of Figures- - - - - - - - - - -x

List of Tables- - - - - - - - - - xiv

List of Appendix- - - - - - - - - - xv

CHAPTER ONE: INTRODUCTION 1

1.1 Background to the study- - - - - - - -1

1.2 The area of study- - - - - - - - - -2

1.3 Statement of the problem- - - - - - - - -6

1.4 Justification of the study- - - - - - - - -6

1.5 Aim and objectives- - - - - - - - - -6

CHAPTER TWO: LITERATURE REVIEW 8

2.1 Definitions and background- - - - - - - -8

2.2 Geology of the study area- - - - - - - - -9

2.2.1 Crystalline Basement Complex- - - - - - - -11

2.2.1.1 Migmatite-Gneiss Complex- - - - - - - - -11

2.2.1.2 Metasedimentary/Metavolcanic Complex- - - - - - - -11

2.2.1.3 The Older Granite Series- - - - - - - - -12

2.2.2 The Sedimentary Rocks- - - - - - - - -13

2.3 Some previous work in the area- - - - - - - -17

CHAPTER THREE: MATERIALS AND METHODS 23

3.1 Materials- - - - - - - - - - -23

3.2 Theories of the interpretation techniques- - - - - - -23

3.2.1 Basic theory- - - - - - - - - - -23

3.2.2 Vertical derivatives- - - - - - - - - -26

3.2.3 Total horizontal derivative- - - - - - - - -26

3.2.4 Theory of analytic signal technique- - - - - - - -27

3.2.5 Theory of tilt derivatives- - - - - - - - -30

3.2.6 Theory of theta derivative- - - - - - - - -31

3.2.7 Theory of Euler deconvolution- - - - - - - -32

3.2.8 Theory of Werner deconvolution- - - - - - - -33

3.2.9 Theoretical basis for 2-D forward modelling and inversion of the aeromagnetic data- - - - - - - - - - - -35

3.3 Data acquisition- - - - - - - - - -36

3.3.1 Acquisition and usage of shuttle radar topographic mission- - - -37

3.3.2 Acquisition and processing of high resolution aeromagnetic data- - - -38

3.4 Processing of high resolution aeromagnetic data- - - - -41

3.4.1 Regional–Residual Separation- - - - - - - -42

3.4.2 Upward continuation- - - - - - - - - -45

CHAPTER FOUR: RESULTS AND INTERPRETATION 49

4.1 Vertical derivatives- - - - - - - - - -49

4.2 Total horizontal derivative- - - - - - - - -54

4.3 Analytic signal- - - - - - - - - -56

4.4 Tilt derivatives- - - - - - - - - -59

4.5 Theta angle map- - - - - - - - - -64

4.6 Euler deconvolution- - - - - - - - - -67

4.7 Werner deconvolution- - - - - - - - -76

4.8 2-D forward modelling and inversion of the aeromagnetic data- - - -81

CHAPTER FIVE: DISCUSSION, CONCLUSION AND RECOMMENDATIONS 87

5.1 Discussion- - - - - - - - - - -87

5.2 Conclusion- - - - - - - - - - -90

5.3 Recommendations- - - - - - - - - - -91

REFERENCES 92

APPENDIX A 105

LIST OF FIGURES

Fig. 1.1: Map of the study area- - - - - - - -3

Fig. 2.1: Geology map of the study area- - - - - - -10

Fig. 3.1: Field due to dipole- - - - - - - - -24

Fig. 3.2: Topography and bathymetry map of the study area - - - - -38

Fig. 3.3a: Total magnetic field intensity map of the study area-- - - -40

Fig. 3.3b: Shaded relief map of the total magnetic field intensity of the study area- - - - - - - - - -41

Fig. 3.4: Regional magnetic field intensity map of the Study area- - - -43

Fig. 3.5a: Residual magnetic field intensity map of the study area- - - -44

Fig. 3.5b: Shaded relief map of the residual magnetic field intensity of the study area -45

Fig. 3.6a: Residual magnetic field intensity map of the study area upward continued to a height of 2000 m- - - - - - - -47

Fig. 3.6b: Shaded relief map of the upward continued residual magnetic field intensity of the study area- - - - - - - - - -48

Fig. 4.1a: First vertical derivative map of the study area- - - - -50

Fig. 4.1b: Shaded relief map of the first vertical derivative of the study area- - -51

Fig. 4.1c: Contour map of the second vertical derivative of the study area- - -52

Fig. 4.1d: Second vertical derivative map of the study area- - - - -53

Fig. 4.1e: Shaded relief map of the second vertical derivative of the study area- -54

Fig. 4.2a: Total horizontal derivative map of the study area- - - - -55

Fig. 4.2b: Shaded relief map of the total horizontal derivative of the study area- -56

Fig. 4.3a: Analytic signal map of the study area- - - - - -58

Fig. 4.3b: Shaded relief map of the analytic signal of the study area- - -59

Fig. 4.4a: Tilt derivative map of the study area- - - - - -61

Fig. 4.4b: Shaded relief map of the tilt derivative of the study area - - -62

Fig. 4.4c: Total horizontal derivative of the tilt derivative map of the study area- -63

Fig. 4.4d: Shaded relief map of the total horizontal derivative of the tilt derivative of the study area- - - - - - - - - -64

Fig. 4.5a: Theta angle map of the study area- - - - - - -66

Fig. 4.5b: Shaded relief map of the theta angle of the study area- - -67

Fig. 4.6a: Euler deconvolution solution plots of the study area (N = 0.0)- - -69

Fig. 4.6b: Euler deconvolution solution plots of the study area (N = 1.0)- - -70

Fig. 4.6c: Euler deconvolution solution plots for contact superimposed on the first vertical derivative map of the study area- - -- -71

Fig. 4.6d: Euler deconvolution solution plots for dyke/sill superimposed on the first vertical derivative map of the study area- - - -- -72

Fig. 4.6e: Euler deconvolution solution plots for contact superimposed on the second vertical derivative map of the study area- - - -- -73

Fig. 4.6f: Euler deconvolution solution plots for dyke/sill superimposed on the second vertical derivative map of the study area- - - - - -74

Fig. 4.6g: Euler deconvolution solution plots for contact superimposed on the analytic signal map of the study area- - - - - - - -75

Fig. 4.6h: Euler deconvolution solution plots for dyke/sill superimposed on the analytic signal map of the study area- - - - - - - -76

Fig. 4.7: Shaded relief map of the second vertical derivative showing the profiles from which residual upward continued data were extracted and used for computation of Werner deconvolution solutions- - - - -78

Fig. 4.8a: Werner plots for profile $P_{1A}P_{1B}$- - - - - - -79

Fig. 4.8b: Werner post on second vertical derivative map for profile $P_{1A}P_{1B}$- - -80

Fig. 4.9: Shaded relief map of the second vertical derivative showing profiles from which the residual data were extracted and used for 2-D forward modelling and inversion- - - - - - - -83

Fig. 4.10a: Forward and inverse model interpretation of residual magnetic anomalies along profile P1a-P1b- - - - - - -84

Fig. 4.10b: Forward and inverse model interpretation of residual magnetic anomalies along profile P2a-P2b- - - - - - -85

Fig. 4.10a: Forward and inverse model interpretation of residual magnetic anomalies along profile P3a-P3b- - - - - - -86

LIST OF TABLES

Table 2.1: The stratigraphic units of eastern Dahomey Basin- - - - -15

Table 4.1: Werner deconvolution results for the ten profiles- - - - -81

LIST OF APPENDIX

APPENDIX A: Werner deconvolution solutions and posts for the ten profiles on second vertical derivative map- - - - - 105

`CHAPTER ONE

INTRODUCTION

1.1 Background to the study

Geophysical method is known to provide a relatively rapid and cost-effective means of obtaining information of the subsurface covering large areas. The method involves the use of various techniques which includes magnetic technique. Magnetic method is a geophysical survey technique that exploits differences in magnetic properties of minerals with the objective of characterising the earth's subsurface.

The technique requires the acquisition of measurements of amplitude of magnetic field at discrete points along survey lines that are distributed regularly throughout the area of interest.

The amplitude of magnetic field measured is the vector sum of:

1. The earth's main field which originates from dynamo action of conductive fluids in the earth's outer core (Merrill *et al*., 1996).
2. An induced field caused by magnetic induction in magnetically susceptible earth materials polarized by the main field (Doell and Cox, 1967).
3. A field caused by remanent magnetism of the earth materials (Doell and Cox, 1967).
4. Others, usually less significant field caused by solar, atmospheric (Telford *et al*., 1990) and cultural influences.

It is the induced and remanent fields that are of particular interest to the geophysicists, because the magnitudes of these fields are directly related to the magnetic susceptibility, spatial distribution and concentration of the local crustal materials.

Once the main field and other minor source effects are removed from the observed magnetic field data through various data reduction and processing methods, the processed data will then serve as an indicator of spatial distribution and concentration of the magnetically significant minerals. At this point the data are enhanced and presented in readiness for analysis. Most importantly, the analysis leads to an interpretation of structures, lithology, alteration, regolith and sedimentary processes, among many other factors. Aeromagnetic data applications are known in wide variety of geological studies and play an important role in tracing lithological contacts and for recognition of structures like faults, lineaments, dykes and layered complexes. Aeromagnetic data can be used along with geological maps for earth resources evaluation applications (Reeves, 1990). The regional aeromagnetic study of an anomaly map brings out the regional geological pattern and structural features and provides an exceptional background for interpretations for specific purposes (Sharma, 1998). Grauch *et al*. (2001) have noted that the past two decades have seen a revolution in application of aeromagnetic surveys, from interpretation of solely basement structures to detailed examination of structures and lithological variations in the sedimentary section as well.

1.2 The area of study

The southwest zone of Nigeria comprises of six culturally homogenous states; namely: Ekiti, Lagos, Ogun, Ondo, Osun and Oyo states. The zone is bounded by Kwara and Kogi states in the north, Edo state in the east, the Republic of Benin in the west and the Atlantic Ocean in the south. It is therefore encompassed by longitude 2° 30′ E and 6° 00′ E and latitude 5° 25′ N and 9° 20′ N. The study area forms part of southwestern zone of Nigeria and is bounded by longitude 2° 30′ E and 5° 00′ E and latitude 6° 00′ N and 8° 00 ′ N (Fig. 1.1).

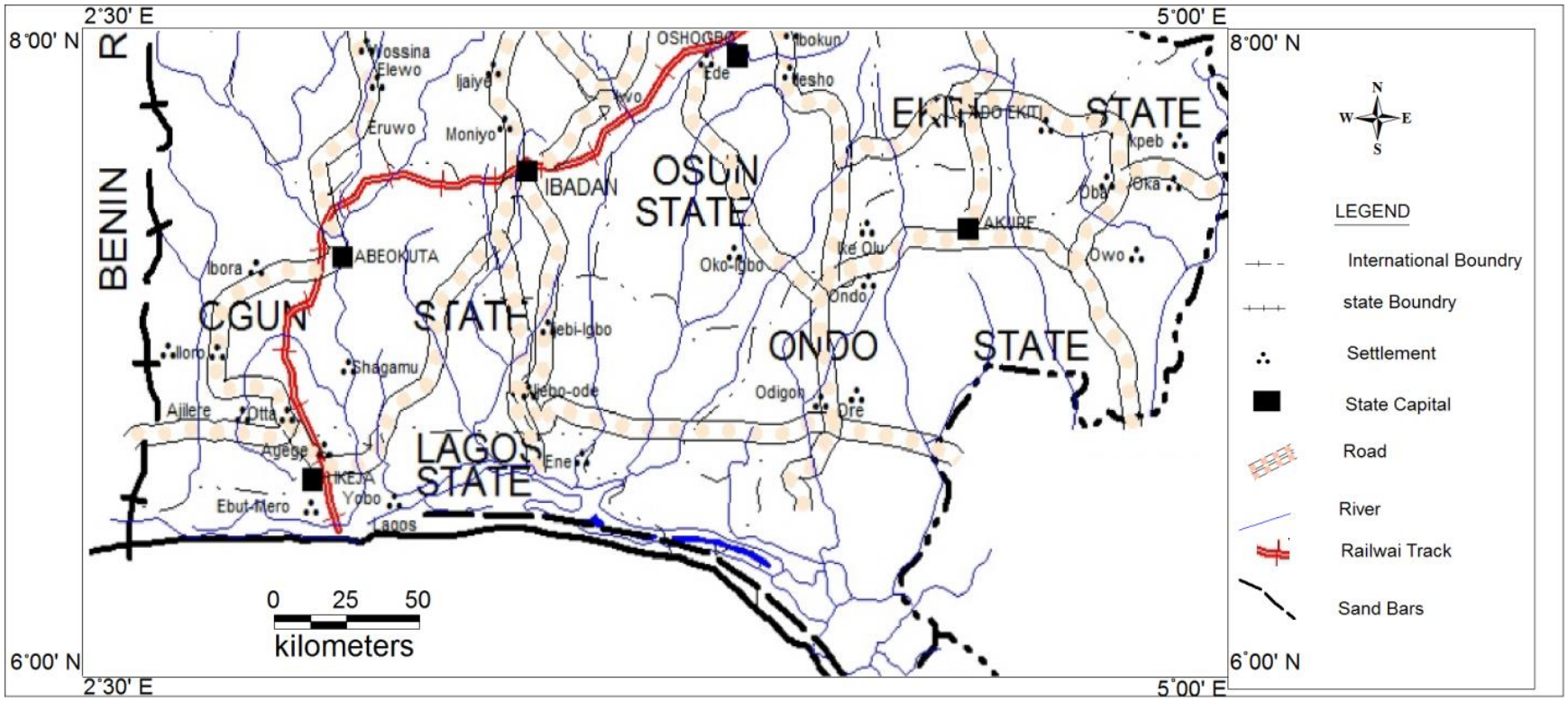


Fig.1.1: Map of the study area (adapted after NGSA, 2008).

The area is quite accessible by number of roads running through the region connecting various towns and villages in the area. Also some major roads run through the region which serves as links from the southwest to the northern and eastern parts of the country.

The relief of the southwest zone rises gradually from about 30 m above sea level at the coastal area to almost a plateau top of about 300 m in the hinterlands (NGSA, 2008). Two distinct physical regions can be identified; the lowland terrain, underlain by Sedimentary Basin and the upland areas marked by the crystalline lithology. The lowland area is characterised by thickly forested, undulating and swampy surface along the coast. Three landforms are identified in the lowland region; these are the northern uplands, the southern uplands, separated by an east-west depression known as Ewekoro depression.

The upland region rises to an elevation of over 300 m above sea level in an area underlain by crystalline Basement Complex of gneisses, migmatites and Metasedimentary as well as Older granites. Consequently, the topography of the zone is characterised by series of whalebacks, inselbergs and conical hills some of which are submerged in thick forest. Some of the known granitic hills are the Idanre hills in Ondo state, Olumo rocks in Ogun state and the series of hills in Ekiti state (*Ekiti means Land of hills*). Similarly, in Ilesha, Effon-Alaye, Osun and Ekiti states respectively and in Ibadan-Iseyin and Upper Ogun Forest Reserve, Oyo state there are moderately low forested and hog-back ridges of quartzite rock. The folded and the isolated hills provide beautiful scenery for geo-tourism. The topmost part of the Ibadan quartzite hill hosts a tourist attraction.

Almost all the major rivers in the zone drain north-south, following the grain of the land, separated by north-south divide responding to the lithological and fracture controls. On the crystalline

Basement Complex, the drainage pattern is dendritic as the directions of flow are subjected to foliation and joint directions in the terrains. The bigger rivers have consequently increased in their size through the process of river capture, especially noticed in Olokemeji area (Jones and Hockey, 1964). The sedimentary area in the southern part show features of superimposed drainage, as evidenced by incised meanders in mature valleys. In the Ewekoro depression, the coastal strip and areas underlain by river alluvium, much of the terrain is waterlogged for the greater part of the year. The major drainage lines in the zone are Yewa, Ogun, Ena, Oshun, Shasha and Oni. It is remarkable that none of these empties directly into the sea. They all flow into the lagoon complex. River Ogun is unique in its pronounced development of meanders and ox-bow lakes; it is at present building a delta into the Lagos lagoon.

The southwestern zone is influenced by tropical climate, characterised by two distinct climate regimes: the dry and the wet seasons. The wet season occurs from March to October, although at the coastal areas rains are experienced nearly throughout the year. The dry season occurs between November and March. The temperature ranges between 20°C to 34°C with hot month being in February (NGSA, 2008 and Ojo, 2007). August is the coldest months of the year, while December-January are noted for dusty and cold harmattan winds conveyed from the Sahara by the north-east trade winds.

The vegetation is the tropical rain forest, especially in the southern region, and derived savanna in the extreme northern parts. Thick and high vegetation are usually prevalent in the mountainous areas of Idanre, Olumo and Ekiti hills and the riverine areas. The coastal areas are noted for swampy vegetation with thick undergrowth.

1.3 Statement of the problem

Several geological and geochemical studies have been carried in the southwestern region of Nigeria (Wright, 1976; Danbatta, 2008; Kolawole and Anifowose, 2011 and Akinmosin *et al.*, 2013). The studies were mainly carried out because of the variety of rock types and the economic importance of some minerals that are associated with the rocks. Numerous geophysical studies have also been carried out (Ajakaiye *et al.,* 1991; Onyedim, 2007; Adepelumi *et al.,* 2008; Akintorinwa *et al.,* 2010; Badmus *et al*., 2013; Osinowo and Olayinka, 2013; Abraham *et al*., 2014; Osinowo *et al.*, 2014 and Oladunjoye *et al*., 2016). The surveys on the other hand failed to provide information on the regional tectonic framework of the southwestern Nigeria because the studies were on a local scale.

1.4 Justification of the study

A regional study of high resolution aeromagnetic anomaly data provide information about regional geological patterns and features. It is hoped that this research work will be valuable for providing knowledge that will lead to better understanding of the geology and other linear features as well as developing a better understanding of the crustal structure of the study area.

1.5 Aim and objectives

The aim of this study is to identify and delineate subsurface structures within part of southwestern Nigeria by producing comprehensive structural maps of the study area which will improve information on the regional geology.

The objectives of this work are:

1. To identify existing and new structures within the study area.

2. To perform enhancement techniques on high resolution aeromagnetic data such as the derivatives in order to map out the subsurface structures.
3. To compute Euler deconvolution on the gridded data in order to characterise the mapped structures in terms of their depths.
4. To compute Werner deconvolution along profiles in order to characterise the mapped structures in terms of their depths, susceptibilities and dips.
5. To determine details of conspicuous structures within the study area.

CHAPTER TWO

LITERATURE REVIEW

2.1 Definitions and background

Faults are ruptures along which the opposite walls have moved pass each other (Billings, 2006). The essential feature is differential movement parallel to the surface of fracture. Some faults are only few centimetres long, and the total displacements are measured in millimetres. At the other extreme, there are faults that are hundreds of kilometres long with a displacement measured in kilometres.

Faults may be classified on the basis of their geometry or their genesis, but the most satisfactory genetic classification at present is based on the nature of the relative movement along the fault:

1. A thrust fault or thrust is a fault along which the hanging wall has moved up relative to the footwall. Three categories are usually recognised. A reverse fault is a thrust that dips more than 45^{o}, the term thrust fault is one that dips less than 45^{o}, but overthrust is used for a fault that dips less than about 10^{o} and has a large net slip.
2. A normal fault is a fault along which the hanging wall has moved relatively downward.
3. Strike-slip faults also called wrench faults are those along which displacement has been essentially parallel to the strike of the fault that is the dip-slip component is small compared to the strike-slip component. If an observer approaches a strike-slip fault from one side, the opposite wall has moved relatively either to the right or left.

Goussev and Pierce (2000) defined contact as a boundary (often, a fault) between two blocks of differing susceptibility/density values or rock types. Correlating the analytic signal amplitude maxima and computation of analytic signal is used for delineating geologic boundaries in the subsurface.

Dyke is a crack through which magma flows, the magma subsequently solidifies to form a thin planar igneous body (Matzner, 2001).

The name lineament was introduced by Hobbs (1904) to characterise any linear feature in the ground. From the advent of aerial photograph and later, satellite images in geology, there was an increasingly interest in defining and analyzing linear features of the earth. Then, some names were introduced as synonymous to lineament. O'Leary *et al.* (1976) concluded that lineament is the most suitable term to describe these linear features. The lineaments may be simple or composite, and rectilinear or slightly curved. They must differ from the nearby linear patterns, and are the consequence of underground structures. Sabins (1986) also reviewed the application of lineament name in describing linear features, without any genetic implication. Sabins (1986) also discussed several geomorphic and/or tonal features that may give rise to a lineament. The general connection of negative magnetic lineaments to crustal weakness and fracture zones is reasoned by changes in magnetic susceptibility contrast between the fractured zone and the host rock (Airo and Wennerström, 2010). On many occasions, topographic valleys have developed along the fractured zones and are correlated with magnetic lineaments. Lipponen and Airo (2006) compared topographic and magnetic lineaments along the Päijänne water conveyance tunnel in southern Finland and found a correlation between brittle, fractured rock within the tunnel and the magnetic directional trends.

2.2 Geology of the study area

The study area is underlain by rock groups of the crystalline Basement Complex of Precambrian to Cambrian age. However about twenty to twenty five percent (20-25%) of the southwestern Nigeria in the southern extremity, bounded by the Atlantic Ocean, is covered by Cretaceous to Recent sediments, accumulated in the narrow Dahomey Basin (Fig. 2.1).

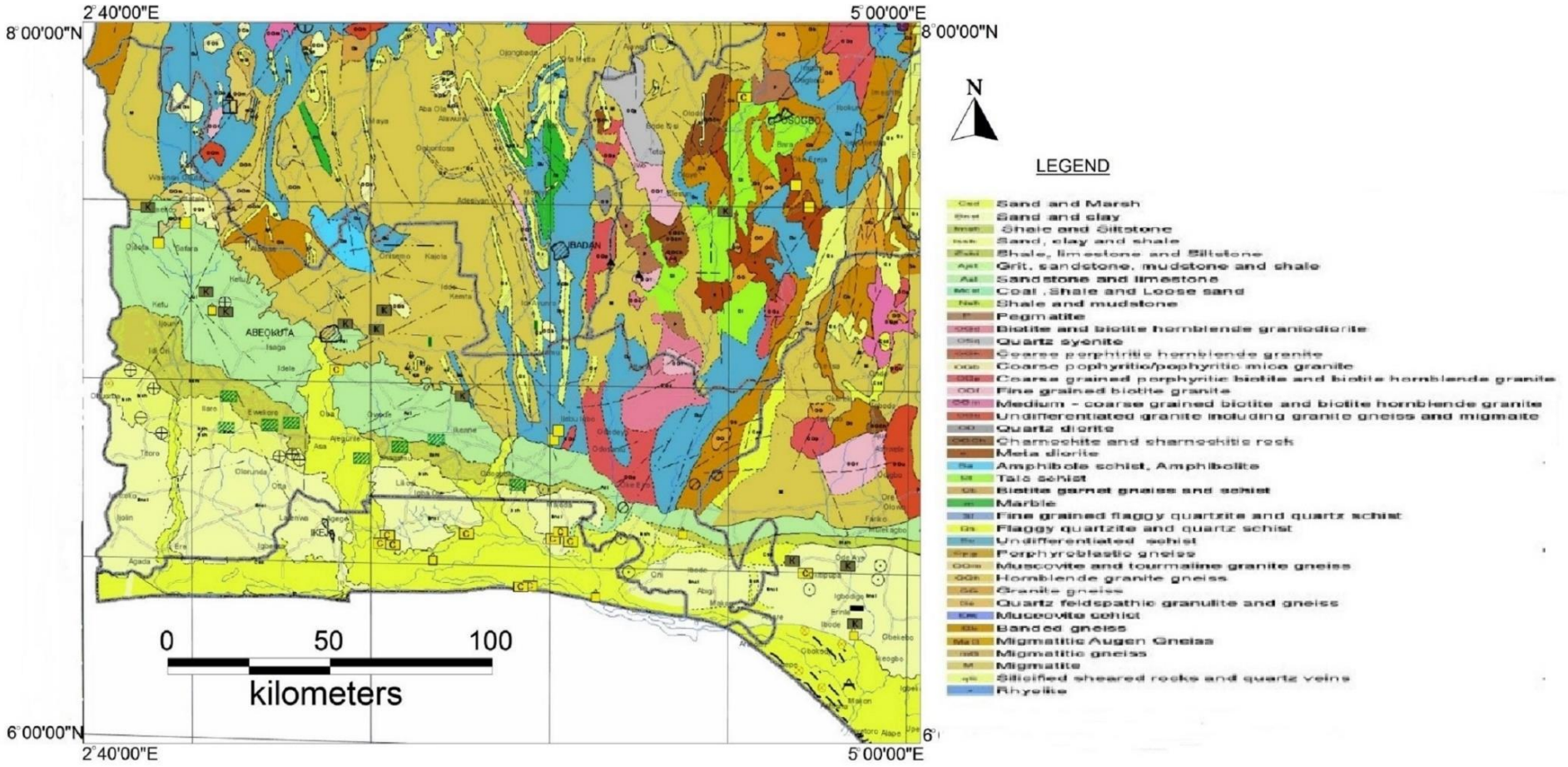


Fig.2.1: Geology map of the study area (adapted after NGSA, 2008).

2.2.1 Crystalline Basement Complex

The lithological units of crystalline Basement Complex are grouped as follows:

i. Migmatite-Gneiss Complex.

ii. Metasedimentary/Metavolcanic Complex.

iii. Older Granite Series (Pan African).

2.2.1.1 Migmatite-Gneiss Complex

This rock group underlies about seventy percent (70%) of the Precambrian Basement Complex rocks in the southwestern Nigeria and it is composed of high grade metamorphic rocks (NGSA, 2008). The gneisses and migmatites are intimately associated in the field. The migmatite is a group of rocks, made up essentially of gneisses and schist as paleosome and granitic rocks, pegmatite and aplite as neosome. The gneisses and migmatites are characterised by intricate folded and banded fabric complicated by quartzo-feldspathic intrusion and quartz rodding's. Relicts of quartzite, marble and calc-silicate rocks occur within the migmatite-gneiss complex. This paragenesis has earned the Precambrian rocks "Older matesediments" (Oyawoye 1972) which have been subjected to at least three periods of Orogeny before the Pan African thermo-tectonic events. Detailed mineralogical, petrological and tectonic evolutions are contained in Oyawoye (1972), Rahman (1988) and other workers. The rock groups are considered mainly by the north-south structural grain.

2.2.1.2 Metasedimentary/Metavolcanic Complex

These are referred to as supracrustal rocks believed to have been in folded into the basement of gneisses and migmatites. The members of rock group have been mapped in troughs trending

roughly north-south, occupying about ten percent (10%) of the total area of southwestern Nigeria (NGSA, 2008). The schistose rocks consist of low to medium grade metamorphic rocks, composed of pelitic schist, quartz schist, banded iron formation, marble and calc-silicates plus subordinate amount of ultramafic rocks, amphibolites, metadiorites, and talc schist. Apart from the pelitic schists, psamitic rocks are abundant in the zone and they are of two generations; the older generation; often refers to as Ibadan quartzite, extends to the Iseyin area and are composed mainly of quartz, muscovite and occasionally sillimanite. The younger quartzites and the Effon Psammites (De Swardt, 1953, Elueze, 1998, Ajayi, 2003) are composed of muscovite, quartz, sillimanite and opaque ore which are characteristically schistose, with pale brown resinous colour. The Effon quartzites form sinuous topographic ridges traceable from Ile-Ife - Ilesha, Osun state to Effon-Alaye, Ara and Okemesi in Ekiti state.

The ultra-mafites: amphibolites and metamafites: talc schist, talc-tremolite schist occur with the quartzites and they are more noticeable in the northeastern part of southwestern Nigeria. The metavolcanic rocks have been studied in some detail (Elueze, 1998; Rahman, 1988 and Ajayi, 2003) especially because of its association with gold mineralization in Ilesha and environ and talc occurrences in Ile-Ife - Ilesha axis, Apomu, Iregun and Iseyin districts.

2.2.1.3 The Older Granite Series

The Older Granite Series form the most conspicuous geomorphic features in the southwestern Nigeria, outcropping as batholiths, conical hills, thickly forested highlands, as exemplified in the Igbo-Ora hills in Oyo state, Idanre hills in Ondo state and the Ekiti hills. The Older Granites were emplaced in the Precambrian basement gneisses and metasediments. Consequently, as shown in Fig. (2.1) the Older Granites lithologically consist of coarse porphyritic biotite and biotite-

hornblende granites, fine to medium-grained granites in addition to foliated and migmatitic types, syenites and grandiorites. However, the most widespread of the series are the coarse porphyritic types, which are characterised by large feldspar crystals (Rahman, 1988).

A variety of the Older Granites, possibly of early Pan-African age, are the charnockitic rocks (Olarewaju, 1988). The charnockites are characteristically bluish-green, coarse-grained rocks composed of quartz-hypersthene and basic plagioclase. The restful colours make the charnockites and related rocks attractive as dimension stones.

2.2.2 The Sedimentary Rocks

The Benin (Dahomey) Basin constituting part of a system of West African peri-cratonic (margin sag) basin (Klemme 1975; Kingston *et al*., 1983) was developed during the commencement of the rifting, that are associated with the opening of the Gulf of Guinea, in the Early Cretaceous to the Late Jurassic (Burke *et al.*, 1971; Whiteman, 1982). The crustal separation, which was typically preceded by crustal thinning, was accompanied by an extended period of thermally induced basin subsidence through the Middle-Upper Cretaceous to Tertiary times as the South American and the African plates entered a drift phase to accommodate the emerging Atlantic Ocean (Storey, 1995; Mpanda, 1997).

The Ghana Ridge, presumably an offset extension of the Romanche Fracture Zone, binds the Basin to the west while the Benin Hinge Line, a basement escarpment which separates the Okitipupa structure from the Niger Delta Basin that binds it to the east. The Benin Hinge Line supposedly defines the continental extension of the Chain Fracture Zone.

The onshore part of the Basin covers a broad arc-shaped profile of about 600 km^2 in extent. The onshore section of the Basin attains a maximum width, along its N-S axis, some 130 km around

the Nigerian-Republic of Benin border. The Basin narrows to about 50 km on the eastern side where the basement assumes a convex upwards outline with concomitant thinning of sediments. Along the northeastern fringe of the Basin where it rims the Okitipupa high is a brand of tar (oil) sands and bitumen seepages (Ekweozor and Nwachukwu, 1989).

The stratigraphy of the eastern Dahomey Basin (Table 2.1) has been discussed by many workers and several classification schemes have been proposed. These works include those of Jones and Hockey (1964); Ogbe (1972); Omatsola and Adegoke (1981); Coker *et al*. (1983); Billman (1992); Nton (2001); Elueze and Nton (2004); Nton *et al*. (2006) among others. In spite of all these classification, geologists strongly disagree on ages assigned and nomenclatures of the different lithological units within the Basin. Omatsola and Adegoke (1981) proposed the Cretaceous sequence in the eastern Dahomey Basin as beginning with the Abeokuta Group, made up of three formations from namely; the Ise, Afowo and Araromi Formations. The Ise Formation unconformably overlies the Basement Complex of southwestern Nigeria and consists of conglomerate and grits at the base and in turn overlain by coarse to medium grained sands with interbedded kaolinite. The conglomerates are unimbricated and ironstones occur at some locations (Nton, 2001). The age is Neocomian to Albian.

Table 2.1: The stratigraphic units of eastern Dahomey Basin (adapted after Idowu *et al*., 1993)

Jones and Hockey(1964)		**Omatsola and Adegoke (1981)**			**Agagu (1985)**	
	Age	Formation	Age	Formation	Age	Formation
Quaternary	Recent	Alluvium			Recent	Alluvium
Tertiary	Pleistocene-Oligocene Eocene Paleocene	Coastal Plain Sand Ilaro Ewekoro	Pleistocene-Oligocene Eocene Paleocene	Coastal Plain Sand Ilaro Oshosun Akinbo	Pleistocene-Oligocene Eocene Paleocene	Coastal Plain Sand Ilaro Oshosun Akinbo Ewekoro
Cretaceous	Late Senonian	Abeokuta	Maastritchtian-Neocomian	Araromi Afowo Ise	Maastritchtian-Neocomian	Araromi Afowo Ise
Precambrian Crystalline Basement Rocks						

Overlying the Ise Formation is the Afowo Formation, which is composed of coarse to medium grained sandstones with interbedded shales, siltstones and claystones. The sandy facies are tar-bearing while the shales are organic-rich (Enu, 1990). The lower part of this Formation is transitional with mixed brackish to marginal horizons that alternate with well sorted, sub-rounded sands indicating an estuarine near-shore environment of deposition. Billman (1992) assigned a Turonian age to the lower part of this Formation, while the upper part ranges into the Maastritchtian.

The Araromi Formation overlies the Afowo Formation and has been described as the youngest Cretaceous sediment in the Basin (Omatsola and Adegoke, 1981). It is composed of fine to medium grained sandstone with interbedded limestone, marl and lignite. The Formation contains abundant planktonic foraminifera, ostracods, pollen and spores. Omatsola and Adegoke (1981) assigned a Maastritchtian to Paleocene age to this Formation.

The Ewekoro Formation overlies the Araromi Formation in the eastern Dahomey Basin. It is an extensive limestone body which could be traced from Ghana in the west, to the eastern margin of the Dahomey Basin in Nigeria (Jones and Hockey, 1964). Elueze and Nton (2004) observed that the limestone are of shallow marine origin owing to abundance of coralline algae, gastropods, pelecypods, echinoid fragments and other skeletal debris. It is Paleocene in age.

Overlying the Ewekoro Formation is the Akinbo Formation, the Formation is made up of shale and clay sequence (Ogbe, 1972). The claystones are concretionary and are predominantly kaolinite (Nton and Elueze, 2004). The base of the Formation is defined by the presence of glauconitic band with lenses of limestone (Ogbe, 1972 and Nton, 2001). The Formation is Paleocene to Eocene in age.

The Oshosun Formation overlies the Akinbo Formation and consists of greenish-grey clay and shale with interbedded sandstones. The shale is thickly laminated and glauconitic. According to Okosun (1998), the basal beds consist of any of the following facies; sandstones, mudstones, claystones, clay-shale or shale. This Formation is phosphate-bearing (Jones and Hockey, 1964 and Nton, 2001). According to Okosun (1998) the Formation is Eocene in age.

The Ilaro Formation overlies the Oshosun Formation and consists of massive, poorly, consolidated, cross-bedded sandstones. The youngest stratigraphic sequence in the eastern Dahomey Basin is the Benin Formation. It is also known as the coastal plain sands (Jones and Hockey, 1964) and consists of poorly sorted sands with lenses of clays. The sands are in parts cross-bedded and show transitional to continental characteristics. The age is from Oligocene to Recent.

2.3 Some previous works in the area

Wright (1976) investigated the fracture systems in Nigeria and initiation of fracture zones in the South Atlantic. The study observed two northeast-southwest trending belts of major faults in Nigeria that extend to the West African coast near Accra and Lagos. Their intersections with the coastline coincide with landward projections of the Romanche and Chain fracture zones in the Atlantic.

Ajakaiye *et al*. (1991) analysed the magnetic anomalies in the Nigerian continental mass based on aeromagnetic survey (Jurassic granitic ring and Neogene volcanic and the Benue trough which is considered to be a failed - rift arm). Major intrusive and fault zones were delineated. The results revealed aspects of the regional tectonic framework of West Africa and its relationship with major structures in the adjacent Atlantic Basins.

Onyedim (2007) applied steerable filters in six different azimuth directions to enhance magnetic anomalies due to faults in part of the Basement Complex of southwestern Nigeria. The filtered images facilitated delineation of linear features which were interpreted as fractures in the area. The major fracture directions identified were NNE-SSW, NE-SW, NW-SE and ENE-WSW. The NNE-SSW trending Ifewara fault shows as a fault zone.

Adepelumi *et al*. (2008) conducted an integrated geophysical survey involving ground magnetic and dipole-dipole resistivity across prominent zone of weakness observable in a Landsat multi-spectral scanner and side looking airborne radar images in the Precambrian Basement Complex of southwestern Nigeria. The integrated approach employed in the research confirmed the existence of the Ifewara shear zone.

Danbatta (2008) reviewed the evolution and tectonic framework of the schist belt of western Nigeria. The study concluded that the Nigerian schist belt with Algoma type banded iron formations are ensialic and Eburnean in age, while those without the banded iron formations are ensimatic and Pan African in age.

Akintorinwa *et al*. (2010) carried out geophysical investigation using ground magnetic, very low frequency electromagnetic and dipole-dipole resistivity surveys along segments of the Ilesha-Akure highway located in the Precambrian Basement Complex of southwestern Nigeria with a view to establish the causes of the road pavement failure. The causes of highway pavement failure in the studied highway may have been clayey topsoil/sub-grade soils and near-surface linear features such as faults, fractures and lithological contacts.

Nwankwo *et al*. (2011) made an estimate of heat flow in the northern part of the sedimentary Nupe Basin using spectral analysis of aeromagnetic data, with a view to explore for new and more energy

locations. The results of the analysis show that the geothermal gradient varies between 10 and 45^{o}C km^{-1}, while the heat flows varies between 30 and 120milliWm^{-2}, flows of more than 100miiliWm^{-2} are found in the north-eastern and north-western parts. The regions with anomalous high heat flow values (above 60milliWm^{-2}) were recommended for further investigation.

Samuel (2011) carried out geology, stream sediment geochemical survey and groundwater quality evaluation of Okemesi and environs, southwestern Nigeria. The lithology mapped in the study areas include banded-gneiss, biotite-gneiss, quartzite, biotite schist, quartz-biotite schist and pegmatite with various structures found on the outcrops such as joints, fractures, solution holes, micro folds, banding and above all, the presence of an asymmetric fold was also detected from the cross-section of the geologic map produced. A total of ten active stream-sediments and four borehole water samples were collected over an area of 138.45 km^{2}. Stream sediment samples were digested in aqua regia solution and analysed by inductively coupled plasma-mass spectrometry (ICP-MS) method, while borehole water samples were analysed by spectrophotometer and ICP-MS method. Comparison of the results by plots of concentration of elements against sample locations and statistical description for both sample media showed that most of the elements have high concentration around Ikange, Ayegunle and Makanju area respectively, which all lie in the western part of the study area. The underlying lithology (quartzite) probably played a major role in the distribution of these elements.

Kolawole and Anifowose (2011) carried out a detailed remote-sensing mapping of the lateral extent of Ifewara-Kalangai fault system using satellite imagery field mapping and ground truthing survey. The results obtained from the investigation showed that satellite imagery study of a segment of the mega structure shows a ductile dextral fault zone with a drag towards the NNW direction in Zungeru area.

Abubakar (2012) used a combined GIS, aeromagnetic and remote-sensing techniques within Kushaka schist belt of north-western Nigeria with the aim of assessing their usefulness in delineating geologic features within the study area. The techniques proved to be useful in identifying known and new structures in the area especially when they are used together. Analytical signal function indicates that with the exception of the Kalangai fault system, the rest of the known and new fault systems were shallow.

Akinmosin *et al*. (2013) carried out geophysical survey and sedimentological analysis on the bitumen seepage at Onikitibi south-western Nigeria with a view to elucidate its electrical and lithological characteristic. Electrical resistivity profiling and one of inter-electrode spacing of 5-30 m and 100 m were carried out using the Werner and Schlumberger electrode configuration along the seepage zone. Three samples collected from the exposure were subjected to granulometric analysis in order to determine their particle size distribution and textural characteristics. Geometrically, the seepage extends approximately 14 m (west to east) and 11 m deep. The study also established that the bitumen has high resistivity in contrast to previous values obtained in other parts of the Basin.

Badmus *et al*. (2013) analysed the aeromagnetic data of Ibadan area, southwestern Nigeria with a view to estimate depths to magnetic sources as well as their locations using horizontal gradient magnitude (HGM), analytic signal amplitude (ASA) and local wave number (LWN) methods. The locations and depths to the magnetic contact were estimated from the maxima of the LWN and the ASA functions of the total intensity magnetic data and HGM function of the reduced-to-pole magnetic grid. The results have shown that the estimates of depths limits by both HGM and LWN methods were relatively close and comparable. The ASA method shows the depths to the shallow sources to be higher than expected in the study area.

Ganiyu *et al.* (2013) employed two magnetic data enhancement procedures (reduction to the pole and upward continuation) on aeromagnetic data of Ibadan area in the southwestern Nigeria with the aim of determining their effectiveness in characterising the study area. The results concluded that reduction to the pole together with upward continuation techniques significantly improve the interpretation of magnetic data in terms of discriminating between shallow and deep magnetic sources within the study area.

Osinowo and Olayinka (2013) mapped the basement topography around the Ijebu-Ode geological transition zone in southwestern Nigeria. The study has identified the geological contact between the crystalline basement and sedimentary terrain. The depth range to basement rocks around the transition zone was also delineated, the basal contacts of sedimentary rocks above the crystalline rocks was also established as well as determine the basement topography and structures which served to guide drilling and some engineering construction decisions.

Abraham *et al*. (2014) examined the thermal structure of crust at Ikogosi Warm Spring area using Curie point depth estimates from spectral analysis of aeromagnetic data. The average Curie point depth for the area was 15.1 km, which indicates that the area is promising for further geothermal explorations.

Oladunjoye *et al*. (2016) interpreted high resolution aeromagnetic data of Ogbomosho (sheet 222) to provide a better understanding of the mode of occurrence of the iron ore and associated structural features and geologic model. These were done by subjecting reduced-to-pole (RTP) residual aeromagnetic intensity data to various data filtering and processing techniques involving total horizontal derivative, vertical derivative, upward continuation, downward continuation, Euler deconvolution at different structural indices and analytic signal using Geosoft Oasis Montaj 6.4.2

(HJ) data processing and analysis software. The resultant maps were overlain, compared and or plotted on RTP residual map and or geological map and interpreted in relation to the surface geological map. The study observed that positive magnetic anomalies are associated with contrasting basement rocks; while the negative magnetic anomalies are associated with intrusive bodies. Interpreted lineaments obtained from total horizontal derivative map were separated into two categories namely ductile and brittle based on their character vis-à-vis magnetic anomalies on RTP intensity map. Whilst the brittle lineaments were interpreted as fracture or faults; the ductile lineaments were interpreted as folds or representing the integral fabric of the rock units. The iron ore mineralization is distributed within the eastern portion of the study area with Ajase BIF at relatively greater depth (0.5-2.0 km) compared to Gbede BIF (0.50-0.74 km) and confined probably along a fault lineament or lying conformably on topographic bedrock depression suggesting it is structurally controlled.

The work of Wright (1976) suggested a possibility of the intersection of the NE-SW trending fracture system with those of Romanche and Chain fracture zones in the Atlantic. Results from this work intends to fill this gap. Even though the works of Ajakaiye *et al*. (1991), Onyedim (2007), Adepelumi *et al*. (2008), Akintorinwa *et al*. (2010) and others who have employed the magnetic technique did not extend their work to the margin of the continent which the present study covers. This work therefore intends to find any major subsurface structure that will/might link those of the Ifewara-Kalangai structures to those coming from the Atlantic.

CHAPTER THREE

MATERIALS AND METHODS

3.1 Materials

The materials for this study include software (Geosoft Oasis Montaj (v 6.4.2), Grapher 8, Microsoft Office 2010 and Surfer 12) which were used for the processing and analysis of data, geological map of the study area, topography/bathymetry data and high resolution aeromagnetic anomaly data of the study area.

3.2 Theories of the interpretation techniques

3.2.1 Basic theory

Conceptually, magnetic scalar potential A(r) at a point P is the work done on a unit positive pole in bringing it from infinity by any path against a magnetic field **F**(r). When **F**(r) is due to a positive pole (+p) at a distance r from P, $A(r) = -\int_{\infty}^{r} \boldsymbol{F}(r).\boldsymbol{dr} = p/\mu r$.

But $\mu=1$

$$A(r) = p/r. \qquad 3.1$$

However, since a magnetic monopole cannot exist, we consider a magnetic dipole to get a realistic entity. Referring to Fig. 3.1, we calculate A(r) at an external point.

$$A(r) = \left(\frac{p}{r_1} - \frac{p}{r_2}\right)$$

$$A(r) = p\left(\frac{1}{(r^2+l^2-2lrcos\theta)^{\frac{1}{2}}} - \frac{1}{(r^2+l^2+2lrcos\theta)^{\frac{1}{2}}}\right). \qquad 3.2$$

The vector **F**(r) can be derived by taking the gradient of A(r).

$$\mathbf{F}(r) = -\nabla A(r). \qquad 3.3$$

Its radial component is $F_r = -\partial A/\partial r$ and its angular component is $F_\theta = -\partial A/r\partial\theta$; those are:

$$F_r = -p\left\{\frac{r+l\cos\theta}{(r^2+l^2+2rl\cos\theta)^{3/2}} - \frac{r-l\cos\theta}{(r^2+l^2-2rl\cos\theta)^{3/2}}\right\}. \quad 3.4$$

$$F_\theta = P\left\{\frac{l\sin\theta}{(r^2+l^2+2rl\cos\theta)^{3/2}} - \frac{l\sin\theta}{(r^2+l^2-2rl\cos\theta)^{3/2}}\right\}. \quad 3.5$$

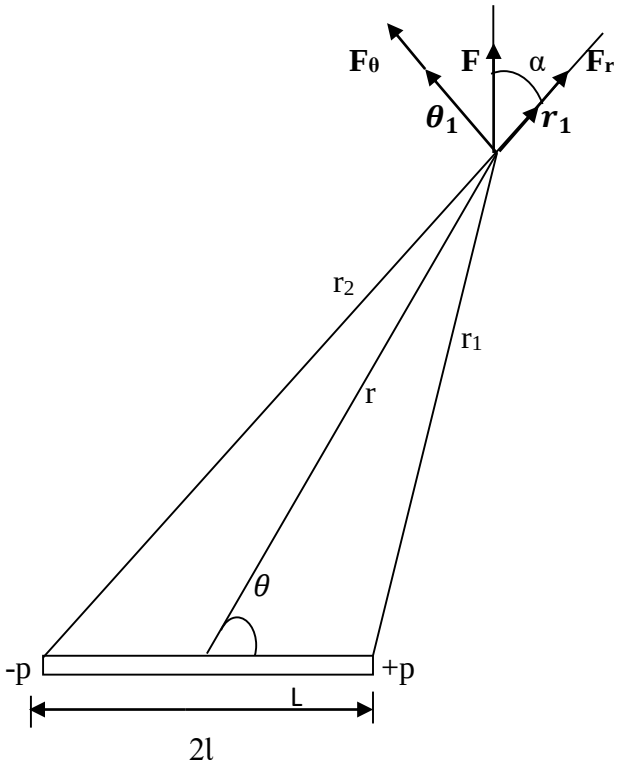


Fig.3.1 Field due to dipole

When r >> l, Equation (3.2) becomes

$$A = |m| \cos\theta / r^2 \quad 3.6$$

Where m is the dipole moment of magnitude m = 2lp.

Equations (3.3) and (3.6) give

$$\mathbf{F} = \left(\frac{m}{r^3}\right)(2\cos\theta\, \boldsymbol{r_1} + \sin\theta\, \boldsymbol{\theta_1}) \quad 3.7$$

Where unit vectors $\boldsymbol{r_1}$and $\boldsymbol{\theta_1}$ are in the direction of increasing r and θ (counter clockwise in Fig. 3.1).

The resultant magnitude is

$$F = |\mathbf{F}| = (m/r^3)\ (1 + 3\ \mathrm{Cos}^2\theta\ )^{1/2}. \qquad 3.8$$

And the direction with respect to the dipole axis is

$$\mathrm{Tan}\propto = F_\theta/F_r = (1/2)\ \tan\theta \qquad 3.9$$

Two special cases, $\theta = 0$ and $\frac{\pi}{2}$ in equations (3.4) and (3.5) are called the Gauss – A (end – on) and Gauss – B (side – on) positions. From equations (3.4) and (3.5) they are given by

$$F_r = 2mr\ /\ (r^2 - l^2)^2,\quad F_\theta = 0 \qquad \theta = 0 \qquad 3.10$$

$$F_r = 0,\qquad F_\theta = m\ /\ (r^2 + l^2)^{3/2} \qquad \theta = \pi/2 \qquad 3.11$$

If $r >> l$, these simplify to

$$F_r = 2m/r^3 \qquad \theta = 0$$

$$F_\theta = m/r^3 \qquad \theta = \pi/2\} \qquad 3.12$$

In geophysical context, magnitude of the earth's magnetic field best modelled to be equivalent to the field due to vertical dipole (with large magnetic moment) at the centre of the earth (as provided by Equation (3.8) along with effect of temporal variations and local anomalies in the field, is what magnetometer measures as total magnetic field in unit of nanotesla (nT) or gamma (γ).

3.2.2 Vertical derivatives

Vertical derivatives emphasise shallower anomalies and can be calculated in either frequency or space domain. These operators also amplify high frequency noise, and special tapering of the frequency response is usually applied to control this problem. Thus first and second vertical derivatives used in this study will be analysed as follows. Vertical derivatives map tends to sharpen the edges of anomalies and enhance shallow features. Vertical derivatives map is much more responsive to local influence than to regional effect. Therefore, vertical derivative (L(r)) as given by Equation (3.13) tends to give sharper image than that of the total field.

$$L(r) = r^n \qquad 3.13$$

Where n is the order of differentiation, and r is the wave number in radians/ground units. Also,

$$r = 2pk \qquad 3.14$$

Where k is cycles/ground unit. Ground unit is the survey ground units used in the grid, examples are metres.

3.2.3 Total horizontal derivative

Total horizontal derivative (THDR) operator estimates the location of lateral changes or abruptness in magnetization (Blakely, 1996). Magnetic susceptibility changes caused by features such as faults can be highlighted by the total horizontal derivative (Blakely, 1996). The THDR given by Equation (3.15) is commonly used for edge-detection in the potential field data (Cordell and Grauch, 1985)

$$\text{THDR} = \sqrt{\left(\frac{\partial M}{\partial x}\right)^2 + \left(\frac{\partial M}{\partial y}\right)^2}\ , \qquad 3.15$$

Where M is the potential field and $\frac{\partial M}{\partial x}$ and $\frac{\partial M}{\partial y}$ are x- and y- directional derivatives of potential field, respectively.

Horizontal gradient magnitude and other derivatives are pretty much an interpretation aid tool. However, the gradient maxima seen on a gradient map could mean different things, and therefore, it is still interpreter's responsibility to find a meaningful interpretation. Another caveat of this technique is that, in a non-near vertical boundary or when two source boundaries occur in close proximity to each other, the gradient maxima are offset from a position directly over the source boundary and this could lead to two peaks maxima, which could be interpreted as two edges (Grauch and Cordell, 1985)

3.2.4 Theory of analytic signal technique

The analytic signal technique is based on the use of the first derivatives of magnetic anomalies to estimate source characteristics and to locate positions of geologic boundaries such as contacts and faults. The forward and inverse 2-D Fourier transform g and *f* respectively of the magnetic field anomaly, **M**, is given by:

$$g(k_x, k_y) = F[f(x, y)]$$

$$= \int_{-\infty}^{\infty}\int_{-\infty}^{\infty} f(x,y)e^{-i(k_x x + k_y y)}\,dxdy \qquad 3.16$$

$$f(x, y) = F^{-1}[g(k_x, k_y)]$$

$$= \frac{1}{4\pi^2}\int_{-\infty}^{\infty}\int_{-\infty}^{\infty} g(k_x + k_y)e^{i(k_x x + k_y y)}dk_x dk_y, \qquad 3.17$$

Where k_x and k_y are the wave numbers in the x- and y-directions respectively. Using Equation (3.16), wave number domain relations can be derived between the Fourier transforms of a magnetic anomaly *M* and of its horizontal and vertical derivatives, as well as relations between the different derivatives of a potential field anomaly (Nabighian, 1972, 1984; Nelson, 1988; Pedersen, 1989).

The three-dimension (3-D) analytic signal (AS) of a potential field anomaly M (magnetic field), can be defined as a complex vector

$$\text{AS (x, y)} = \frac{\partial M}{\partial x}\hat{x} + \frac{\partial M}{\partial y}\hat{y} + i\frac{\partial M}{\partial z}\hat{z}, \qquad 3.18$$

Where i is the complex number and $\hat{x}$, $\hat{y}$ and $\hat{z}$ are the unit vectors in x, y and z directions, respectively (Nabighian, 1972; Roest *et al.*, 1992: Debeglia and Corpel, 1997).

Equation (3.18) satisfies the basic requirement of the analytic signal (Nabighian, 1972, 1984), that its real and imaginary parts form a Hilbert transform pair. This can be achieved by transforming Equation (3.18) into the frequency domain and expressing it in terms of the gradient of the Fourier transform of the magnetic field (Roest *et al*., 1992) which is equivalent to Equation (3.18) in the space domain (Debeglia and Corpel, 1997):

$$\hat{t} \cdot F[\boldsymbol{AS}(x,y)] = \hat{h}\,\nabla F(M) + i\hat{z}\,\nabla F(M). \qquad 3.19$$

The real and imaginary parts of Equation (3.19) being the horizontal and vertical derivatives respectively, form a Hilbert transform pair and are related by the 3-D Hilbert transform operator $i(\hat{h}\cdot\boldsymbol{k})/|\boldsymbol{k}|$ as follows:

$$\begin{aligned}\hat{h}\cdot\nabla F[M] &= i\,h\cdot kF[M]\\ &= i\frac{\hat{h}\cdot k}{|k|}|k|F\,[M] \qquad 3.20\\ &= i\frac{\hat{h}\cdot k}{|k|}\hat{z}\cdot\nabla F[M],\end{aligned}$$

where $\nabla = ik_x\hat{x} + ik_y\hat{y} + |k|\hat{z}$, represents the gradient operator in the frequency domain, $\boldsymbol{k}$ = (k_x, k_y) the wavenumber, $\hat{h} = \hat{x} + \hat{y}$ and $\hat{\imath} = \hat{x} + \hat{y} + \hat{z}$.

According to Roest *et al.* (1992), Equation (3.20) is equivalent to the scalar Equation (17) of Nabighian (1984) and represents a means of calculating the vertical derivative when horizontal derivatives in two perpendicular directions are available.

The absolute value (amplitude) of analytic signal (**AS**) is defined as the square root of the squared sum of the vertical and the two horizontal first derivatives of magnetic field anomaly M given by:

$$|\boldsymbol{AS}(x,y)| = \sqrt{\left(\frac{\partial M}{\partial x}\right)^2 + \left(\frac{\partial M}{\partial y}\right)^2 + \left(\frac{\partial M}{\partial z}\right)^2} \qquad 3.21$$

The shape of the absolute value of the analytic signal is used for interpretation; the amplitude of the analytic signal shows maxima over boundaries/edges.

For the 2-D case, this equation is simplified to

$$|\boldsymbol{AS}(x)| = \sqrt{\left(\frac{\partial M}{\partial x}\right)^2 + \left(\frac{\partial M}{\partial z}\right)^2} \qquad 3.22$$

Using Equation (3.22) Nabighian (1972) showed that for a thin sheet-like body (dyke), the location of the source in the horizontal plane can be deduced from the positive peaks of the amplitude of the analytic signal and the source depth can be estimated as the half width at half maximum of the amplitude of the analytic signal over a thin dyke is independent of the angle of inclination and declination of the magnetic field vector and the magnetization vector.

This is not the case when prismatic 3-D bodies are encountered, especially if their extents are close enough to produce interference effects and thereby affect the shape of the analytic signal amplitude.

Roest *et al.* (1992) determined the analytic signal over a vertical magnetic contrast at a depth d, given by:

$$|A(x)| \propto \frac{1}{x^2+d^2} \qquad 3.23$$

Equation (3.23) indicates that amplitude of the analytic signal has a bell shaped function; with half-maximum half-width that equals the depth to the magnetic source (Nabighian, 1972; Roest *et al.*, 1992).

The absolute value of the analytic signal is often referred to as the energy envelope of a signal (Oppenheim and Schafer, 1975). The absolute value of the analytic signal is the envelope of all possible phase shifts of an observed anomaly. The absolute value of the analytic signal in three dimensions is also envelope over all possible directions of magnetization and inducing field (Roest *et al.,* 1992). The envelope has a maximum that is located over the magnetic contrast. The locations of these maxima thus determine the outlines of magnetic sources.

3.2.5 Theory of tilt derivatives

The analytic signal amplitude for 2-D structures is as in Equation (3.22) and $\theta = tan^{-1}\left[\frac{\partial M}{\partial z} / \frac{\partial M}{\partial x}\right]$ is the local phase.

Tilt derivative (TDR) is similar to the local phase, but uses the absolute value of the horizontal derivative in the denominator

$$\text{TDR} = tan^{-1}\left[\frac{VDR}{THDR}\right], \qquad 3.24$$

Where VDR and THDR are the first vertical and total horizontal derivatives, respectively, of the total magnetic intensity. While VDR can be positive or negative, THDR is always positive (Verduzco *et al.,* 2004). For profiles in the x direction,

$$\text{THDR}= \sqrt{\left(\frac{\partial M}{\partial x}\right)^2} \qquad 3.25$$

And for grids is as in Equation (3.15).

Due to the nature of the arc tan trigonometric function, all amplitudes are restricted to values between $+\pi/2$ and $-\pi/2$ (+90° and -90°) regardless of the amplitudes of VDR or THDR.

This fact makes this relationship function like an automatic gain control (AGC) filter and tends to equalize the amplitude output of total magnetic intensity anomalies across a grid or along a profile.

The total horizontal derivative of tilt derivative (THDR_TDR) is

$$\text{THDR_TDR}= \sqrt{\left(\frac{\partial TDR}{\partial x}\right)^2} \qquad 3.26$$

for a profile and

$$\text{THDR_TDR}= \sqrt{\left(\frac{\partial TDR}{\partial x}\right)^2 + \left(\frac{\partial TDR}{\partial y}\right)^2} \qquad 3.27$$

for a grid. These are equivalent to the absolute value of the local wavenumber.

3.2.6 Theory of theta derivatives

The analytic signal of a magnetic intensity anomaly is defined in 3-D by Roest *et al*. (1992) as in Equation (3.18). Directly over a vertical contact, $\partial M / \partial z = 0$, so that the analytic signal vector makes an angle $\theta = 0$ with the horizontal. Defining $\hat{s}$ as a unit vector along the horizontal direction of the analytic signal, the angle θ is calculated using

$$\text{Cos}\,\theta = \frac{A\cdot\hat{s}}{|A||\hat{s}|} = \frac{\sqrt{(\partial M/\partial x)^2 + (\partial M/\partial y)^2}}{|A|} = \frac{THDR}{|A|} \qquad 3.28$$

Note that $0 < \theta < \pi/2$ because we rely on the horizontal gradient to define the horizontal. Although this method restricts the range of angles and we lose information, the result is a well-defined image that is easy to interpret. Equation (3.28) is the ratio of the magnitudes of the horizontal gradient to the analytic signal, so that the theta map may also be thought of as a normalization of the horizontal gradient. This normalization introduces an effective gain control, such that amplitude information is lost, but low-amplitude features are highlighted (Wijns *et al.,* 2005).

3.2.7 Theory of Euler deconvolution

Thompson (1982) showed that Euler's homogeneity relation could be written in the form

$$(x - x_0)\frac{\partial M}{\partial x} + (y - y_0)\frac{\partial M}{\partial y} + (z - z_0)\frac{\partial M}{\partial z} = N\,(B - M), \qquad 3.29$$

Where (x_0, y_0, z_0) is the position of a magnetic source whose total field M is detected at (x, y, z). The total field has a regional value of B. The degree of homogeneity N may be interpreted as a structural index (Thompson, 1982), which is an exponential component corresponding to the rate at which the field falls off with distance, for a source of given geometry. Sources are simple geometrical object such as a homogenous point source (sphere) $N = 3$, a linear source (line of dipoles or poles, and for a homogenous cylinder, rod, etc.) $N = 2$, for intrusive bodies (thin layer, dyke, etc.) $N = 1$, for a contact, vertex of a block and a pyramid with a big height $N = 0$. The choice of a proper structural index is a function of the geometry of causative bodies. Estimation of the correct structural index is crucial for the successful application of the Euler deconvolution method (Reid *et al.,* 1990). And this is achieved by using the index that produces the best clustering of solutions (Reid, 1995). Incorrect choice of structural index leads to errors in estimated source

depths (Ravart, 1996). Euler deconvolution used the magnetic field and its three orthogonal gradients (two horizontals and one vertical) to compute anomaly source locations (Keating and Pilkington, 2004).

3.2.8 Theory of Werner deconvolution

Werner (1953), introduced Werner deconvolution technique, and realized that the greatest need was for a method to separate an anomaly from the interference caused by adjoining anomalies and to consider the entire anomaly rather than just a few parameters such as maxima, minima, or inflection points, which can be greatly affected by type of interference. With Werner's method, it is necessary still to assume the type of source configuration, examples dykes, and to process the interference correctly. Also, the method assumes initially that the data are perpendicular to geologic strike.

The equation in the total field for a dyke with infinite strike length and depth extent can be written in the form,

$$M(x) = \frac{A(x-x_0)+Bz}{(x-x_0)^2+z^2} \qquad 3.30$$

Where x represents distance along a profile and M is the total magnetic field intensity at x. The constants A and B are functions of the field strength, susceptibility, and the geometry involved (dip, strike, magnetic inclination, declination, etc.); x_o is the horizontal distance along traverse to the point immediately above the top of the dyke; and z is the depth to the top of the dyke. There are four unknown quantities - A, B, x_0, z.

Werner points out that in the simple case where observations are made in a plane over level bounded bodies whose length and depth are infinite and whose strike is perpendicular to the

direction of the profile, the equation for a dyke can be cast into the following interpretation equation:

$$a_o + a_1 x + b_0 M + b_1 x M = x^2 M \qquad 3.31$$

In this equation, *x* and *M* are the same as in Equation (3.30). It follows that

$$a_0 = -Ax_0 + Bz, \qquad a_1 = A,$$
$$b_0 = -x_0^2 - z^2 \text{ And } b_1 = 2x_0. \qquad 3.32$$

Conversely, the horizontal position and depth of the top of the dyke are functions of the parameters of the interpretation Equation (3.31):

$$x_0 = \frac{1}{2} b_1 \quad \text{And} \quad z = \left[\sqrt{-4b_0 - b_1^2}\right]/2 \qquad 3.33$$

Since there are four unknowns, simultaneous solution of the interpretation Equation (3.31) at four x values and their corresponding *M* values will yield solutions for a_o, a_1, b_o, and b_1, and, from Equation (3.33), for x_0 and *z*. In the simple case, the geometric solution is complete. The depth to the top of the dyke (thin sheet) has been determined.

If we now admit the possibility of interference and assume that the interference can be represented by a polynomial of some degree, we can add the interference polynomial to Equation (3.30).

$$M(x) = \frac{A(x-x_0)+Bz}{(x-x_0)^2+z^2} + C_0 + C_1 x + \cdots + C_n x^n, \qquad 3.34$$

Where *n* is the order of the interference polynomial and the C's are the coefficients. We now have a total of (*n* + 5) unknowns and therefore (*n* + 5) points are required to solve for the unknowns. In practice, a first or second order polynomial is generally sufficient, so that 6 or 7 points are required for solution. Werner also presents a simple method of solving the simultaneous equations which

amounts to multiplying the data points by a set of linear operators, thus greatly reducing the labour involved. Although this represents the first attempt to deal automatically with interference, with Werner's method it is necessary still to assume the type of source configuration, e.g., dykes, and to process the interference correctly. Also, the method assumes initially that the data are perpendicular to geologic strike.

Werner's theory is valid for all semi-infinite, homogenous, thin-sheet bodies, whatever their strike, dip, or remanent magnetization, and at any magnetic latitude.

Werner's theory was extended to incorporate another geometric form (contact) (Hartman *et al.*, 1971). Thin-sheets are actually bounded by two planes called interfaces. In the case of thin sheets, the individual interfaces are too close together for their anomalies to be separately distinguishable. In general, this is true if the width of the sheet is less than the depth to the top edge of the sheet. By the integration of a sufficient number of thin sheets, a body can be made broad enough so that the magnetic anomaly from each of the interfaces is distinct. This extension of a thin sheet theory results from the fact that the magnetic anomaly for a thin sheet is precisely the same as the derivative of an anomaly for a similar positioned interface. Therefore, by applying Werner's formulas to the total field and to the two gradients, Hartman *et al.* (1971) were able to identify and calculate the pertinent characteristics of thick sheets and individual interfaces, as well as those of thin sheets. Solutions are found from any set of equally spaced points, and these points need not be pre-determined or critical points along the profile, such as inflexion points, maxima, or minima.

3.2.9 Theoretical basis for 2-D forward modelling and inversion of the aeromagnetic data

The 2-D forward modelling and inversion methods to be used in calculating the magnetic model response are based on the methods of Talwani *et al.* (1959) and Talwani and Heirtzler (1964), and

make use of the algorithms described by Won and Bevis (1987). Two-and-a-half dimensional calculations are based on Rasmussen and Pedersen (1979). The GM-SYS inversion routine to be used utilizes a Marquardt inversion algorithm (Marquardt, 1963) and the USGS computer program, SAKI (Webring, 1985) to linearize and invert the calculations (Tom *et al.*, 2009).

3.3 Data acquisition

Shuttle radar topographic mission and aeromagnetic data are very useful in a wide variety of geological and geophysical studies and play a leading role in tracing lithological contacts and delineating geological structures as well as drainages and vegetation (Kogbe, 1985 and Muhammad, 2009). When used with geological maps, aeromagnetic data can be useful in evaluation of earth resources (Kowalik and Glen, 1987; Adepelume *et al.,* 2008 and Abubakar, 2012). A regional study of an aeromagnetic anomaly map brings out the regional geological patterns and structural features and provides exceptional background information for interpretation to suite specific purposes Sharma (1998). The speed of coverage of large and inaccessible areas for subsurface investigation is an additional advantage of the use of shuttle radar topographic mission (SRTM) and aeromagnetic data.

Aeromagnetic survey has been widely used for mapping of anomalies. When guided by structural and geological observations, it serves as a means of identifying anomalous sources; their depths, dimension, magnetization, extending geological mapping area of poor exposure and in providing structural frameworks for inferring information about tectonic evolution, mineralization etc. (Kowalik and Glen,1987; Adepelume *et al*., 2008 and Abubakar, 2012).

The aeromagnetic survey of the study area is part of the high resolution airborne geophysical surveys of Nigeria involving magnetic, radiometric and limited electromagnetic surveys. Fugro

Airborne Survey Limited conducted the data acquisition using wing aircrafts. The survey was flown in drape mode using real time differential global positioning system at a sensor mean terrain clearance of 80-100 m. Traverse and Tie line spacing were 500 m and 2000 m respectively in NW-SE and NE-SW directions and the data were recorded at a sampling interval of 100 m (NGSA, 2010).

3.3.1 Acquisition and usage of shuttle radar topographic mission data

Shuttle radar topographic mission (SRTM) gridded data covering the study area were acquired from Nigerian Geological Survey Agency (NGSA). The gridded data were converted into a map using Oasis Montaj software as shown in Fig. (3.2). From the Figure, two distinct physical regions can be identified; the lowland terrain underlain by sedimentary basin and the upland areas remarked by the crystalline lithology. The elevation of the lowland in the zone rises from 4 to 62 m above sea level while that of the upland rises from 73 to 381 m. The depth below sea level ranges between -8 m and -747 m.

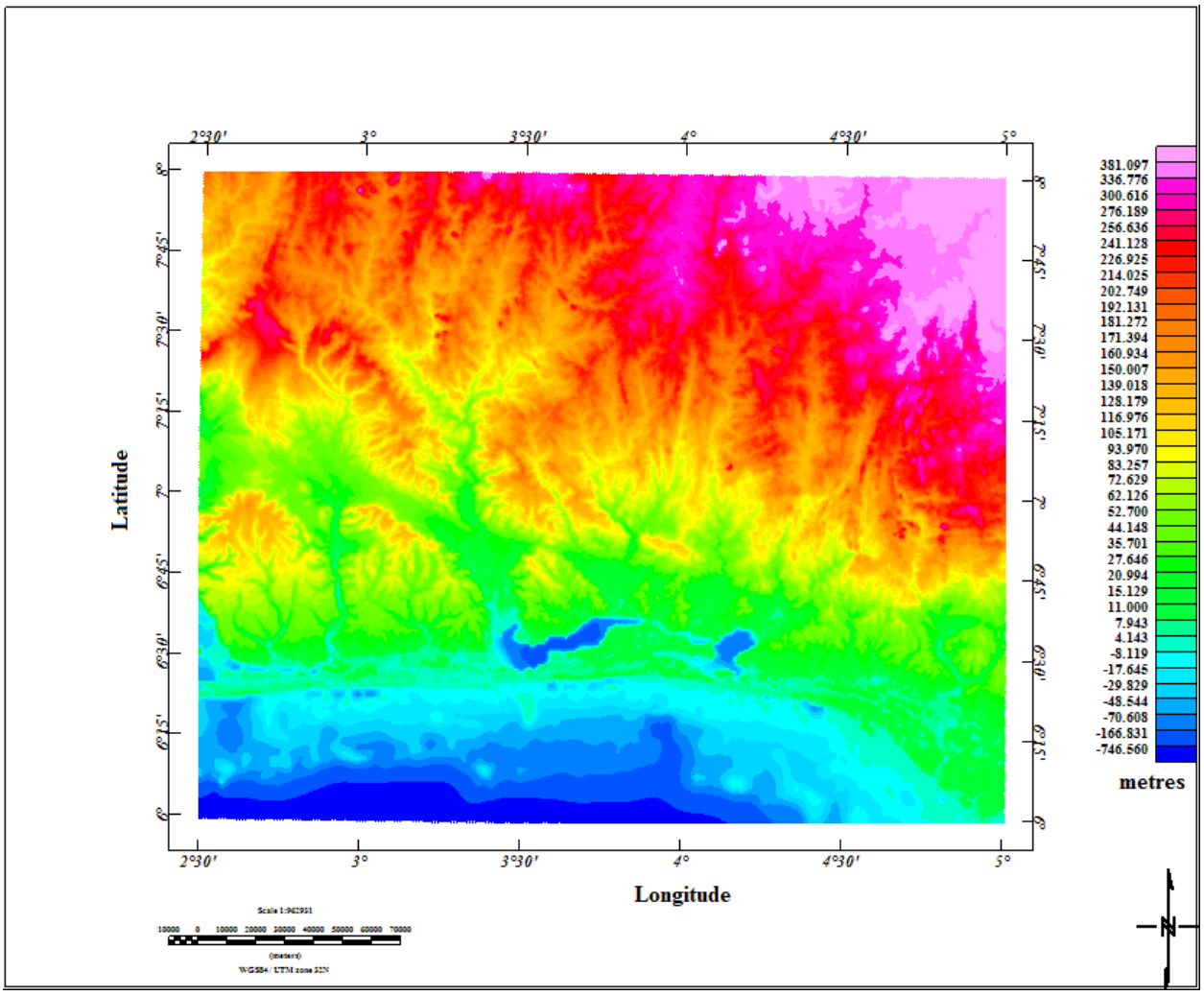


Fig. 3.2: Topography and bathymetry map of the study area.

3.3.2 Acquisition and processing of high resolution aeromagnetic data

High resolution aeromagnetic data of the study area sheets: 239, 240, 241, 242, 243, 259, 260, 261, 262, 263, 278, 279, 280, 281, 282, 278^{A}, 279^{A}, 280^{A}, 281^{A} and 296 were acquired from the Nigerian Geological survey Agency (NGSA) and processed using a suite of appropriate software. The data for each sheet, covers half-degree sheet were on a scale of 1:100000. The data were initially pre-processed by Fugro Airborne Survey and Consultant teams, pre-processing operation include micro leveling, removal of cultural effects as well as filtering for noise contents.

The pre-processed data were quality controlled for isolated spikes and other spurious data which bear no correlation with geology. Butterworth filtering processing was applied to remove any possible cultural noise and other outrageous noise in order to increase the signal to noise ratio while minimizing other noise energies in the data. Total magnetic intensity maps of the study area comprising of the sheets (Figs. 3.3a-b) were plotted using the Oasis Montaj software (version 6.4.2). The composite map (Fig. 3.3a) is presented in shaded relief (Fig. 3.3b). The features in shaded relief imaging are enhanced when aeromagnetic data are treated as topography that is illuminated from different directions by an artificial light source to accentuate the finer details that are perpendicular to the illumination direction (Kowalik and Glen, 1987; Broome, 1990). The missing data corresponding to the white portions is as a result of no survey being conducted at such areas. With the combined coloured and shaded relief maps, both long wavelength and short wavelength features are effectively displayed.

The total magnetic field intensity ranges between 32923 and 33127nT. A magnetic relief of 204 nT is attributed to differences in magnetic mineral content between various lithologies, and to the variation in the depth to magnetic rocks (Bird, 1997). Comparing the geology and the total magnetic intensity maps, there is a sharp correlation between the geologic and total magnetic field intensity territorial boundaries. Most of the anomalies trend NE-SW, some trend NW-SE and few trend E-W.

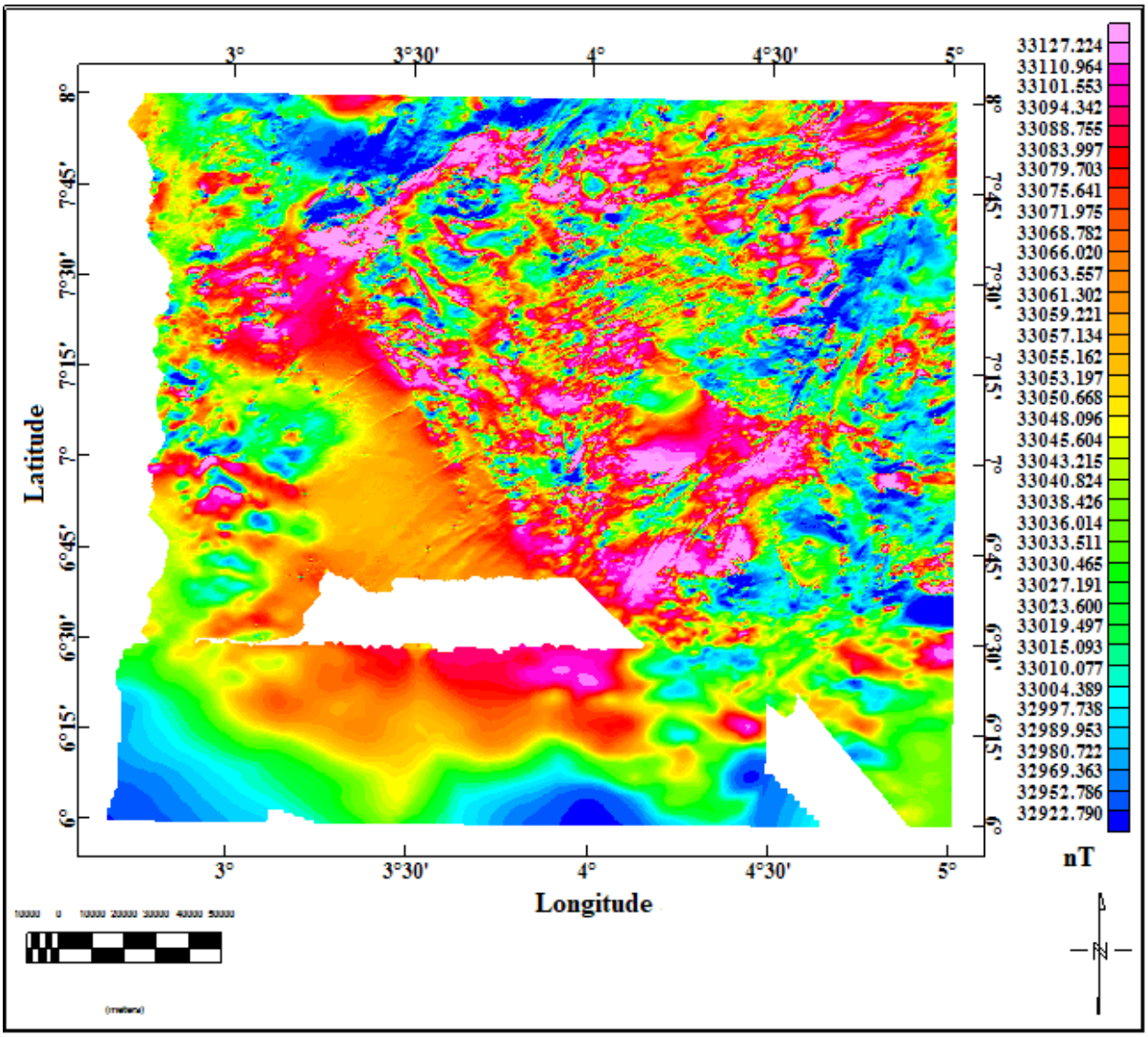


Fig. 3.3a: Total magnetic field intensity map of the study area.

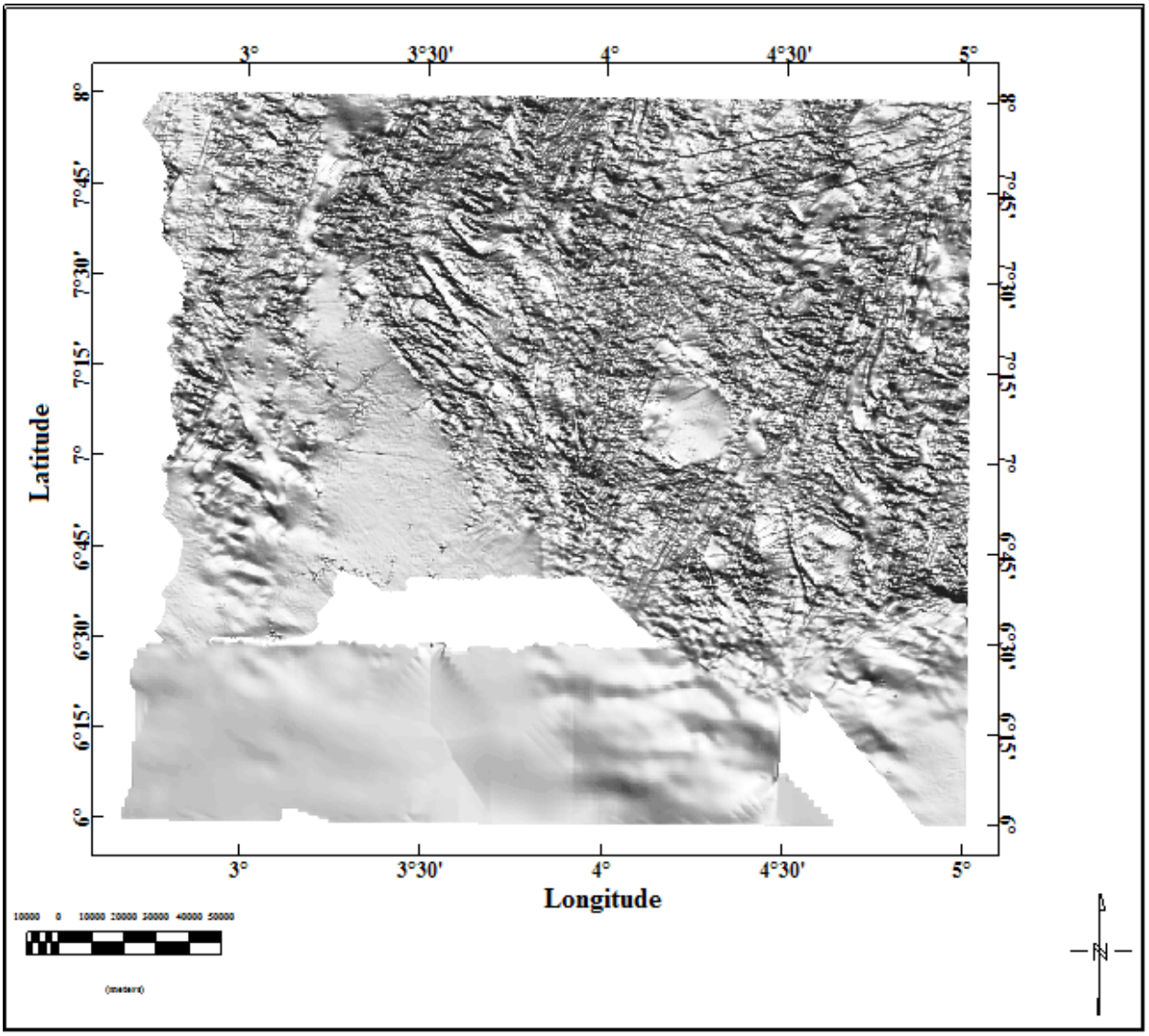


Fig. 3.3b: Shaded relief map of the total magnetic field intensity of the study area.

3.4 Processing of high resolution aeromagnetic data

Data processing are the series of steps taken to remove both signal and spurious noise from the data that are not related to the geology of earth's crust. This process prepares the dataset for the interpretation by reducing the data to contain only signal relevant to the task using filtering techniques (regional-residual separation and upward continuation).

3.4.1 Regional–residual separation

All regional-residual potential field separation methods are based on the fact that the regional field is smooth and its spectrum is dominated by relatively low frequencies. In this work, the polynomial fitting method which is the most flexible and most applied of the analytical methods for determining regional magnetic field (Skeels, 1967; Johnson, 1969 and Dobrin, 1976) was used. In this method, marching of regional field by a polynomial surface of low order express the residual features as random error. The treatment is also based on statistical theory. The observed data were used to compute, usually by least square method, which is the mathematical describable surface giving the closest fit to the magnetic field that can be regional field and the residual field is the difference between the magnetic field values as actually mapped and the regional field thus determined.

The least-square method was applied to the aeromagnetic data of the study area. All the regional fields were calculated as a two-dimensional first-degree polynomial surface. To eliminate the regional field, a plane surface was fitted to the data by multiple regression least-square criteria established by the mathematical concept of (Skeels, 1967; Johnson, 1969 and Dobrin, 1976).

The polynomial coefficients were used to compute the regional field data (Fig. 3.4). A mapping software (Surfer 12) was used to subtract the values of the regional field from the total magnetic values at grid points. The data were processed to generate the residual field maps (Figs. 3.5a and 3.5b). It was observed that the trend pattern of the regional field is NE-SW. The direction of the regional field is in conformity with the suspected structures arising from the Atlantic Ocean. Most of the structures on the residual maps are in the same direction with the regional field, which shows the authenticity of the regional field.

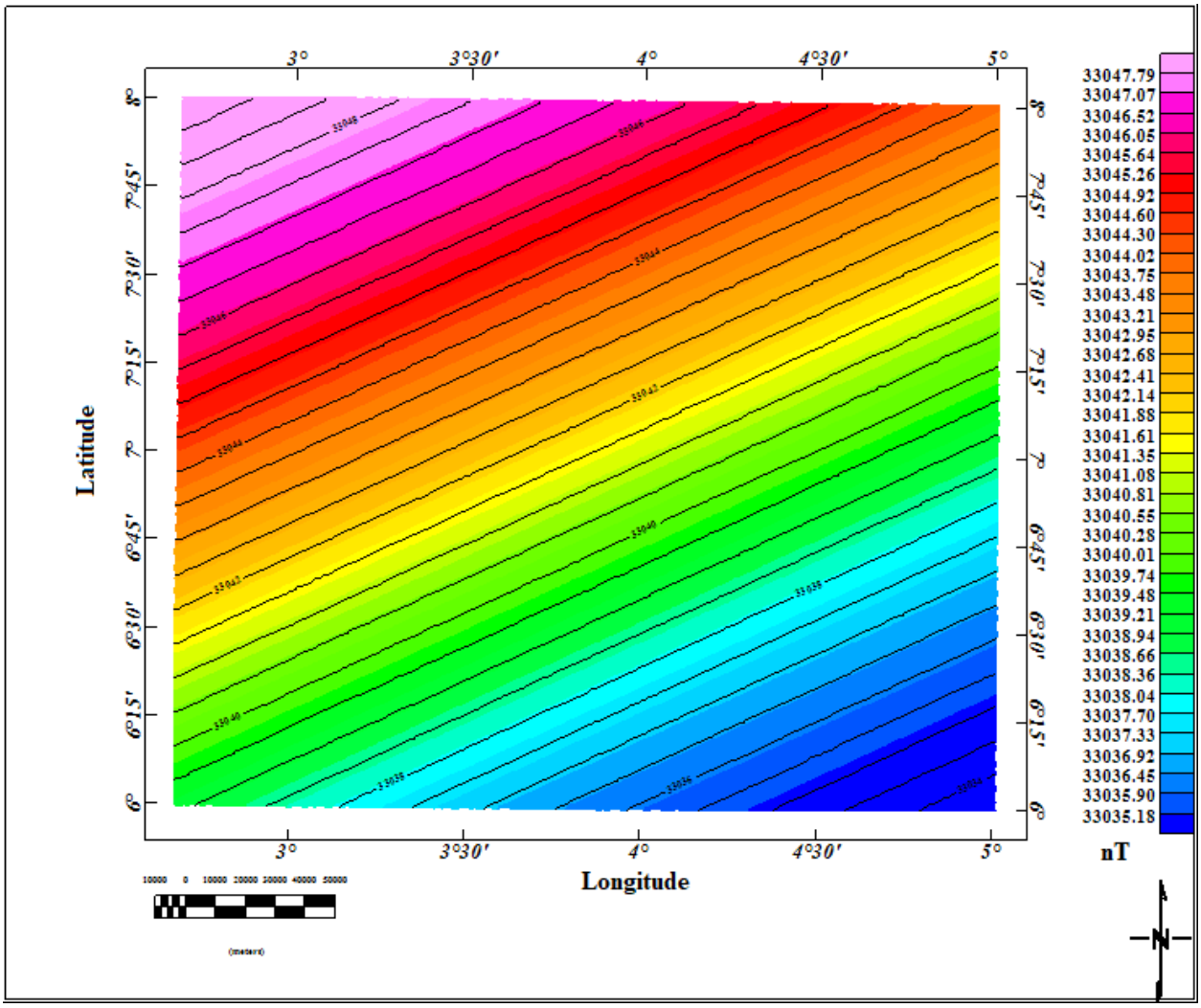


Fig. 3.4: Regional magnetic field intensity map of the study area.

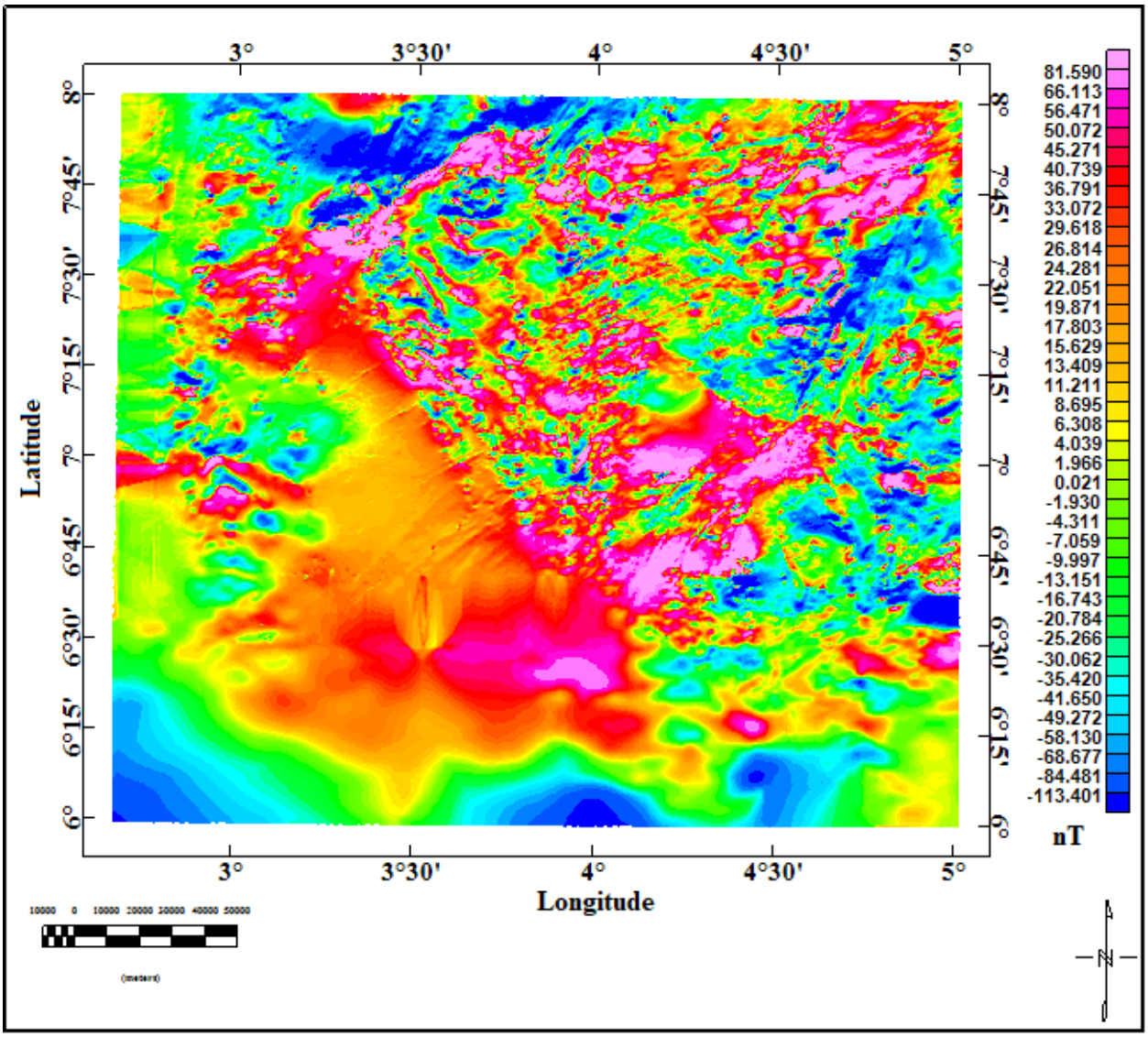


Fig. 3.5a: Residual magnetic field intensity map of the study area.

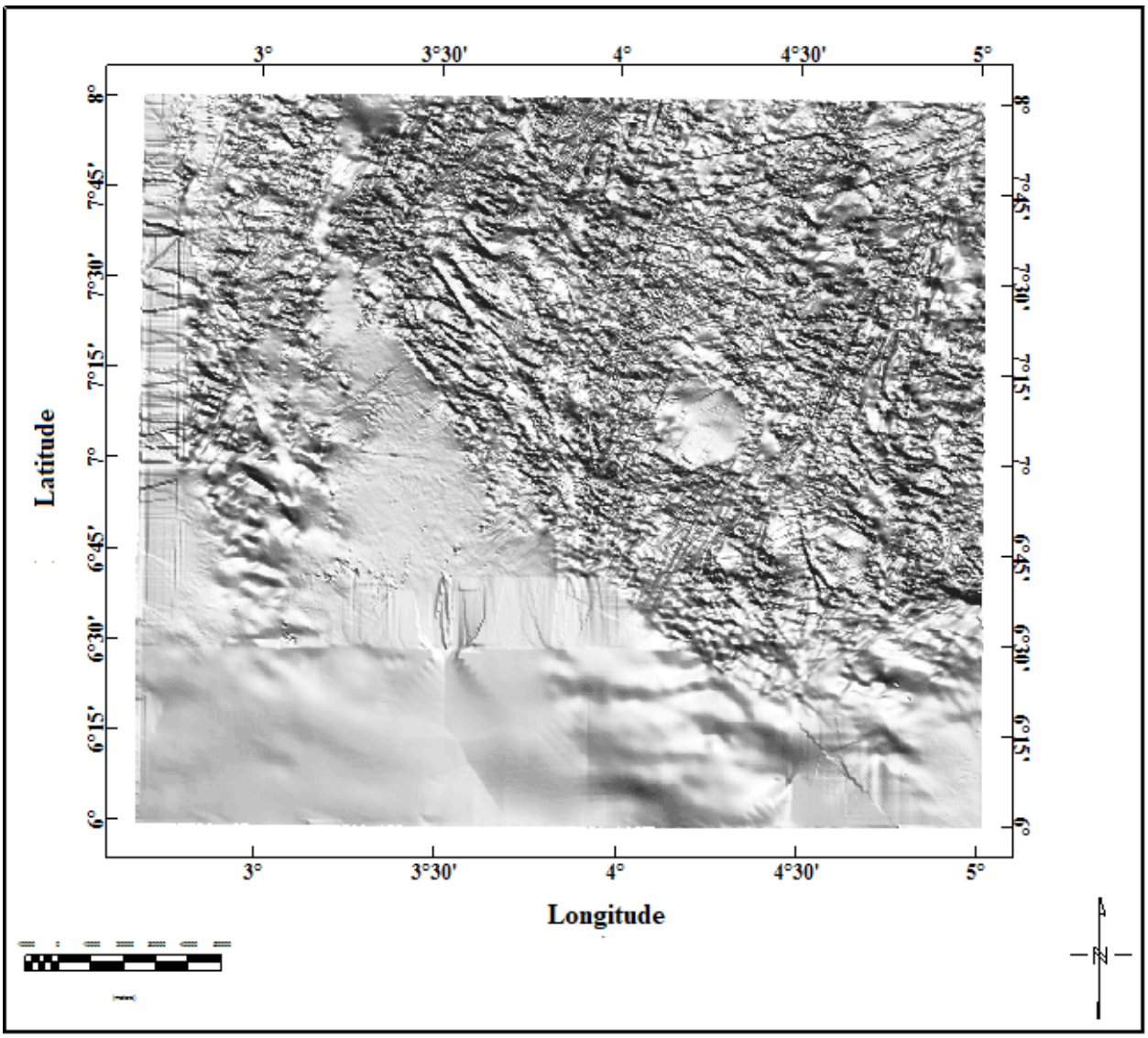


Fig. 3.5b: Shaded relief map of the residual magnetic field intensity of the study area.

3.4.2 Upward continuation

Filtering represents a major component of magnetic data processing. As a rule, digital filters as used for signal enhancement unit is to remove unwanted noises and enhance desired signals. The filtering technique in this study was performed using upward continuation. The upward continuation filter technique is a form of a low-pass filter, which is preferable to an ordinary low-pass filter because the upward continuation map is usually devoid of the ringing artifact or Gibbs

phenomena, which is often characteristic of a broadband low-pass filtered map. The Gibbs phenomenon occurs on the anomaly map where the amplitude of the data is rapidly changing. In the frequency domain, the truncation of the frequency spectrum with a rectangular window (step function window) causes the Gibb's effect, which is expressed as short wavelength ringing in the space domain data (Papoulis, 1962; Ku *et al*., 1971). The upward continuation transformation calculates the magnetic field at an elevation higher than that at which it was originally measured. This transformation attenuates near-surface effects and accentuates the anomalies from deeper magnetic sources (Blakely, 1996). The residual aeromagnetic data were upward continued to a height of 2000 m (where the noise level of the second vertical derivative grid appears to be very low). This transformation highlights the longer spatial wavelength anomalies at the expense of the shorter wavelength anomalies (Figs. 3.6a and 3.6b). In spite of the upward continuation, certain short wavelength anomalies were preserved, superimposed on regional anomalies. These anomalies have their origin in shallow geological structures.

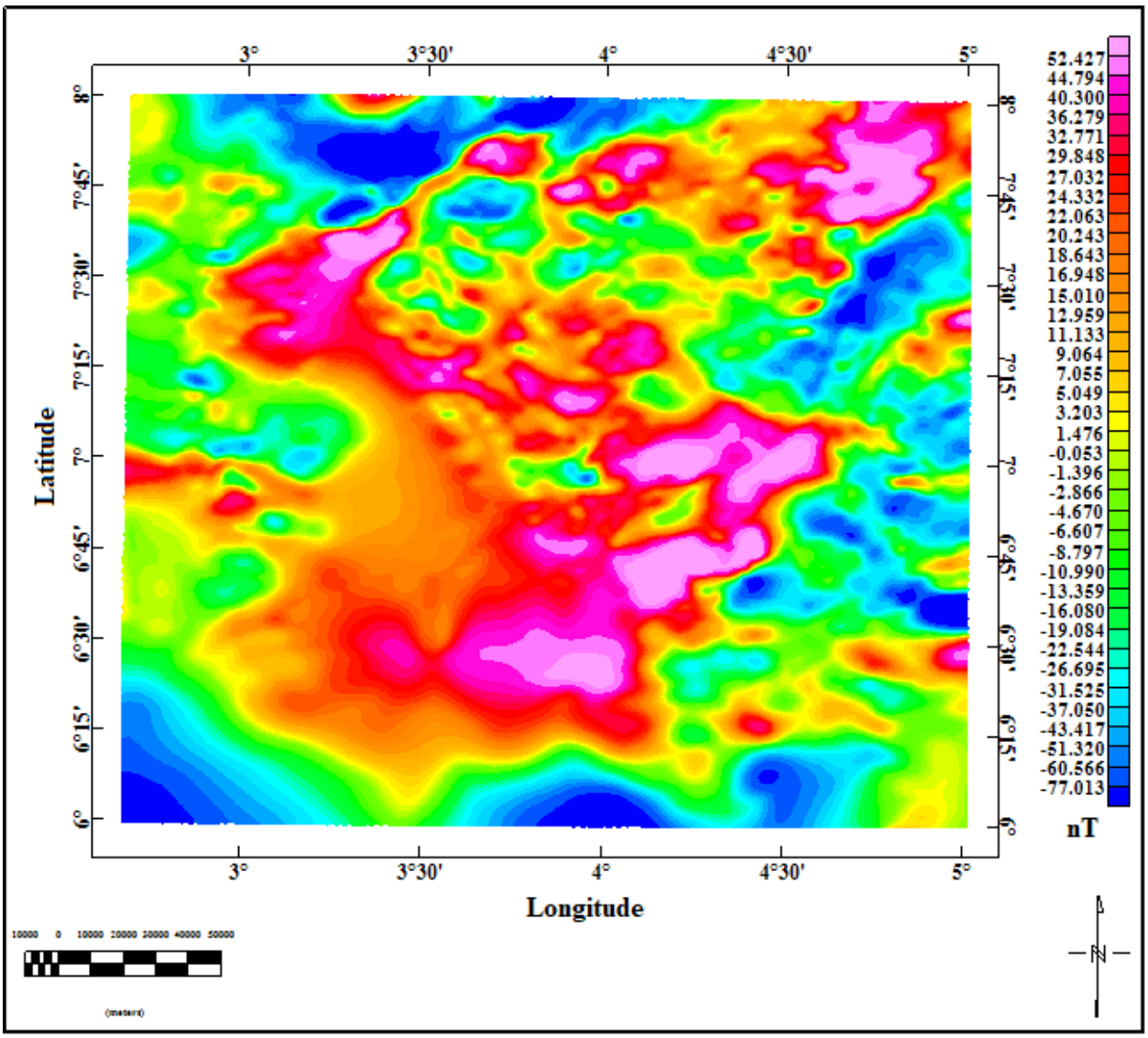


Fig. 3.6a: Residual magnetic field intensity map of the study area upward continued to a height of 2000 m.

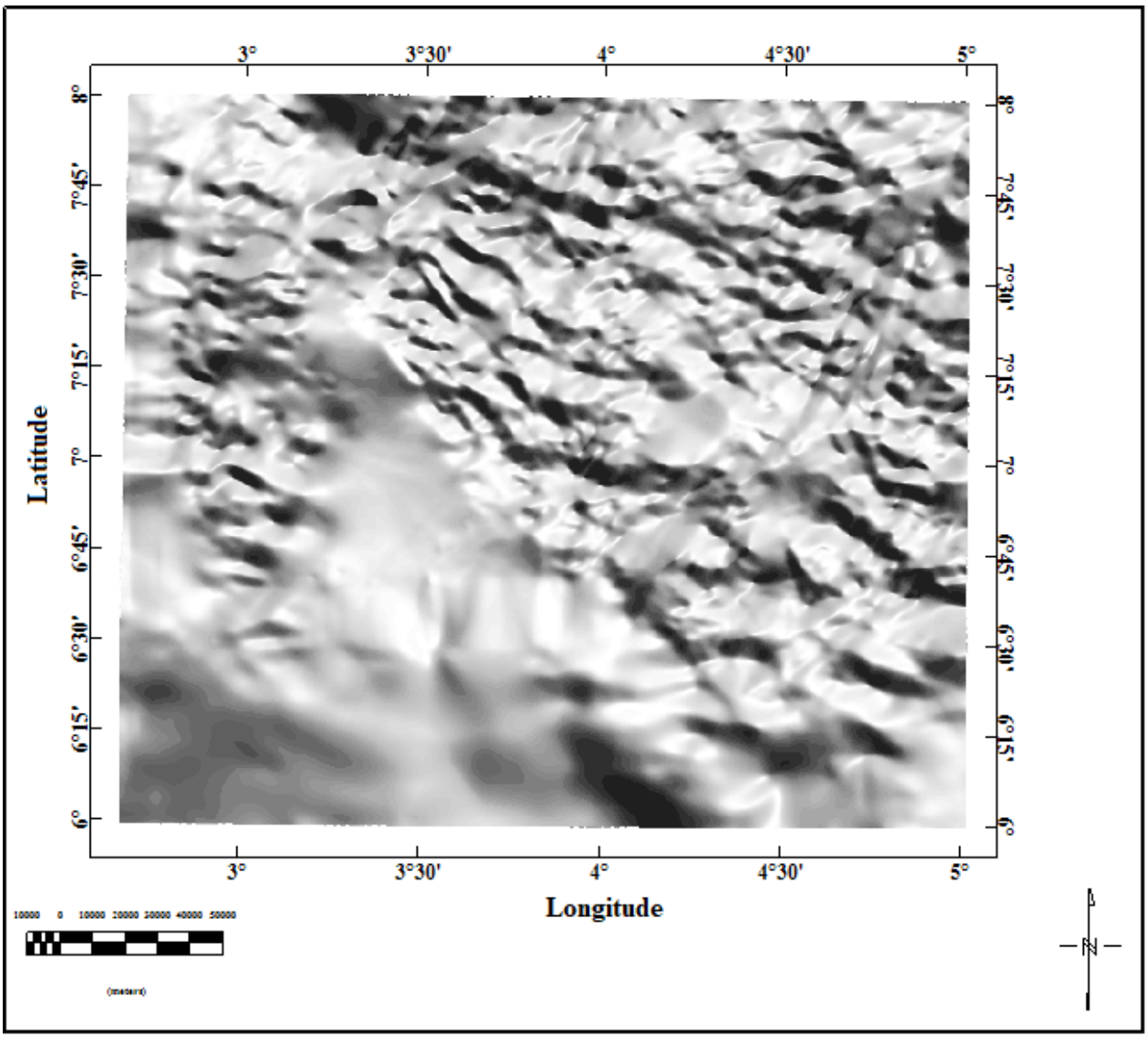


Fig. 3.6b: Shaded relief map of the upward continued residual magnetic field intensity of the study area.

CHAPTER FOUR

RESULTS AND INTERPRETATION

4.1 Vertical derivatives

This is a technique that uses potential field derivatives to suppress deep-seated long wavelength anomalies to enhance field component that are associated with shallow features. It also resolves interference between adjacent anomalies. Mostly used for delineating near surface lineaments and contacts (Tarlowski *et al*., 1997). The first vertical derivative or vertical gradient (FVD) can be thought of as component of the rate of change of the anomaly values as the potential-field data are upward continued. The first vertical derivative of the total magnetic field anomaly map is shown in Figs. 4.1a and 4.1b.

The second vertical derivative is the vertical gradient of the first vertical derivative. First vertical derivative data have become almost an important tool in magnetic interpretations. Second vertical derivative has even more resolving power than the first vertical derivative, but its application requires high quality data because of its greater enhancement of noise (Figs. 4.1c, 4.1d and 4.1e). It was shown by Hood and McClure (1965) that second vertical derivative is zero and rapidly changes sign at a point vertically over a contact. In magnetic data interpretation, second vertical derivatives are used to delineate the plain-view boundaries of intra-basement anomaly sources and are also found to be effective for enhancement of magnetic anomalies (Sharma, 2002). The zero-point (of the second vertical derivative) of the image map indicates the spatial locations of the magnetic source edges which in effect outline anomalous areas.

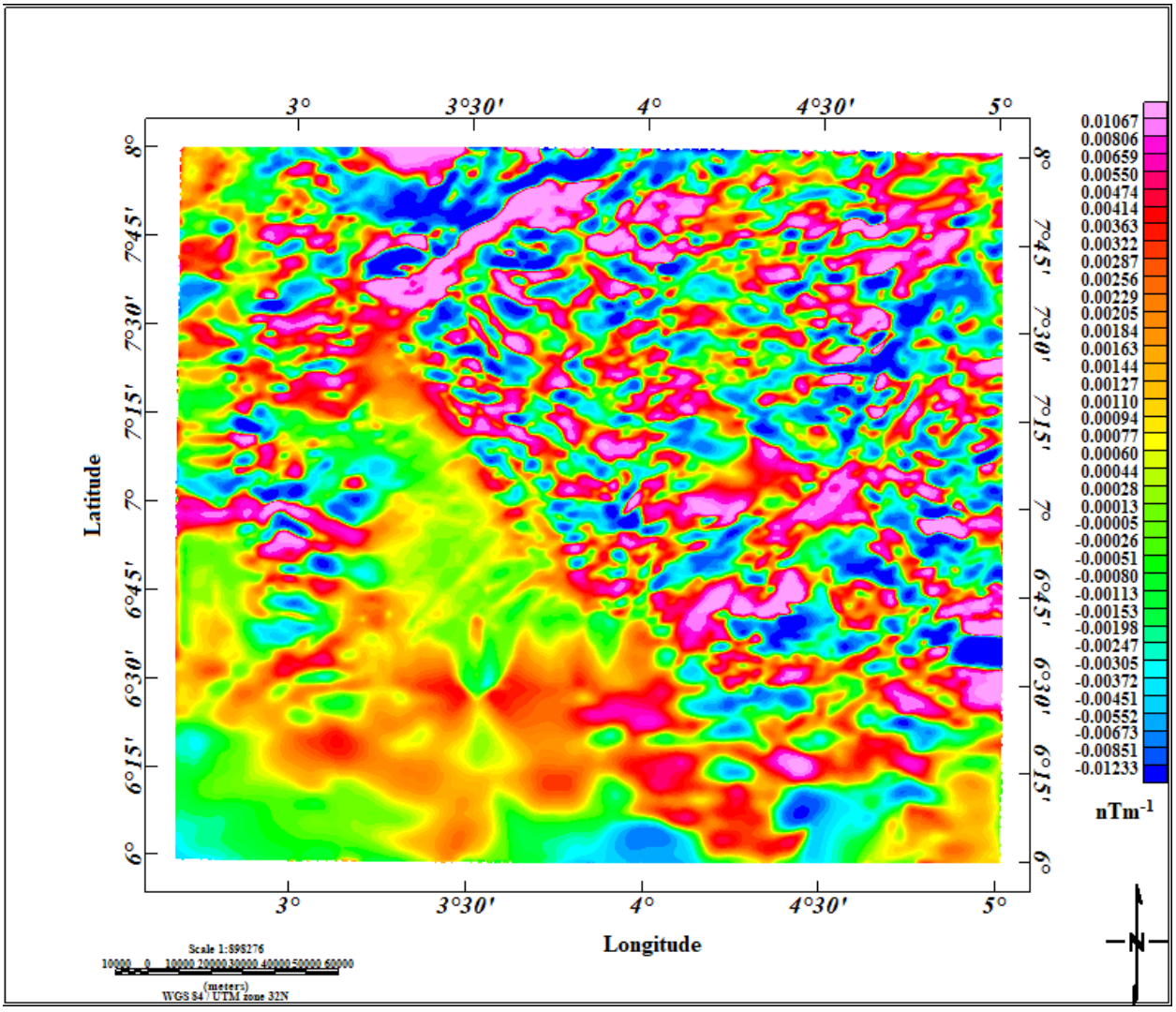


Fig. 4.1a: First vertical derivative map of the study area.

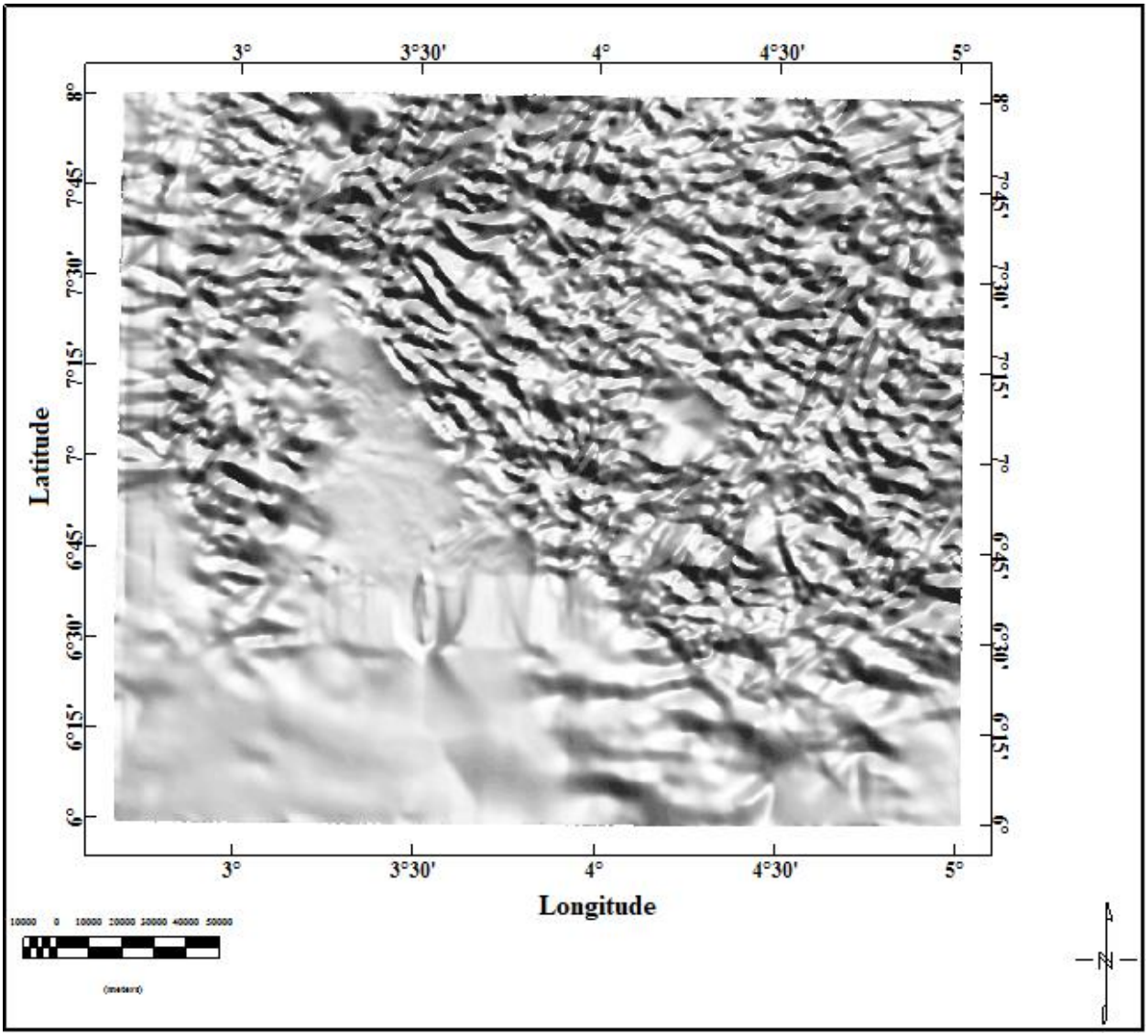


Fig. 4.1b: Shaded relief map of the first vertical derivative of the study area.

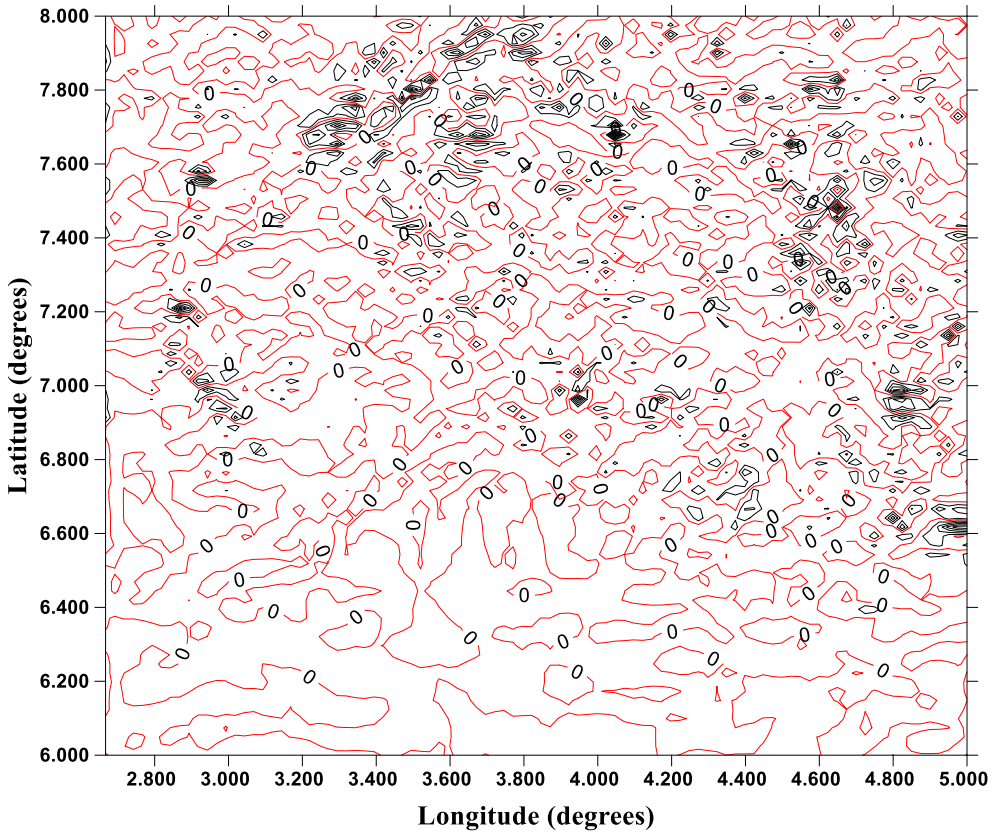


Fig. 4.1c: Contour map of the second vertical derivative of the study area.

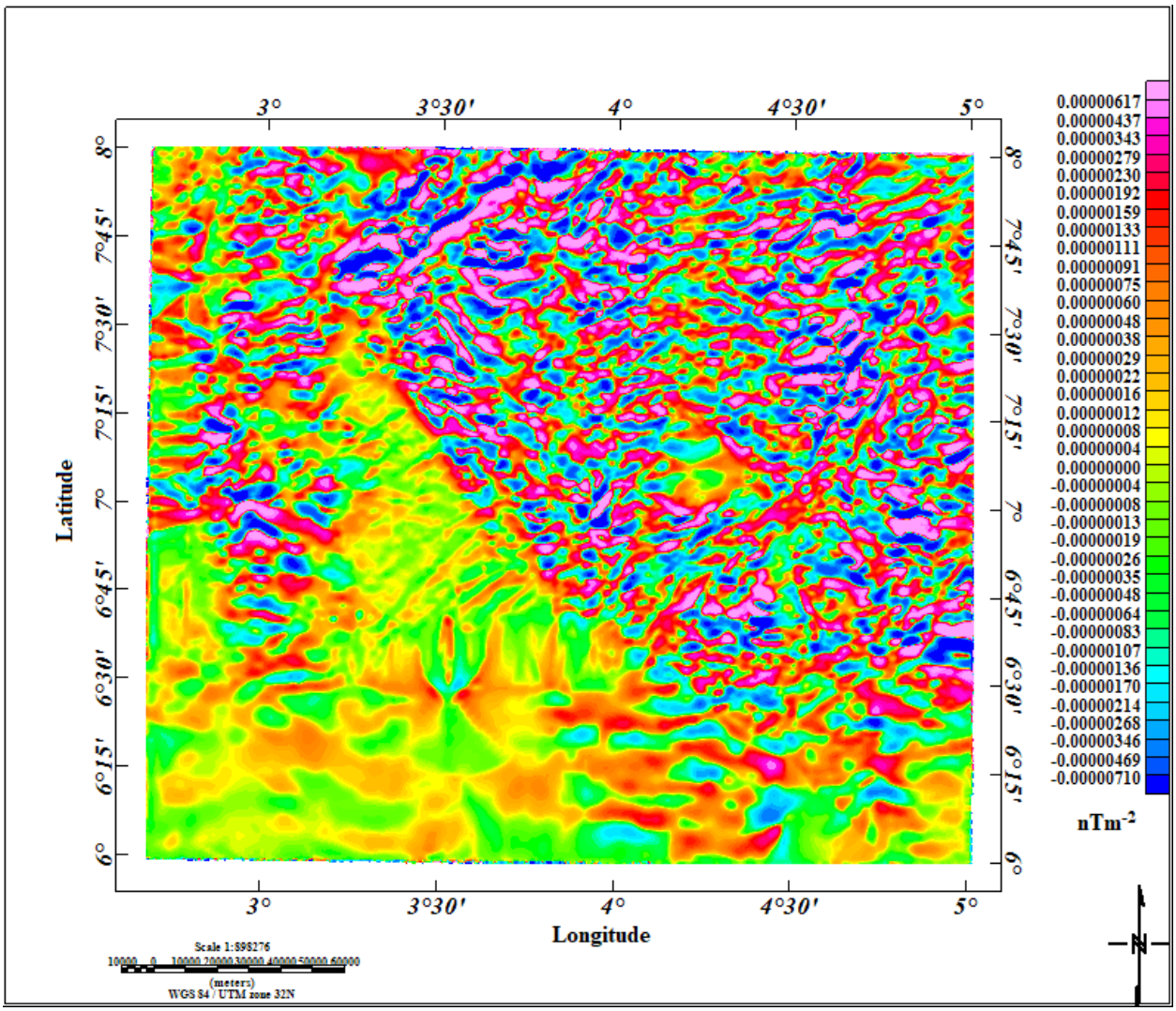


Fig. 4.1d: Second vertical derivative map of the study area.

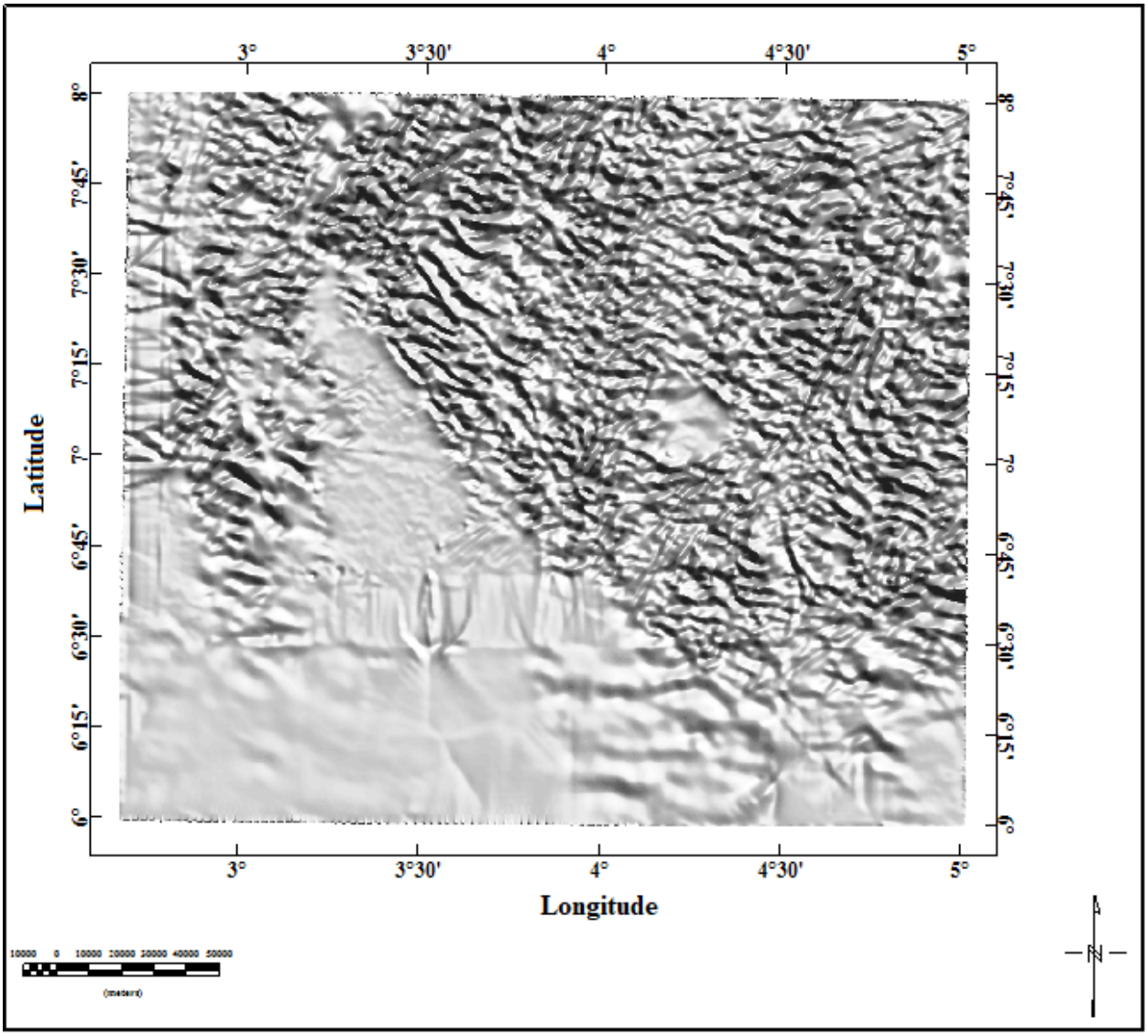


Fig. 4.1e: Shaded relief map of the second vertical derivative of the study area.

4.2 Total horizontal derivative

After the upward continuation correction of aeromagnetic data, a magnetic body is spatially more directly associated with the related magnetic response. Total horizontal derivative was employed because it enhances shallow anomalies in data, making it an important tool for outlining edges of magnetic basement blocks and faults or other magnetic bodies, in addition it also highlights linear features related to contacts, in the data set (Milligan and Gunn, 1997). The total horizontal

derivative (THDR) defined by Equation (3.15) was applied to the total magnetic field anomaly (residual field data upward continued to 2000 m) data (m) to produce the total horizontal derivative maps (Fig. 4.2a and 4.2b). Horizontal-gradient maxima occur over the steepest parts of potential-field anomalies, and minima over the flattest parts. It was reported that the bodies are delineated by maxima, while the centres are indicated by minima (Cordell and Grauch, 1985).

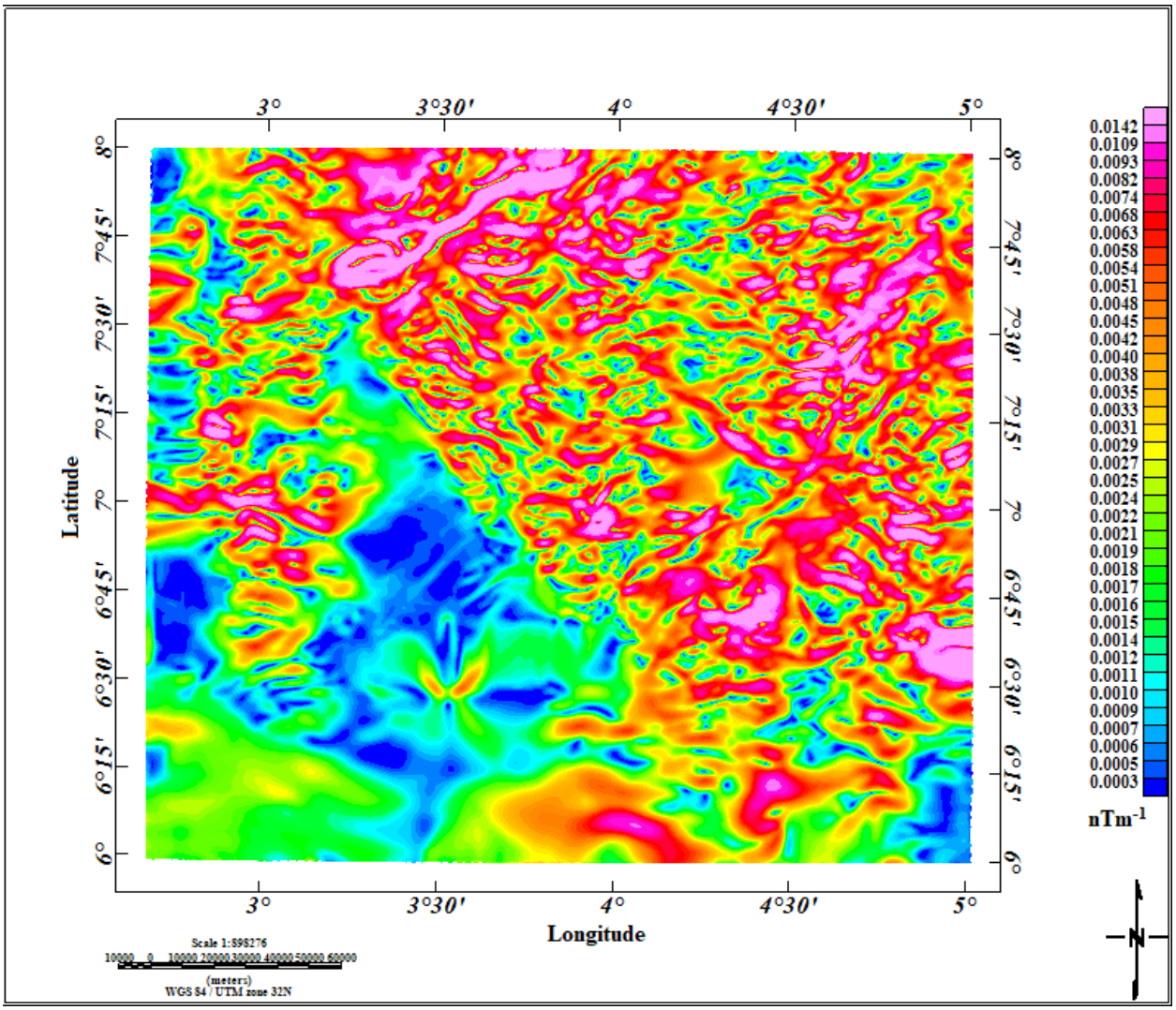


Fig. 4.2a: Total horizontal derivative map of the study area.

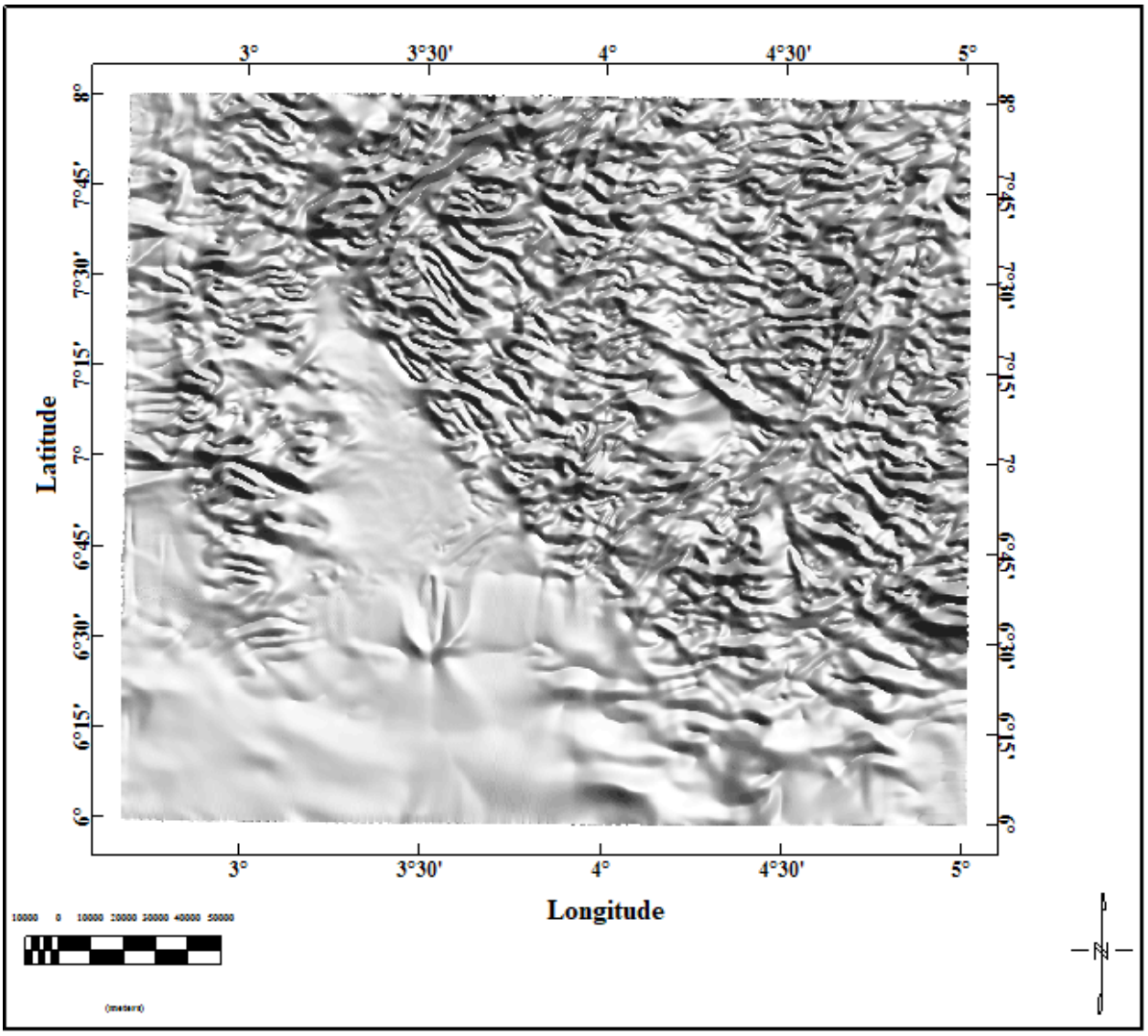


Fig. 4.2b: Shaded relief map of the total horizontal derivative of the study area.

4.3 Analytic signal

The analytic signal or total gradient is formed through the combination of the horizontal and vertical gradients of the magnetic anomaly. It is based on the calculation of the first derivatives of magnetic anomalies to estimate source characteristics. This is a filter applied to magnetic data and

is aimed at simplifying the fact that magnetic bodies usually have a positive and negative peak associated with it, which in many cases make it difficult to determine the exact location of the causal body.

The analytic signal has a form over causative body that depends on the locations of the body (horizontal coordinate and depth) but not on its magnetization direction (Ansari and Alamdar, 2009). The amplitude of analytical signal was first developed by Nabighian (1972) in 2-dimensions and later extended to 3-dimensions (Nabighian, 1984 and Roest *et al*., 1992). Defined by Equation (3.21), the analytical signal modulus (ASM) was applied to the total magnetic field anomaly (residual field data upward continued to 2000 m) data to produce the maps (Fig. 4.3a and 4.3b). This enhancement approach has been widely used as a tool in outlining geologic boundaries such as contacts and faults regardless of direction of magnetization.

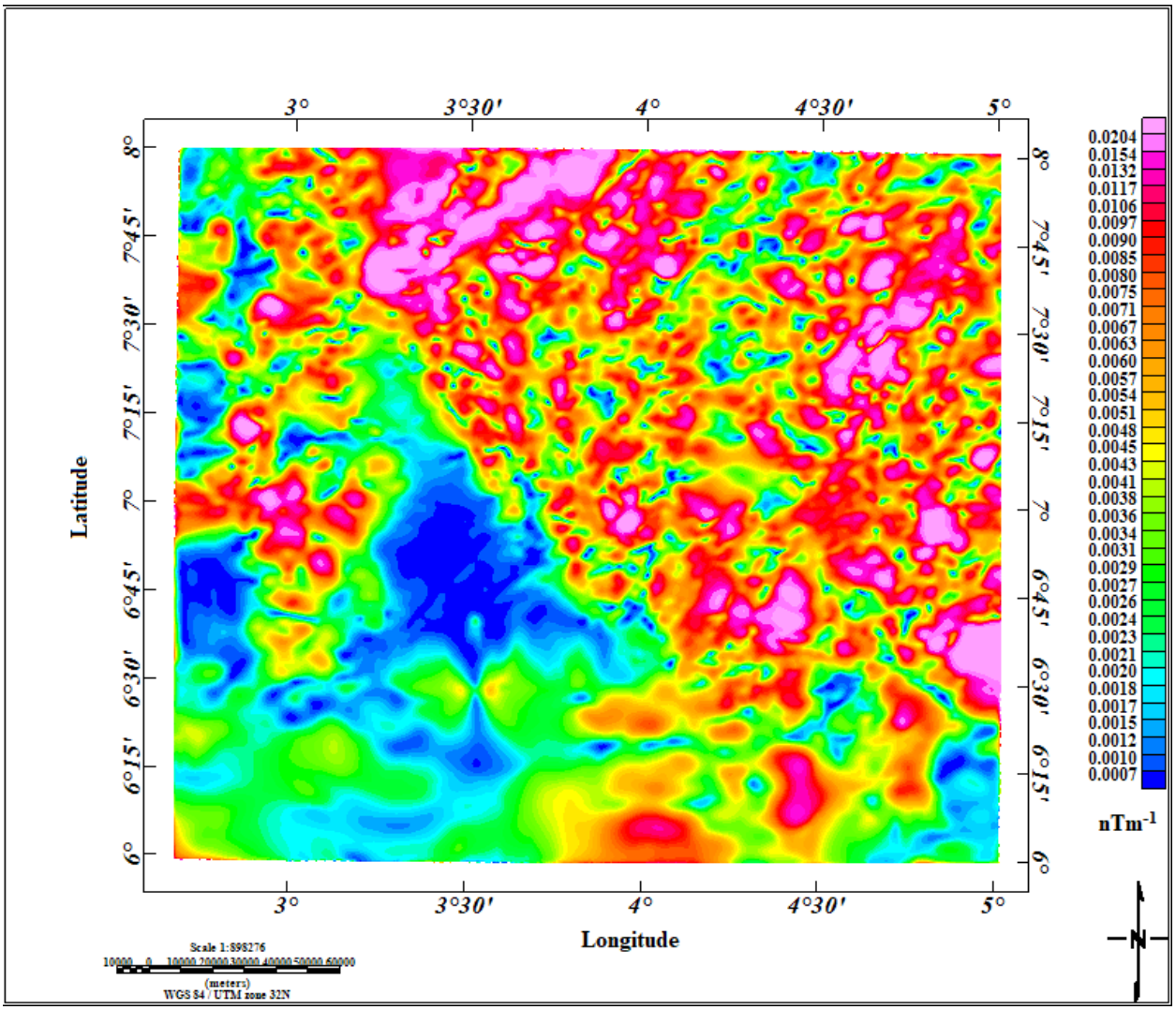


Fig. 4.3a: Analytic signal map of the study area.

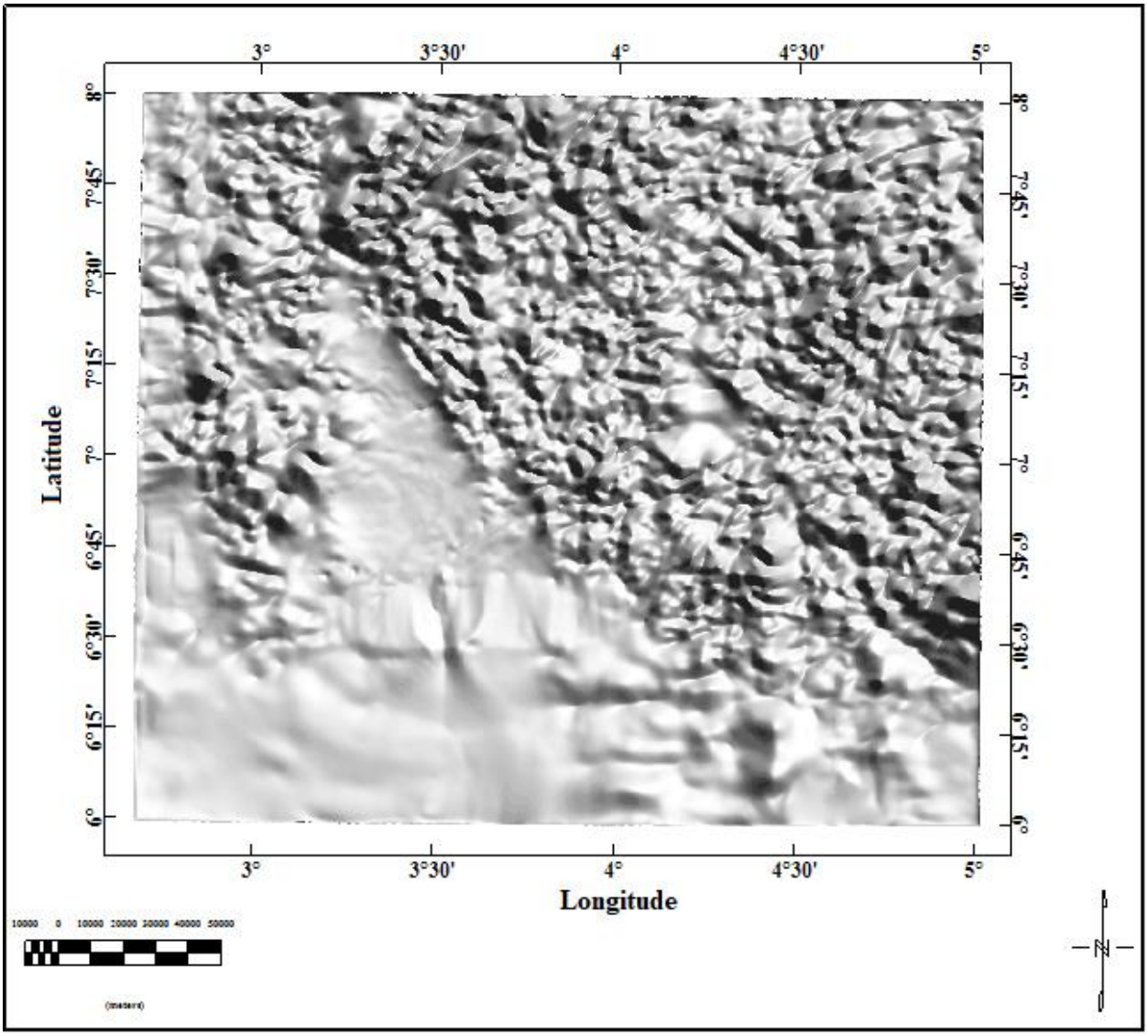


Fig. 4.3b: Shaded relief map of the analytic signal of the study area.

4.4 Tilt derivatives

Tilt derivative and horizontal derivative of the tilt derivative of a magnetic data can help in determining the magnetic source shape, continuity and geologic edges. Both techniques excel in their ability to map subtle basement features.

These techniques are more effective than their contemporary vertical derivatives because they can effectively discriminate between signal and noise in the data and normalize magnetic anomaly amplitude. Tilt derivative acts like an automatic-gain control (AGC) because, unlike other magnetic derivatives whose amplitude responses are linked to the total magnetic intensity amplitude (amplitude fall-off with depth), tilt derivative is independent of the total magnetic intensity's amplitude. It depends on the ratio between vertical derivative and the absolute value of the horizontal derivative, and the reciprocal of the source depth. Thus, it does not depend on its amplitude for resolution (Verduzco *et al*., 2004). That means that subtle basement features will have amplified amplitude and therefore will be enhanced as much as already amplified features. Tilt derivative also has an advantage of responding well to both shallow and deep sources, and the zero value of the tilt derivative is near the edges of the anomaly body. Defined by Equation (3.24), the nature of the arc tan trigonometric function make all amplitudes to be restricted to values between $+\pi/2$ and $-\pi/2$ (+90° and -90°) regardless of the amplitudes of the vertical derivative or total horizontal derivative.

The tilt derivative (TDR) defined by Equation (3.24) was applied to the residual magnetic field data upward continued to 2000 m to produce maps (Fig. 4.4a and 4.4b).

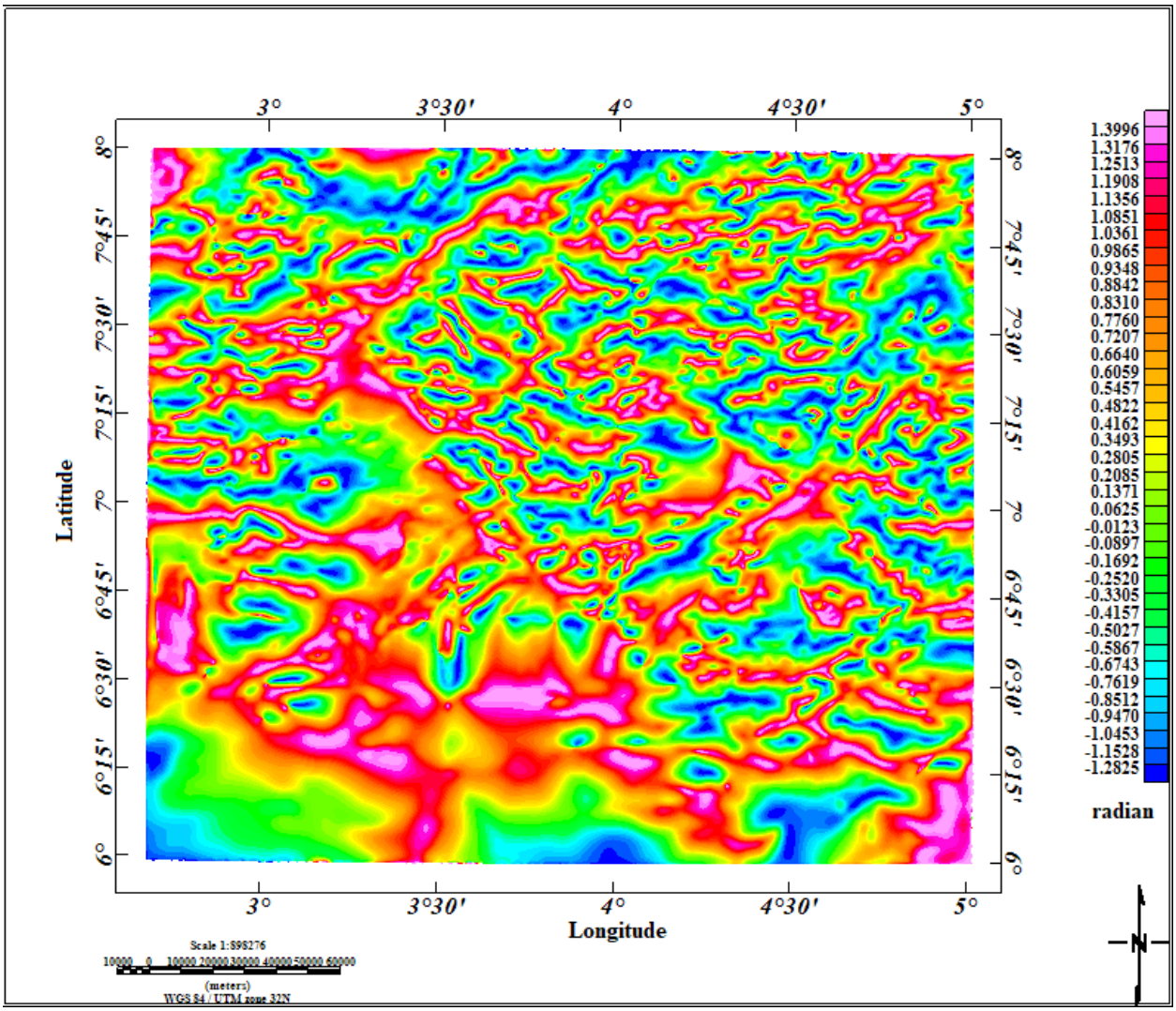


Fig. 4.4a: Tilt derivative map of the study area.

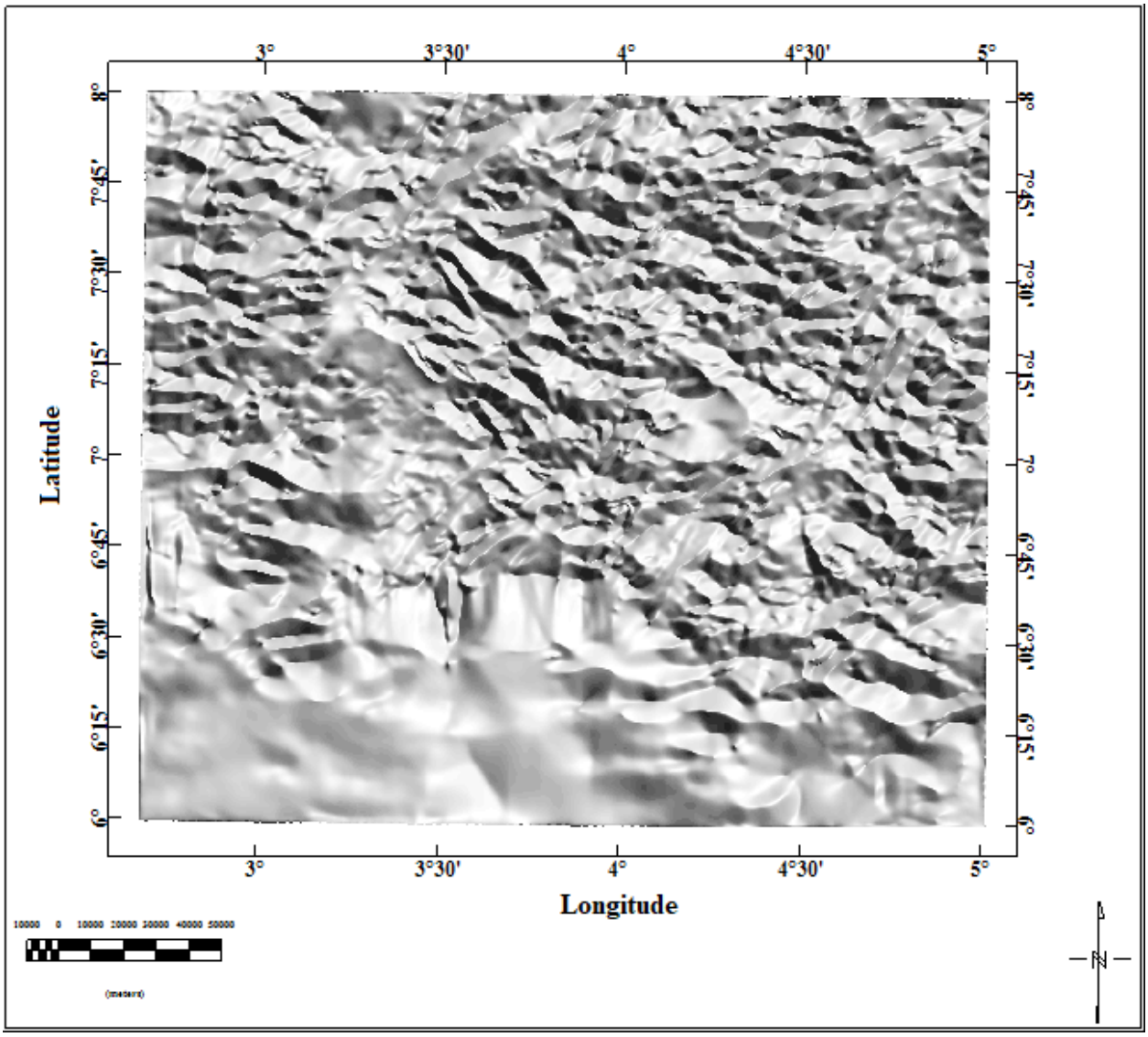


Fig. 4.4b: Shaded relief map of the tilt derivative of the study area.

The total horizontal derivative of tilt derivative defined by Equation (3.27) for a grid are equivalent to the absolute value of the local wave number. The total horizontal derivative of the tilt angle technique, proposed by Verduzco *et al*. (2004), is independent of the magnetic inclination and intensity, besides enhancing and centralizing the maximum amplitudes over the source limits. Such attributes are of the highest relevance for the qualitative interpretation of potential field data. However, it is also noted that the anomaly amplitudes are attenuated with the models' depths,

besides the profusion of noises, hindering the structural interpretation (Bongiolo and Ferreira, 2012). The total horizontal derivative of the tilt angle of the filtered aeromagnetic data were computed and maps were subsequently plotted (Fig. 4.4c and 4.4d).

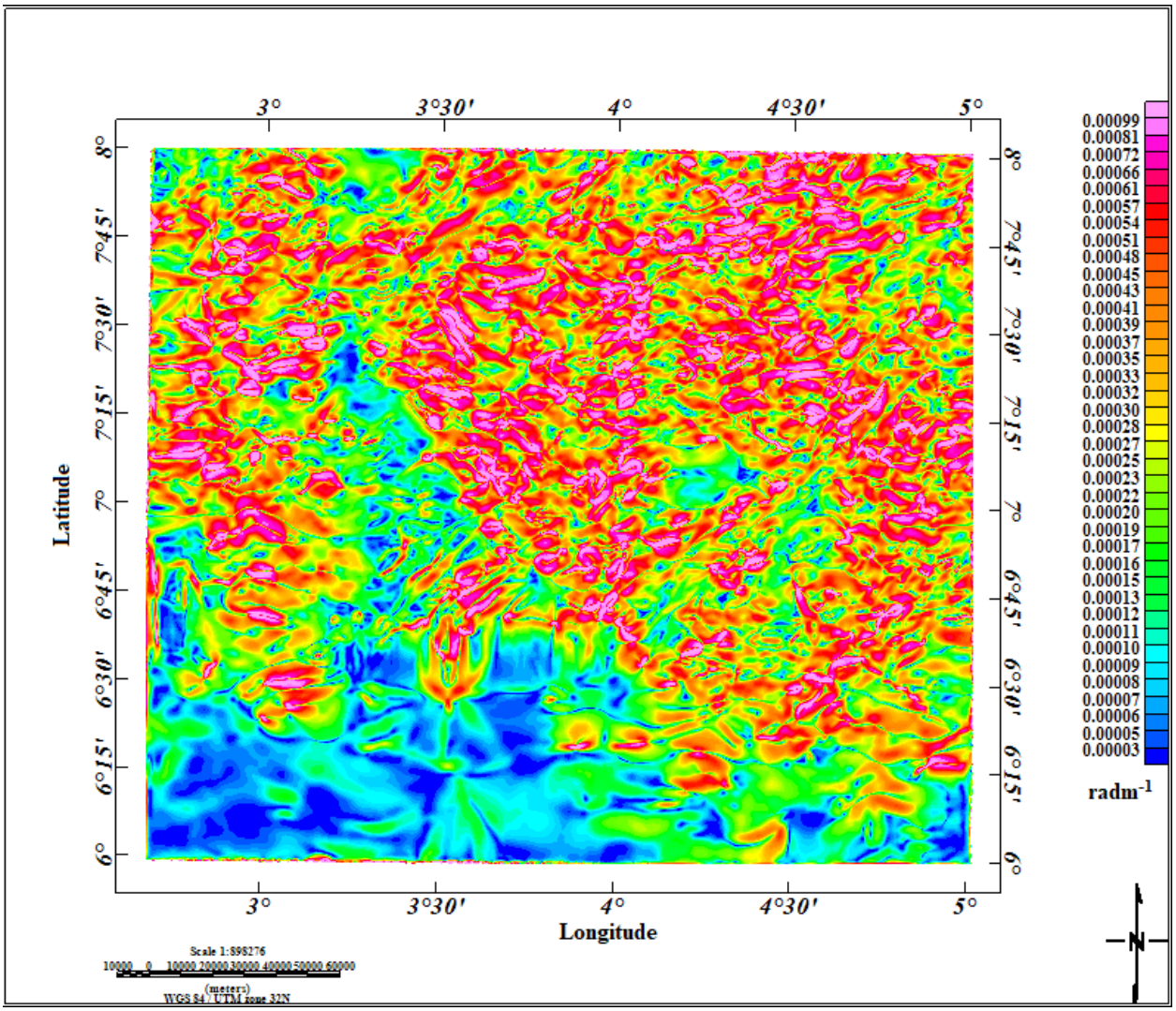


Fig. 4.4c: Total horizontal derivative of the tilt angle map of the study area.

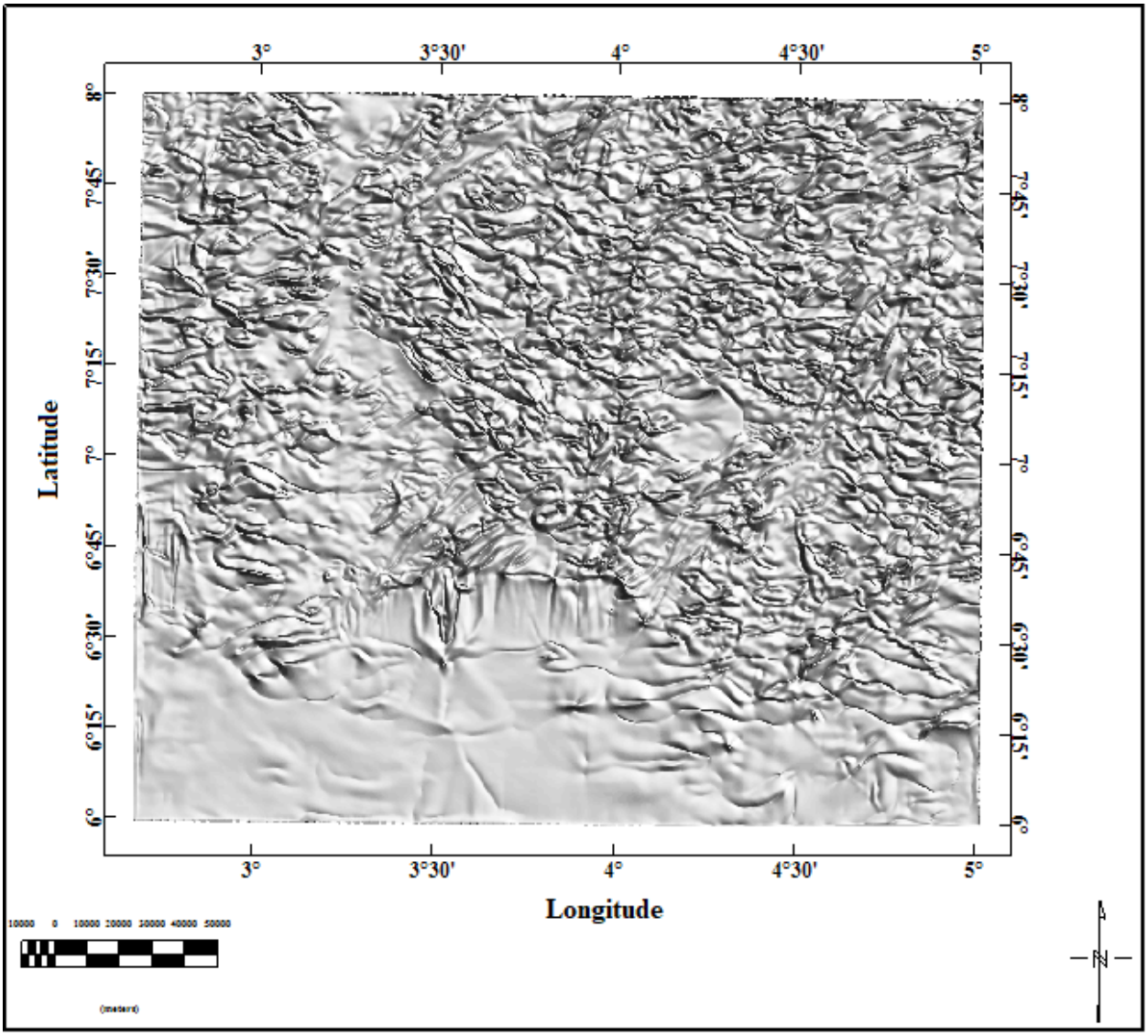


Fig. 4.4d: Shaded relief map of the total horizontal derivative of the tilt angle of the study area.

4.5 Theta angle map

Theta angle defined by Equation (3.28) is the ratio of the magnitudes of the total horizontal gradient to the analytic signal amplitude, so that the theta map may also be thought of as a normalization of the horizontal gradient. This normalization introduces an effective gain control, such that amplitude information is lost, but low-amplitude features are highlighted in a manner similar to automatic gain control (Wijns *et al.*, 2005).

Wijns *et al*. (2005) proposed the theta map, which uses the amplitude of the analytic signal to normalize the total horizontal derivative. It can be considered an image of either the cosine of the angle between the analytic signal and the horizontal, or the normalized horizontal gradient of total magnetic intensity.

The theta map is a simple and effective processing tool for delineating magnetic contacts, it also affords the possibility of discriminating between vertical and dipping contacts (Wijns *et al*., 2005). It also displays the edges of the shallow and deep bodies simultaneously (Li, 2013).

The theta angles of the filtered aeromagnetic data were computed and the maps were subsequently plotted (Fig. 4.5a and 4.5b).

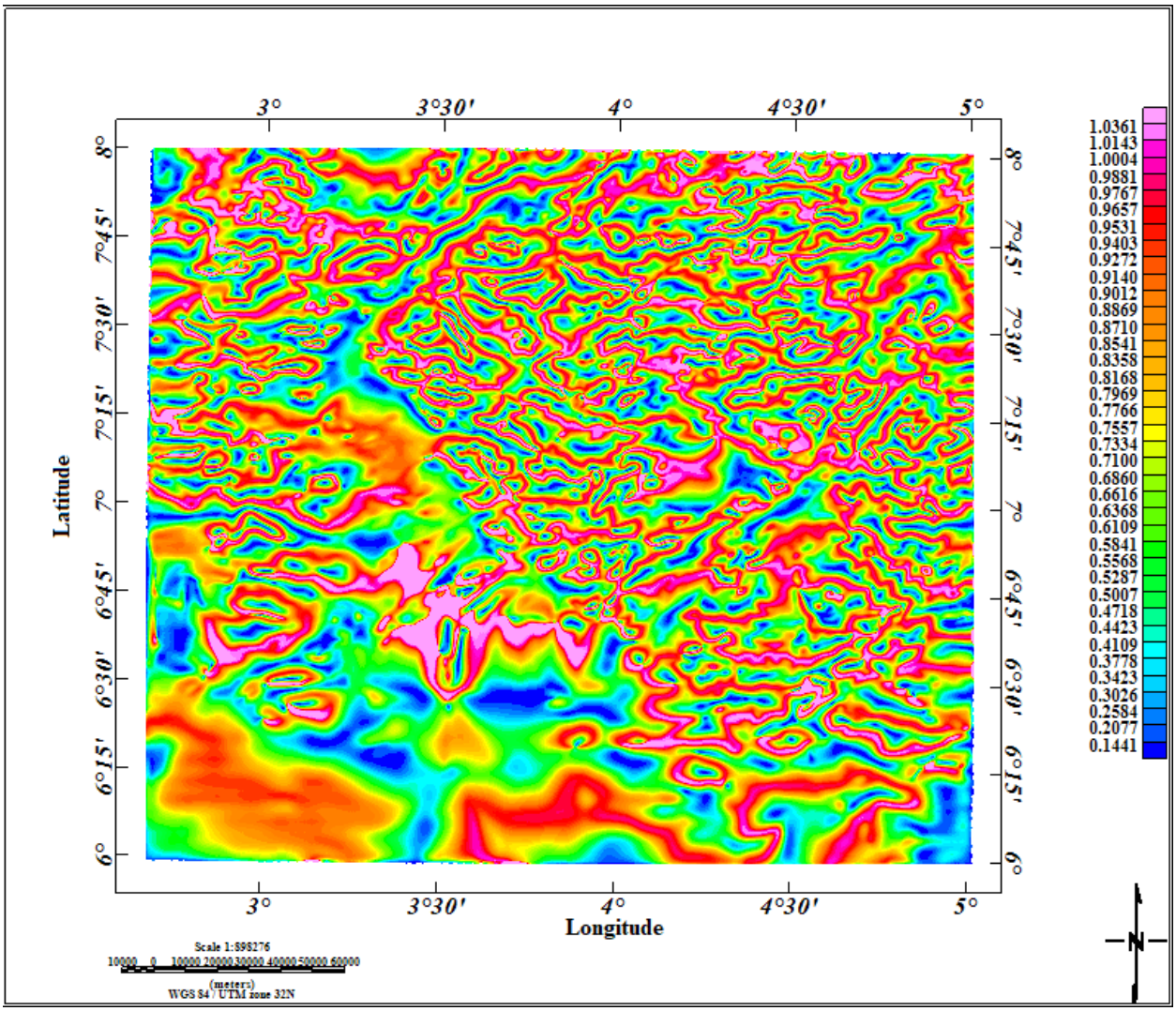


Fig. 4.5a: Theta angle map of the study area.

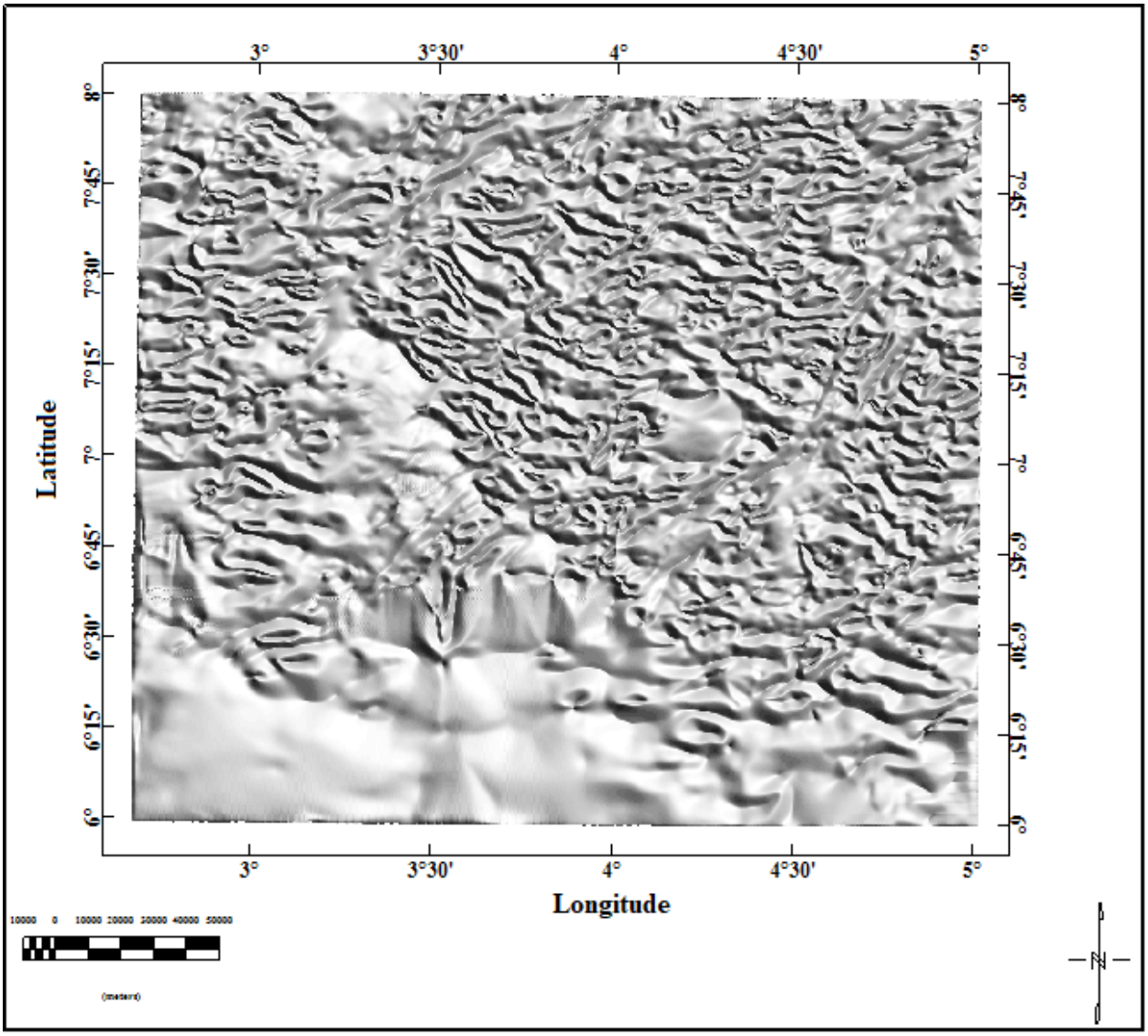


Fig. 4.5b: Shaded relief map of the theta angle of the study area.

4.6 Euler deconvolution

Euler's homogeneity relation has attracted sporadic interest from geophysicists over the years because it serves as a fast means of processing a magnetic grid to derive trends and depth estimates in an automatic or semiautomatic manner (Reid *et al.*, 1990). Thompson (1982) suggests that a 3-D implementation of EULDPH algorithm could be used to analyse mapped magnetic data. This methodology utilizes the total potential field and its related gradients (X, Y, and Z components) to

derive the rate of change of potential field with respect to distance from the source location and depth. The degree of homogeneity of the rate of change of the three gradient components is directly related to geometry of the source body and is commonly referred to as the structural index (Thompson, 1982).

Processed aeromagnetic data were subjected to Euler's deconvolution operation to determine depths to magnetic sources as done by Thompson (1982); Reid *et al*. (1990); Mushayandebvu *et al*. (2001) and Hsu *et al*. (2002). The standard Euler deconvolution method was employed. The standard method examined all grid locations and retained only those locations with valid solutions. Results of the standard Euler deconvolution method were compared and the closest solution to the geologic model was accepted.

Filtered aeromagnetic data (residual magnetic field data upward continued to 2000 m) were used as the starting grid for the Euler deconvolution because of its relatively high signal to noise ratio. Euler deconvolution processing parameters such as structural index, maximum % depth of tolerance, window size and maximum distance were carefully selected to improve the integrity of the solution results from the study area especially since the depth range between the shallowest source and the deepest source is relatively small. However, Euler deconvolution has been successfully used in Basement Complex environments for mineral exploration and other investigations (Cooper, 2008), as well as used with high degree of precision in near surface investigation for locating unexploded ordinance.

Structural indices values of 0.0 and 1.0 were used based on the assumed geological models of the source to be individual contacts or dykes/sills. The obtained solutions were further refined by using windowing technique in order to reduce uncertainty to the barest minimum (Figs. 4.6a - h).

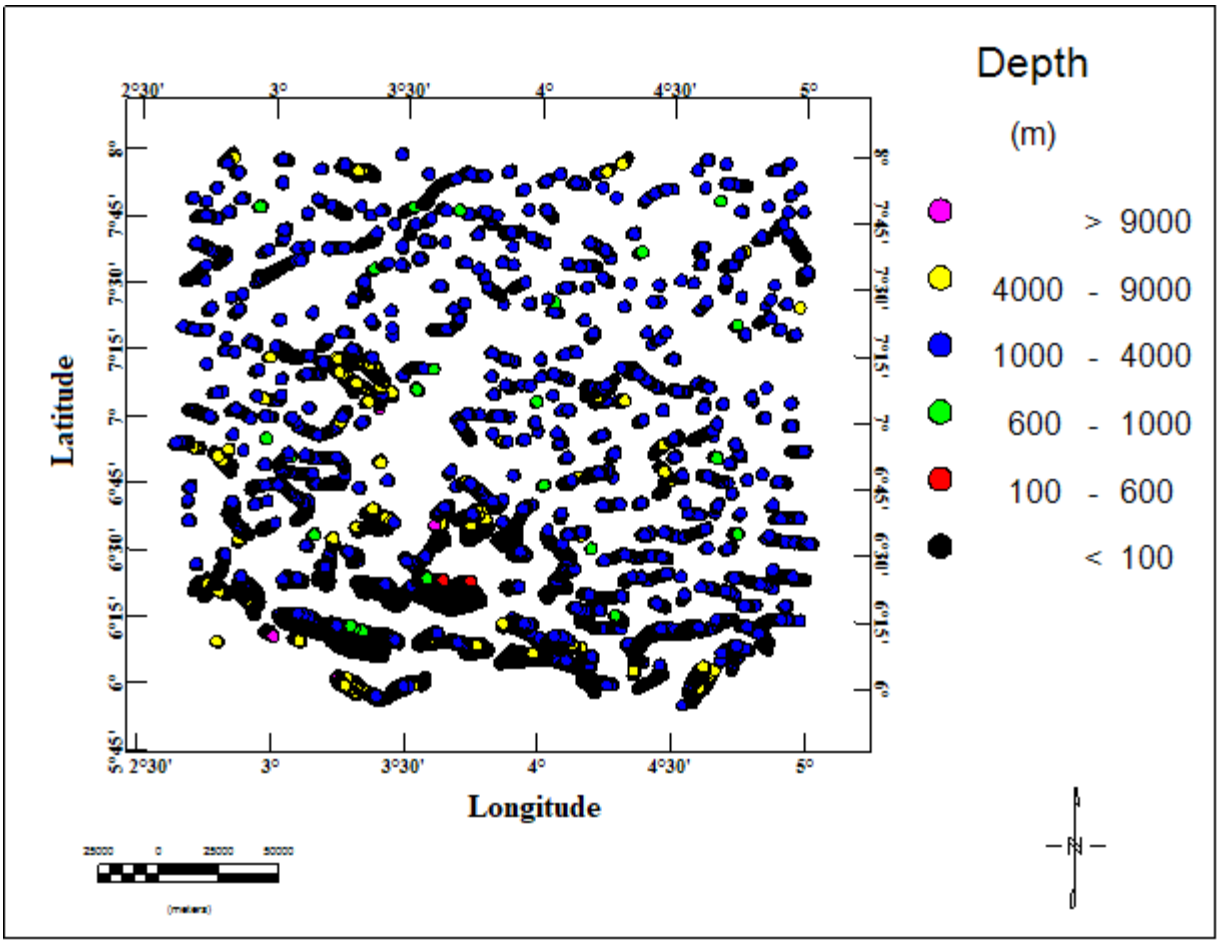


Fig. 4.6a: Euler deconvolution solution plots of the study area (N = 0.0).

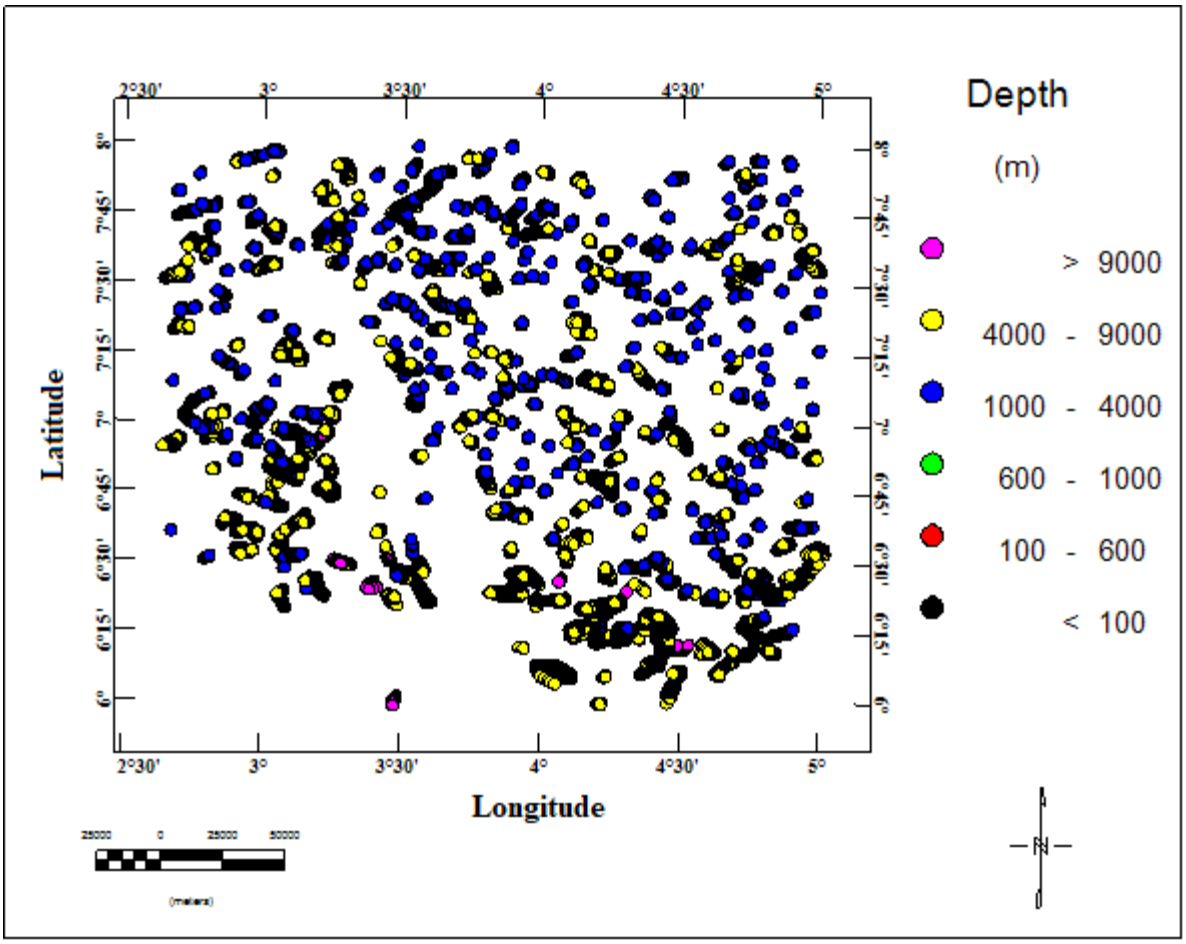


Fig. 4.6b: Euler deconvolution solution plots of the study area (N = 1.0).

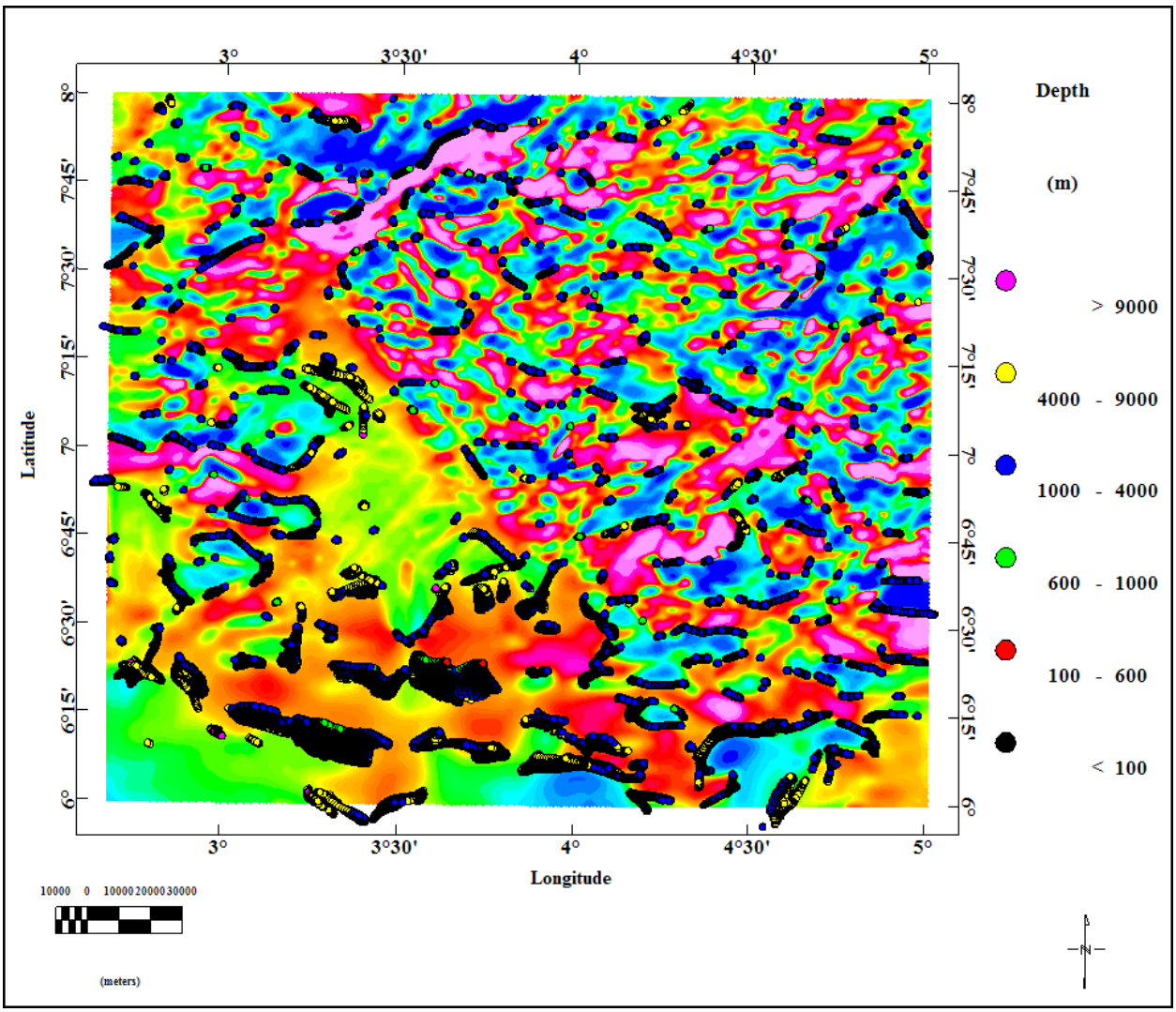


Fig. 4.6c: Euler deconvolution solution plots for contact superimposed on the first vertical derivative map of the study area.

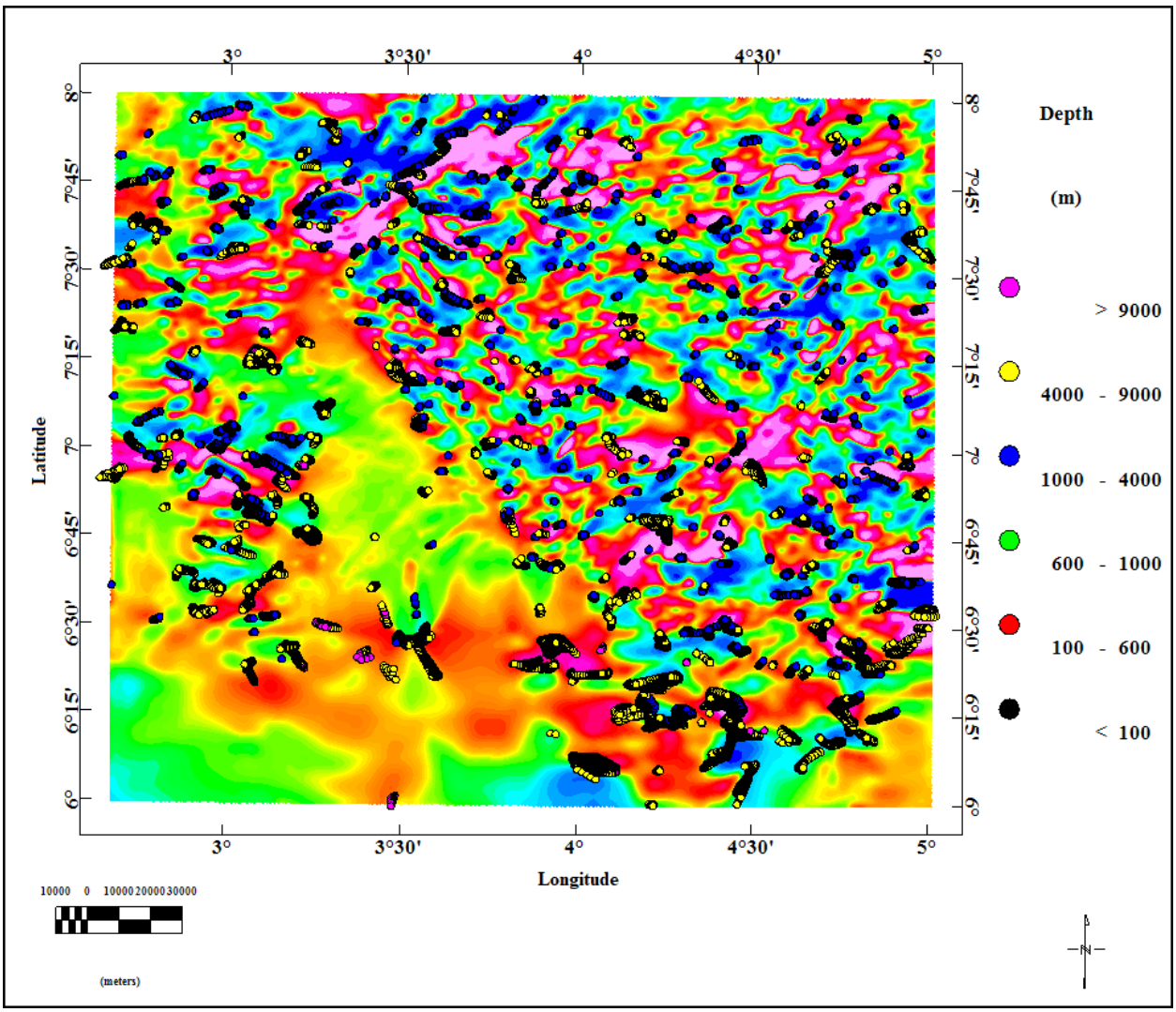


Fig. 4.6d: Euler deconvolution solution plots for dyke/sill superimposed on the first vertical derivative map of the study area.

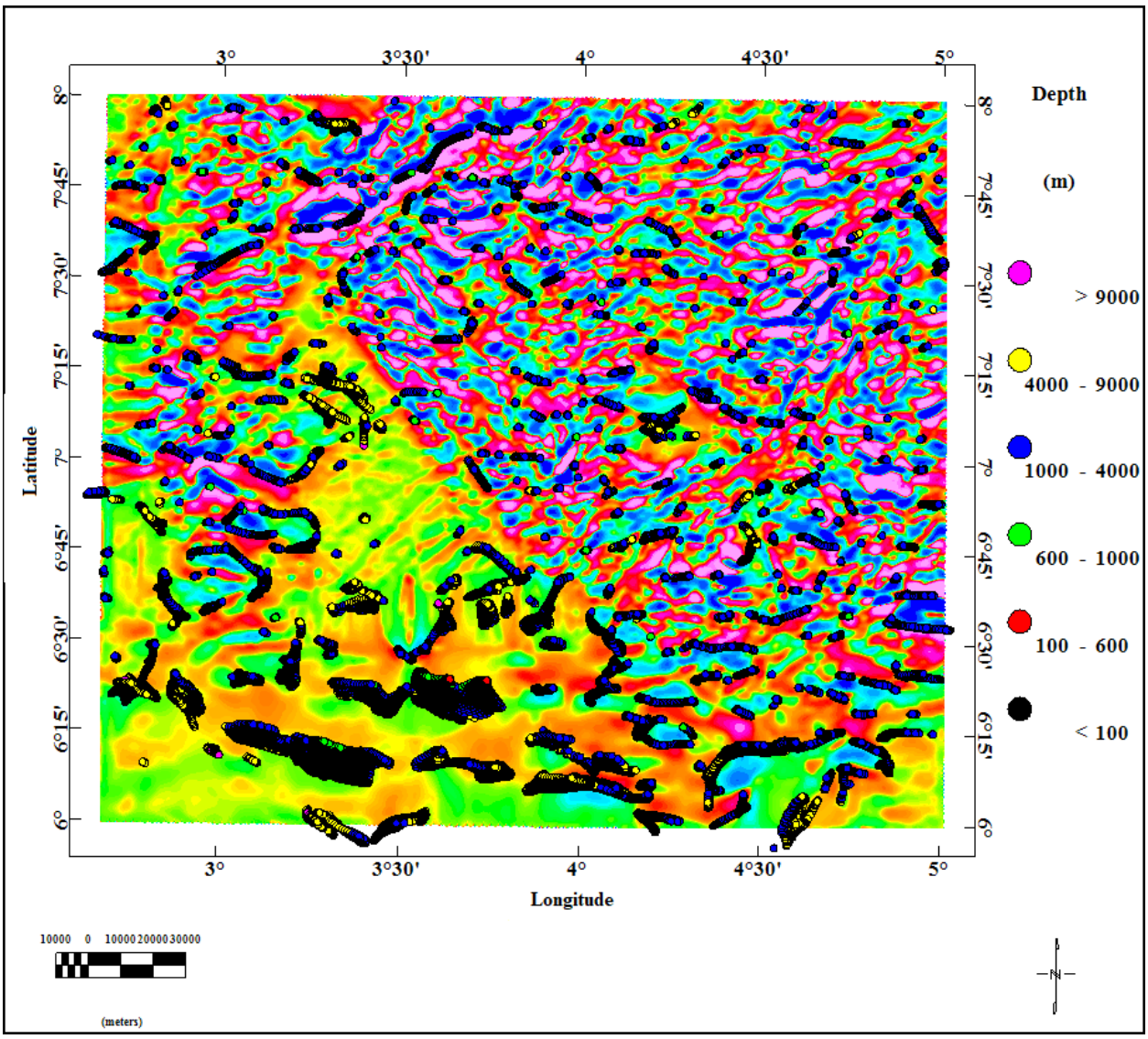


Fig. 4.6e: Euler deconvolution solution plots for contact superimposed on the second vertical derivative map of the study area.

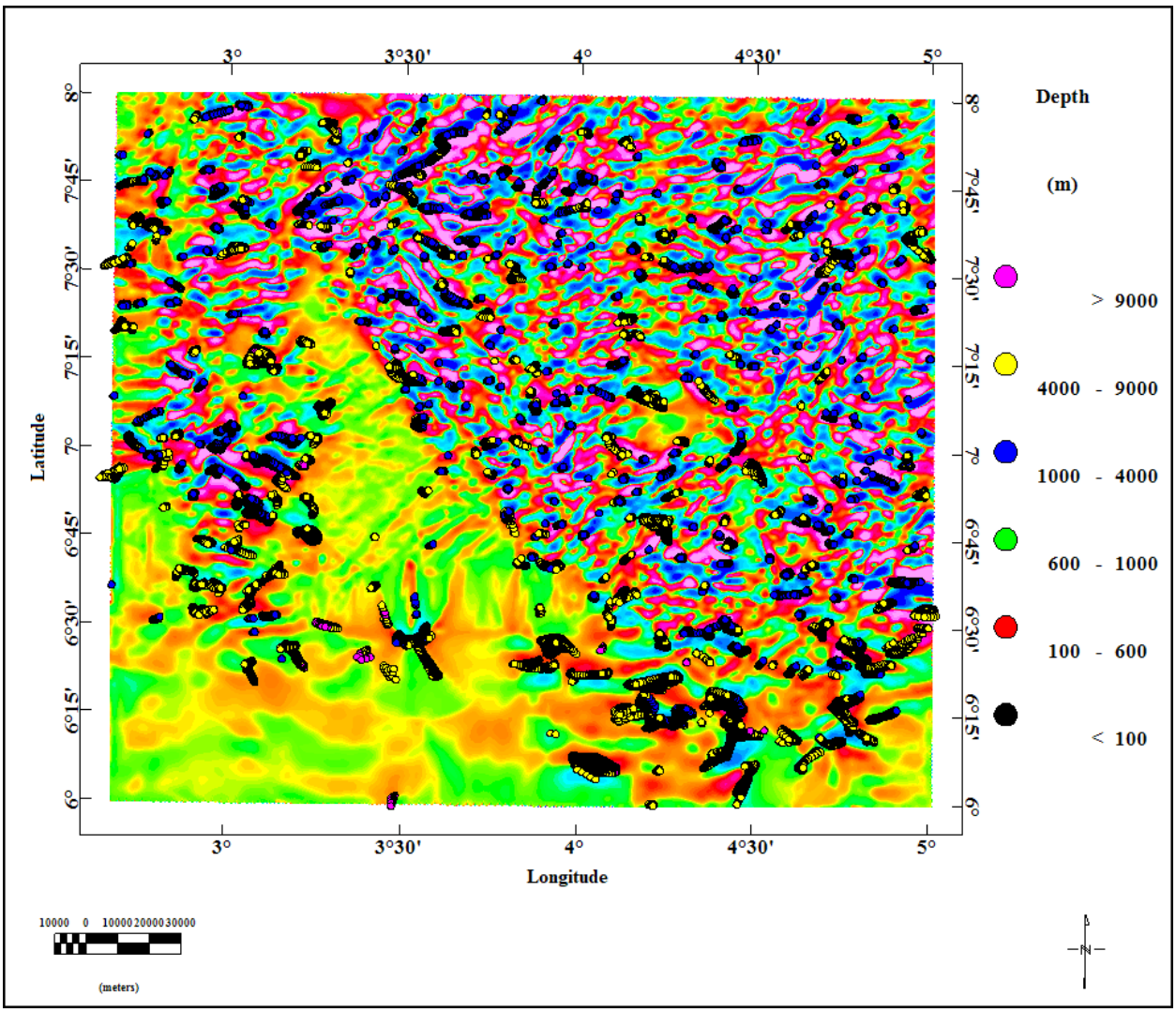


Fig. 4.6f: Euler deconvolution solution plots for dyke/sill superimposed on the second vertical derivative map of the study area.

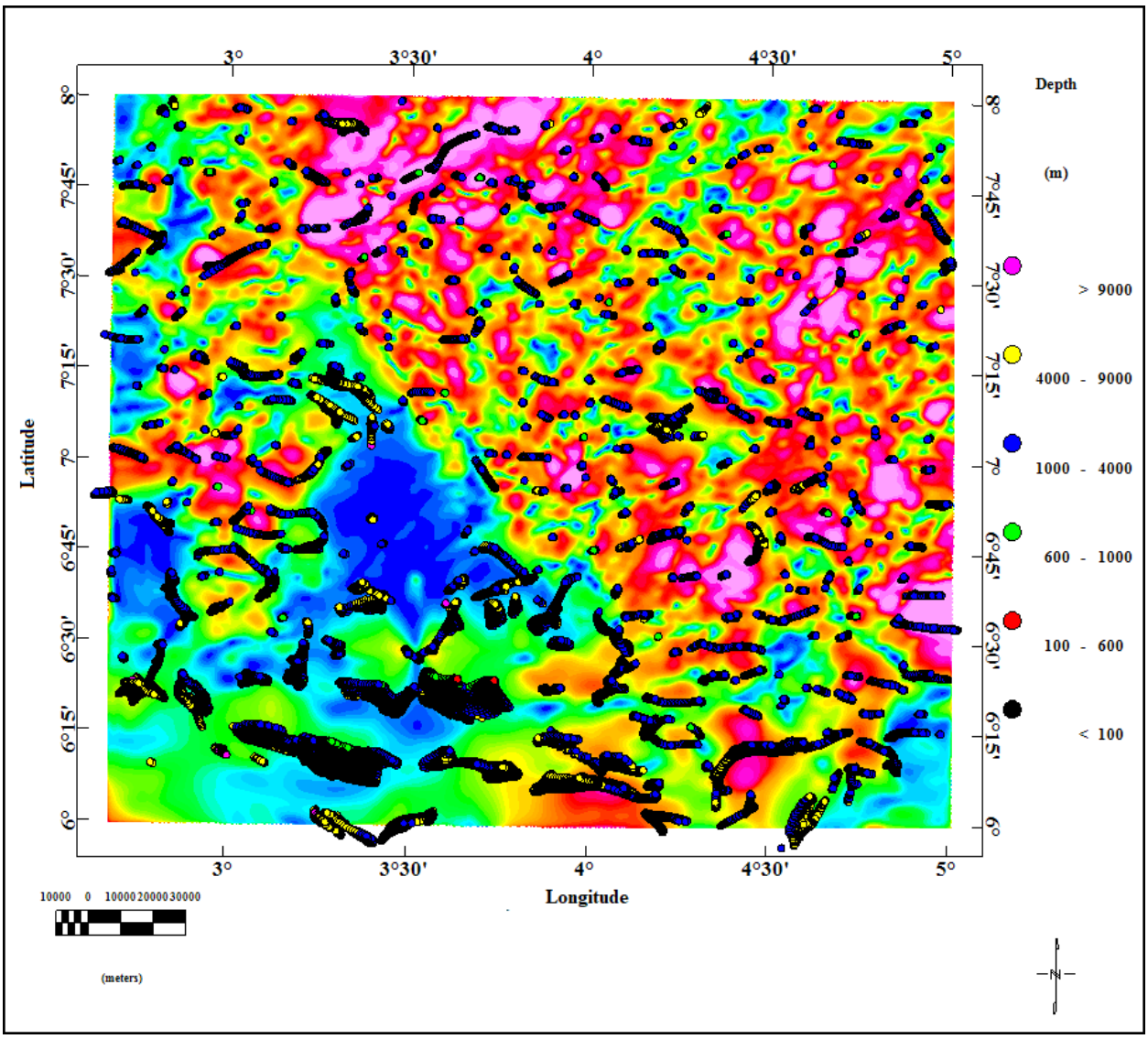


Fig. 4.6g: Euler deconvolution solution plots for contact superimposed on the analytic signal map of the study area.

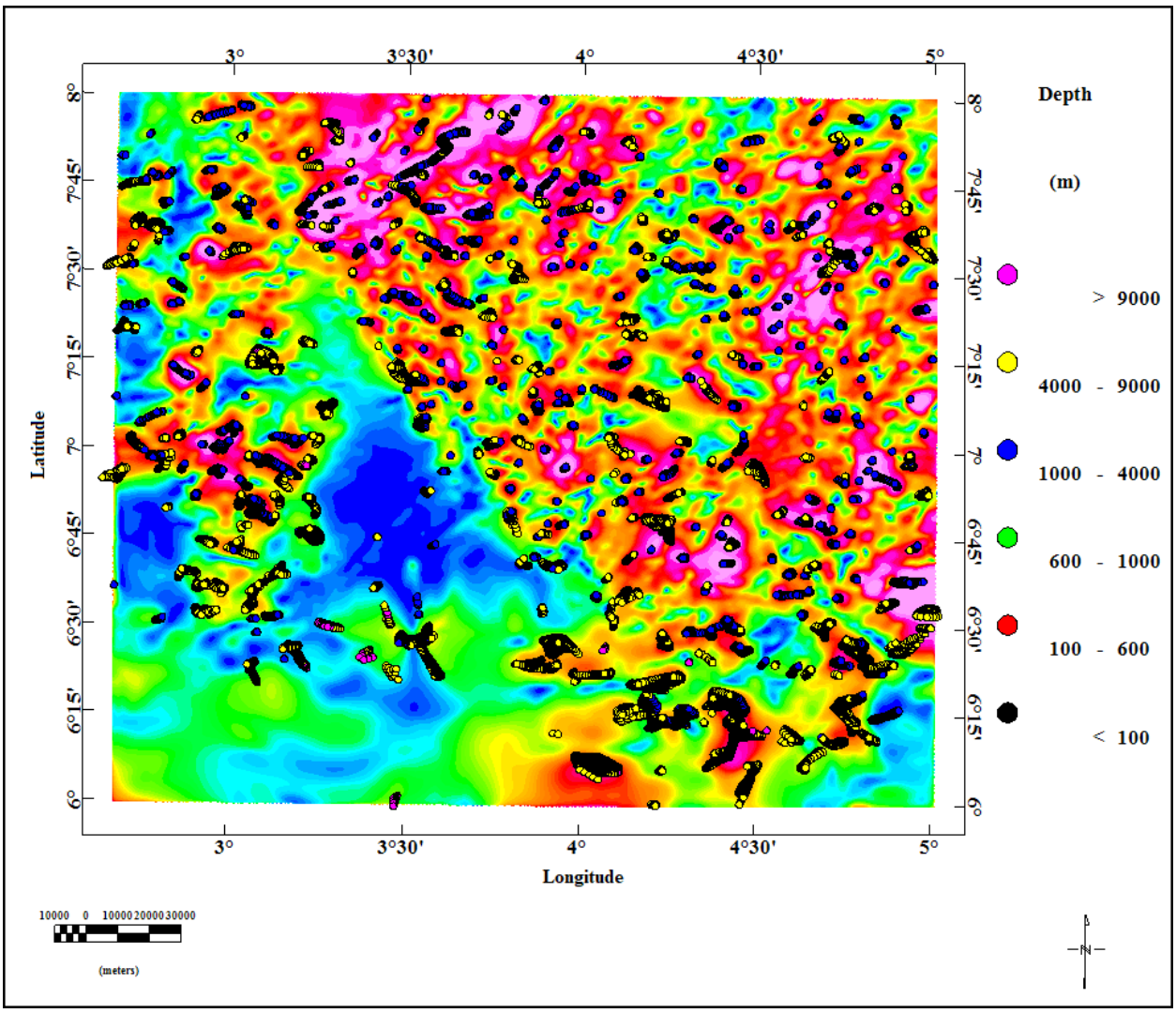


Fig. 4.6h: Euler deconvolution solution plots for dyke/sill superimposed on the analytic signal map of the study area.

4.7 Werner deconvolution

Aeromagnetic data have been largely used in delineating surface and subsurface structures that have good magnetic susceptibility contrast from the host rock. Werner deconvolution modelling technique for automatic analysis of magnetic data is a powerful tool for the interpretation of magnetic data on a profiles in particular; the technique is a valuable aid to the interpretation of deep crustal structures. The analysis of profiles allows the interpretation of data as recorded.

However, the direct interpretation methods must assume that the profiles are normal to the strike direction and that the bodies extend to large distances on either side of the profile.

The Equations for the total magnetic field due to thin sheets and the edges of a thick body (Werner Equations) are used to compute the depth to the top, susceptibility contrast, and the dip of these features from a given total magnetic field profile. The term "Werner deconvolution" refers to a set of algorithms whose feature is the linearization of a two-dimensional (2-D) inverse problem for the parameters of a magnetic dyke or contact by clearing the denominators of the rational functions that describe their anomalies (Kilty, 1983; Hansen and Simonds, 1993).

The Werner deconvolution operator is a sliding window that moves along the profile and continually solves for the four unknowns. The parameters of the operator consist of:

i. The size of the window, which will influence the estimated depth of the anomalies.
ii. How the window size is moves on the profile, which controls the number of generated solutions.
iii. Parameters that exclude the spurious solutions (caused by noise which have been taken care of by upward continuation).

Werner deconvolution usually generates a cluster of solutions around the "real" solution due to multiple passages with different window length. If thin sheets (dykes or sills) are present, their anomalies are recognized and analysed from the total field data, while interfaces (dipping contacts or changes in slope of a particular surface) are analysed from the measured vertical gradient data and the computed horizontal derivative of the total field. Typically, an anomaly will produce both a thin-sheet solution and an interface solution.

Werner deconvolution was applied to the filtered aeromagnetic data along ten profiles (Fig. 4.7). The profiles were drawn across anomalies located on the second vertical derivative shaded relief map. Oasis Montaj (version 6.4.2) software was applied to the filtered data for the ten profiles, which yielded the Werner deconvolution solutions. Grapher 8 software was used to obtain the Werner plots.

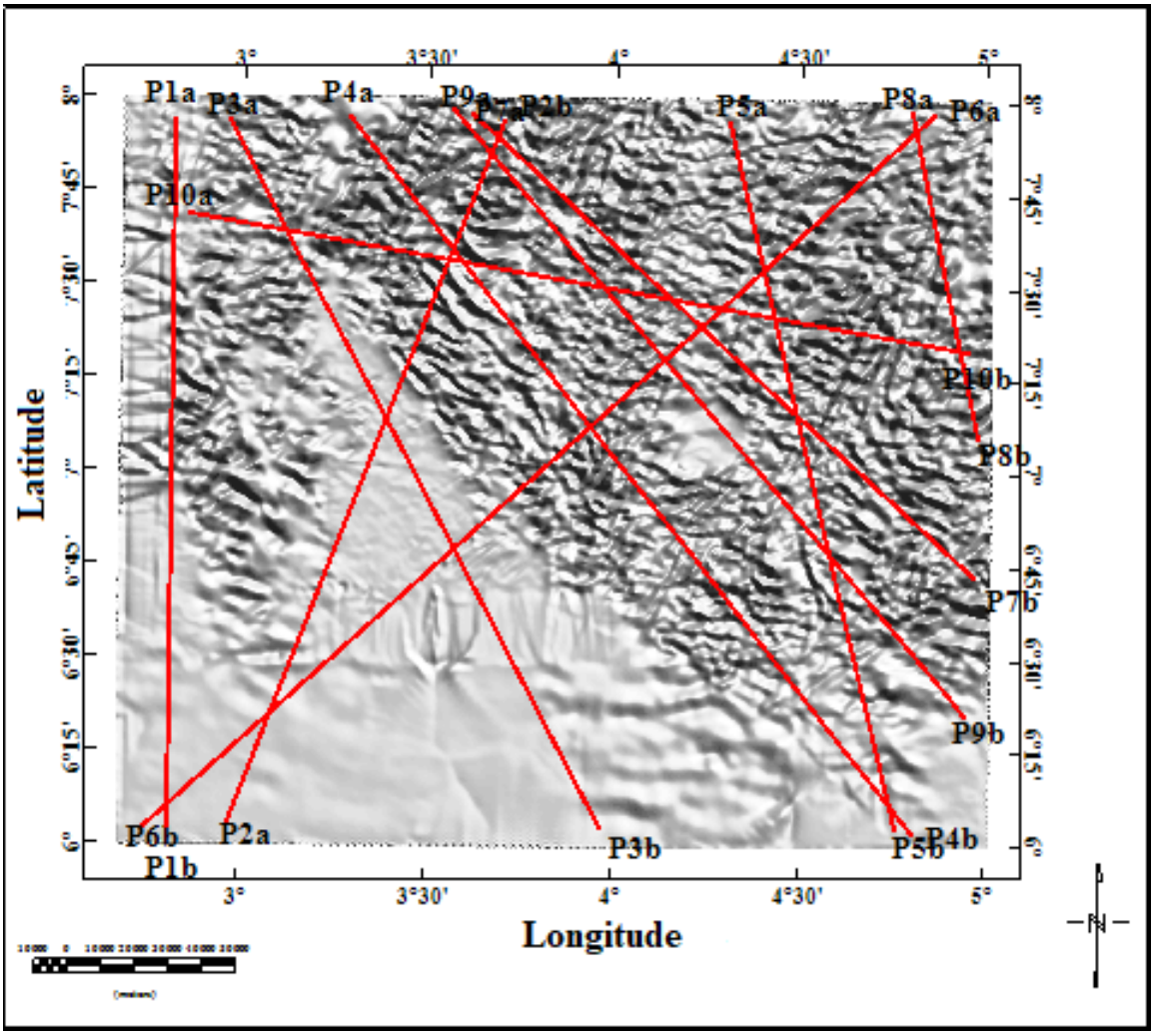


Fig. 4.7: Shaded relief map of the second vertical derivative showing profiles from which the residual upward continued data were extracted and used for computation of Werner deconvolution solutions.

Figs. 4.8a and b are the Werner deconvolution modelling results for profile 4. The Werner deconvolution results for the ten profiles are given in Table 4.1 and Appendix A are the plots for the filtered aeromagnetic intensity field data and their corresponding Werner deconvolution modelling results.

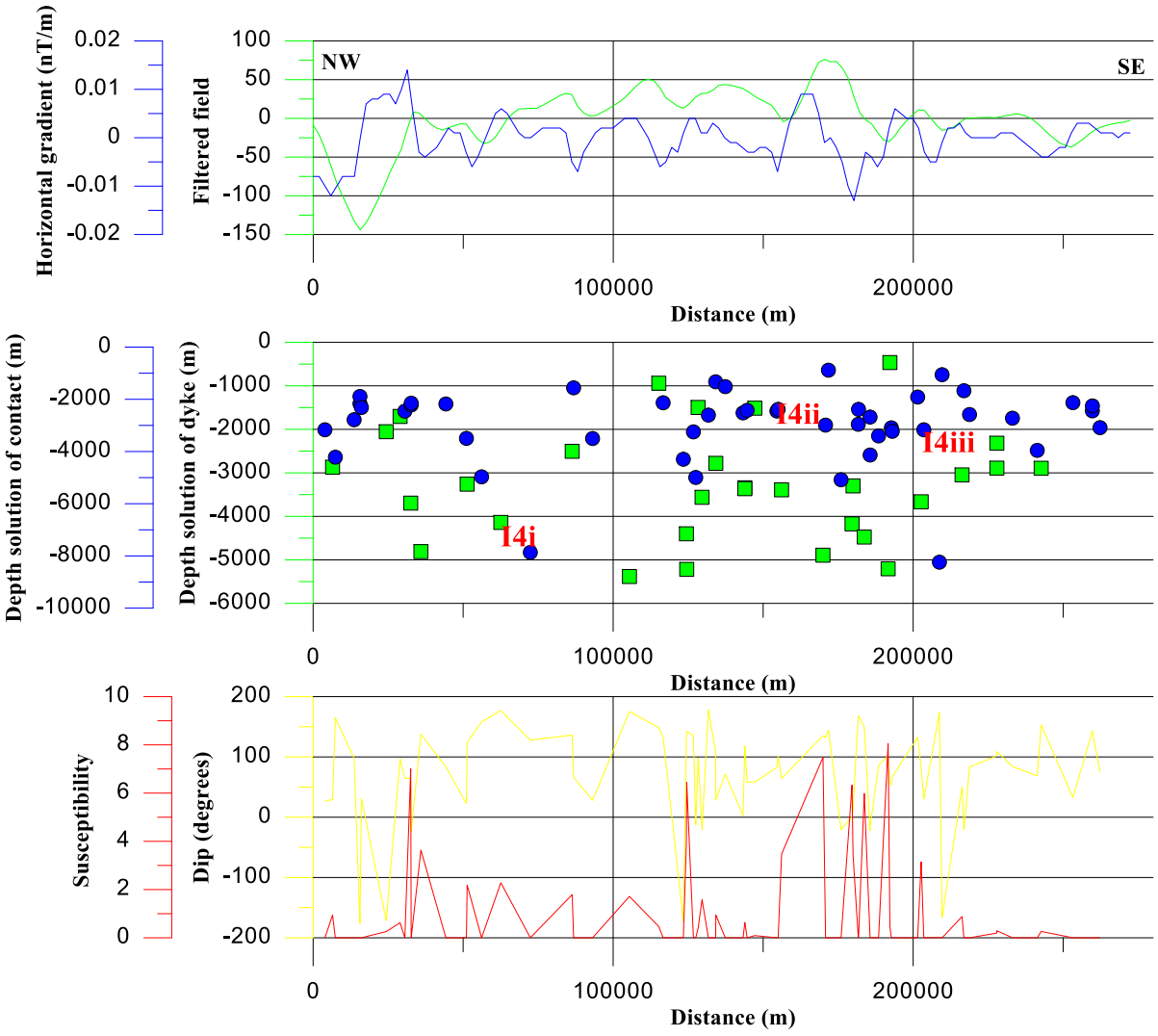


Fig. 4.8a: Werner plots for profile P_{4A} P_{4B}.

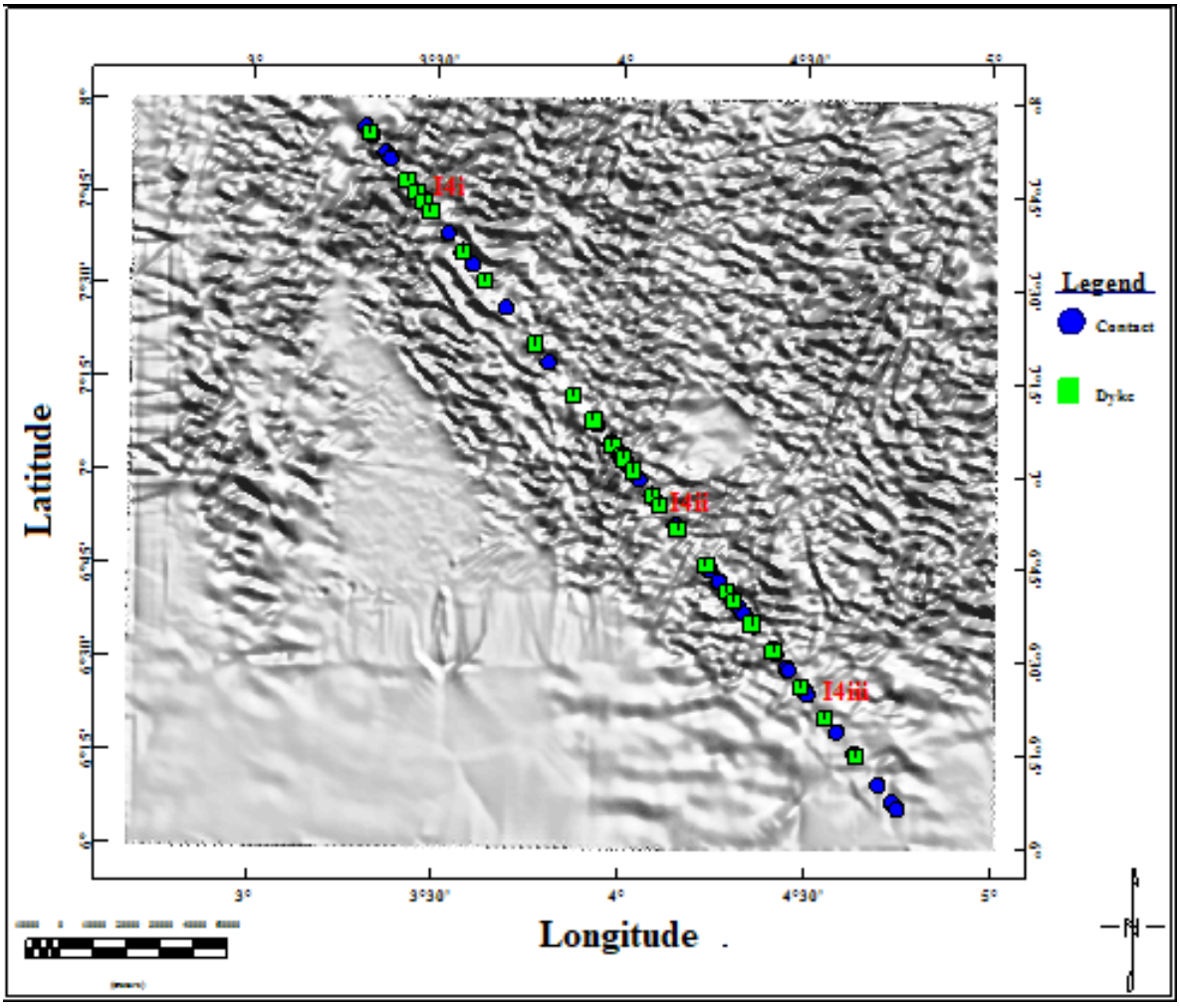


Fig. 4.8b: Werner post on second vertical derivative map for profile P_{4A} P_{4B}.

Table 4.1: Werner deconvolution results for the ten profiles

Profiles	Estimated depth (km)	Estimated angle of dip (degree)	Average susceptibility
P_{1A} P_{1B}	5.0	36	1.4447
P_{2A} P_{2B}	3.8	65	1.4569
P_{3A} P_{3B}	3.8	54	1.7707
P_{4A} P_{4B}	3.2	67	0.9839
P_{5A} P_{5B}	4.1	59	2.8517
P_{6A} P_{6B}	3.2	75	1.8107
P_{7A} P_{7B}	3.0	68	2.7693
P_{8A} P_{8B}	3.9	50	2.5037
P_{9A} P_{9B}	1.4	81	0.0323
P_{10A} P_{10B}	1.7	78	0.0825

4.8 2-D forward modelling and inversion of the aeromagnetic data

To quantitatively interpret the magnetic data (Fig. 4.9), the GM-SYS profile of Oasis Montaj software was used. The GM-SYS profile is a programme for calculating the magnetic response from a geologic cross-section model. Forward modelling involves creating a hypothetical geologic model and calculating the geophysical response to that earth model while inversion, optimization or inverse modelling involves the reverse procedure. Starting with the observed geophysical response, an earth model that will provide the best fit to that data is calculated. Because magnetic calculations are non-linear, the calculations use an iterative process. Two-dimensional (2-D) models assume the earth is two dimensional; i.e. it changes with depth (the Z-direction) and in the direction of the profile (X-direction; perpendicular to strike). 2-D models do not change in the

strike direction (Y-direction). The priori information obtained from geologic map, and the magnetic data were used in GM-SYS profile of Oasis Montaj software for the 2-D forward modelling and inversion of the aeromagnetic data (Fig. 4.9). The profiles in Fig.4.9

(P1a P1b - P3a P3b) were chosen on the magnetic map and were subsequently interactively employed in the 2-D forward and inversion, optimization, or inverse modelling. The aeromagnetic anomalies are trending mainly in the NE-SW and NW-SE directions with occasional W-E. The first two profiles in Fig. 4.9 (P1a P1b and P2a P2b) were therefore chosen perpendicular to the strike of the causative structures of the area while the third profile (P3a P3b) was chosen to cut across the two main lithologies (i.e. Basement and Sedimentary) and suspected structures. Figs. 4.10a - c show the aeromagnetic data profiles and their corresponding earth models generated from the GM-SYS profile of Oasis Montaj software used.

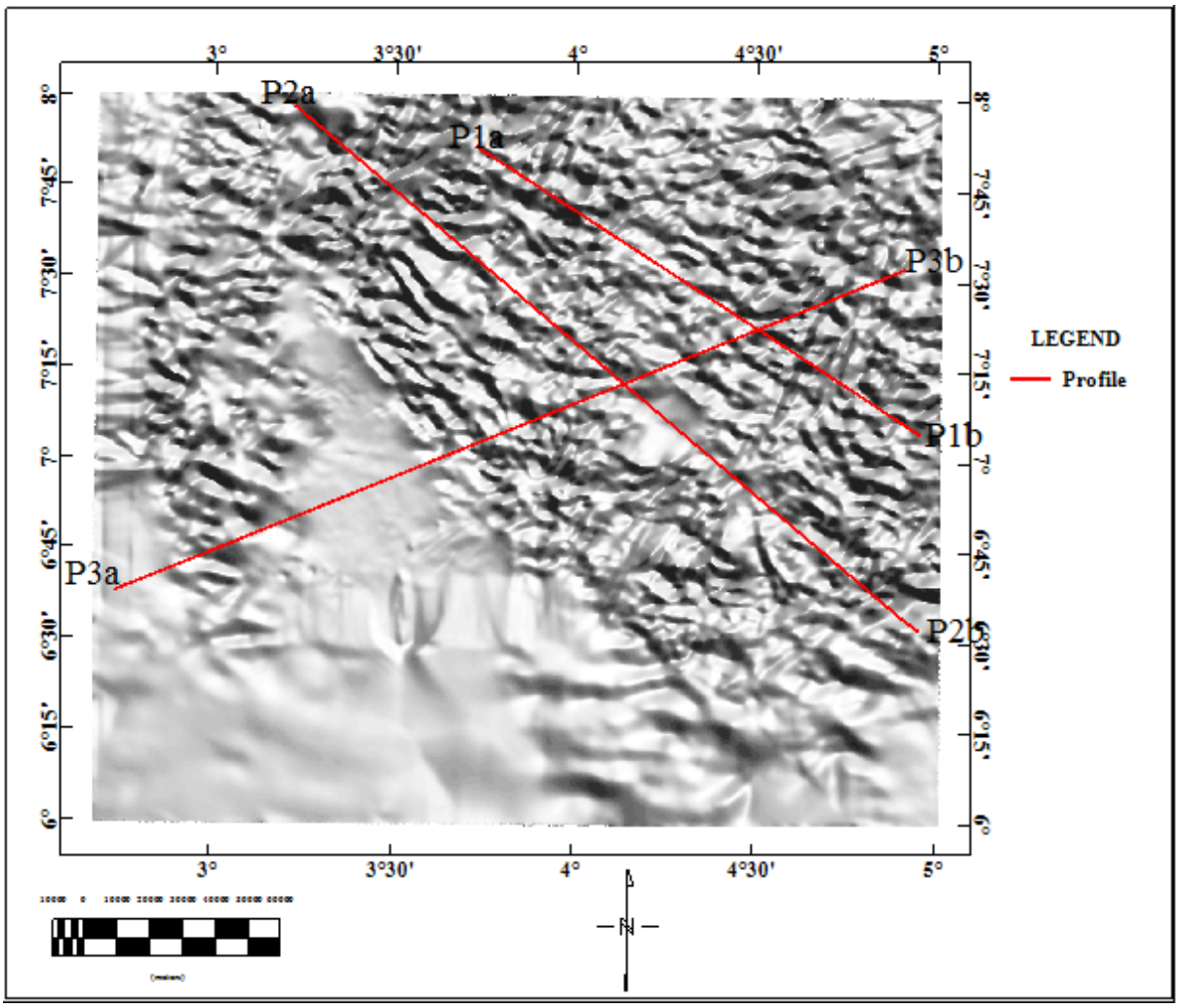


Fig. 4.9: Shaded relief map of the second vertical derivative showing profiles from which the residual data were extracted and used for 2-D forward modelling and inversion.

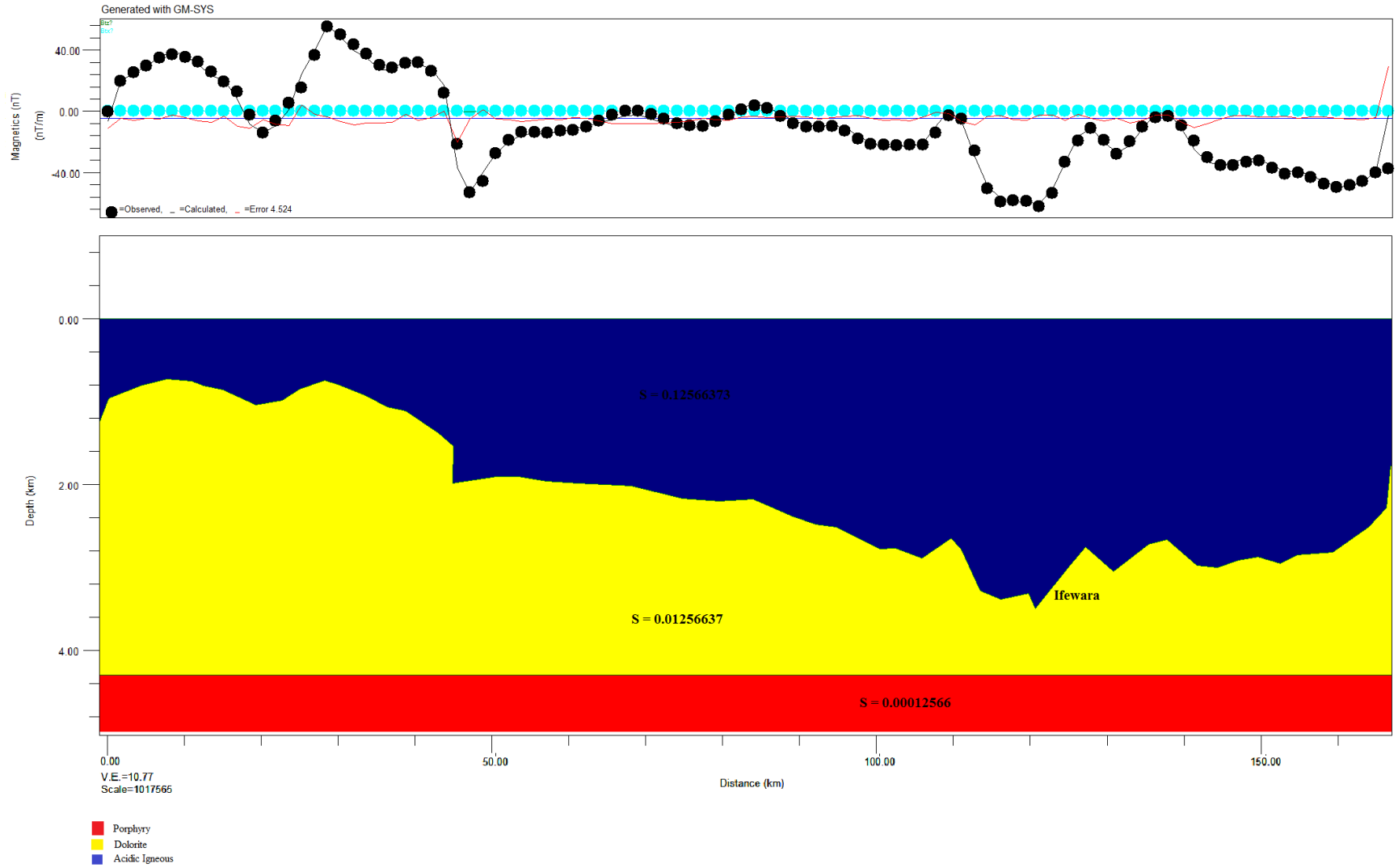


Fig. 4.10a: Forward and inverse model interpretation of residual magnetic anomalies along profile P1a-P1b.

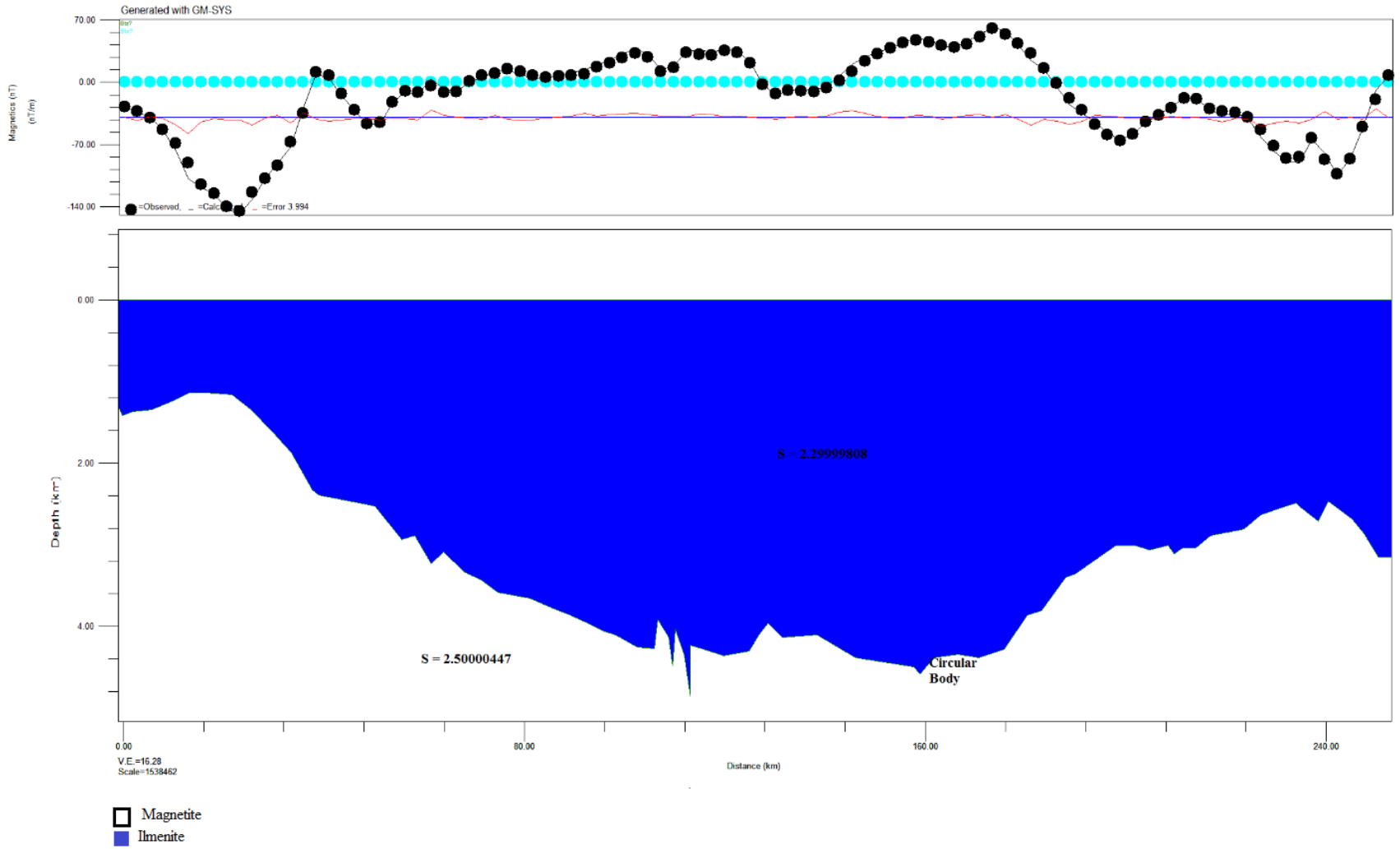


Fig. 4.10b: Forward and inverse model interpretation of residual magnetic anomalies along profile P2a-P2b.

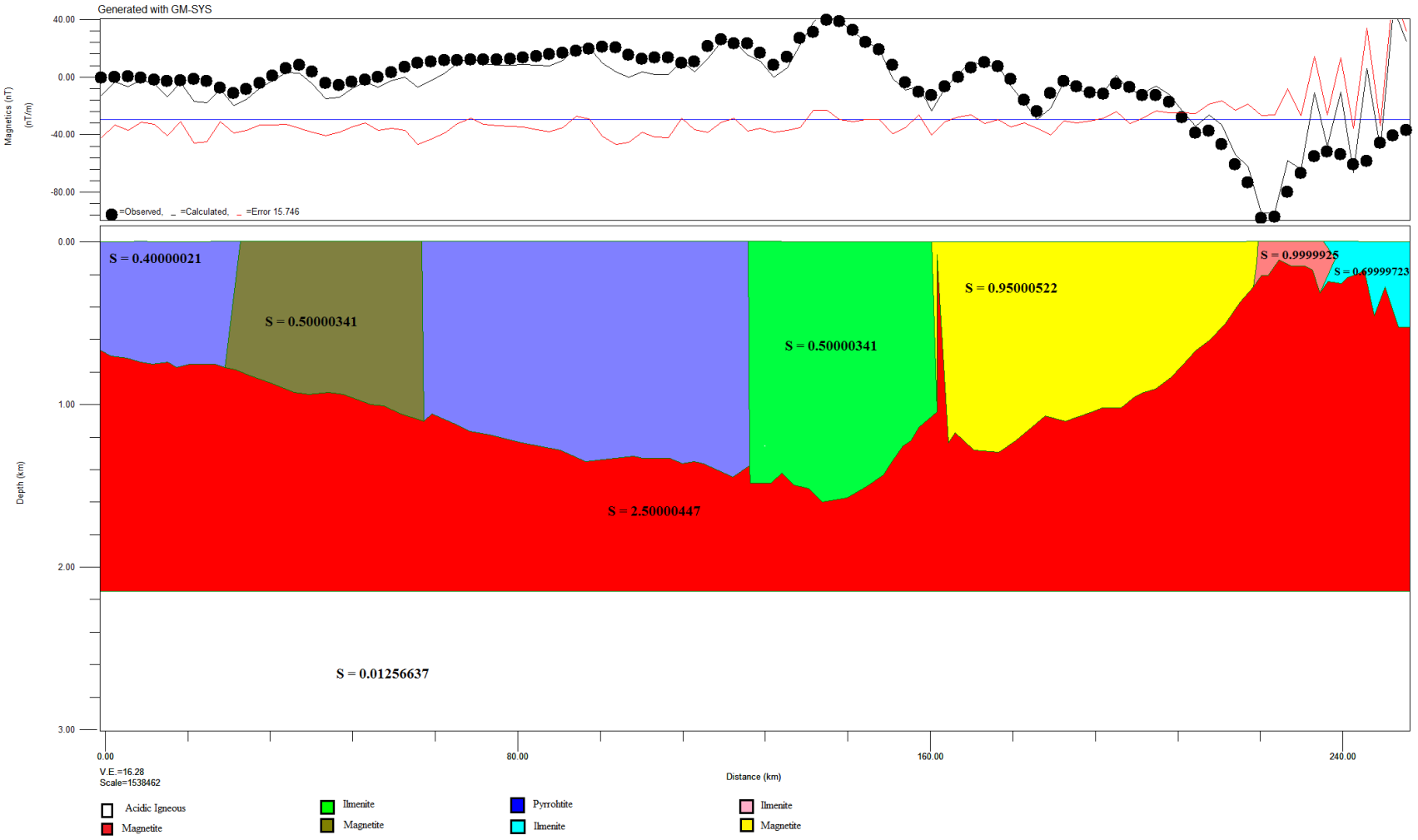


Fig. 4.10c: Forward and inverse model interpretation of residual magnetic anomalies along profile P3a-P3b.

CHAPTER FIVE

DISCUSSION, CONCLUSION AND RECOMMENDATIONS

5.1 Discussion

Visual studies of total magnetic field intensity, regional field, residual field and upward continued maps (Figs. 3.3 - 3.6) of the study area revealed variations in magnetic field intensity. The direction of the regional field (NE-SW) is in conformity with the suspected structures coming from the Atlantic Ocean. The observations made on total magnetic field intensity and residual field maps are more visible on the upward continued maps (Figs. 3.6a - b) because the data has been enhanced. Regions of magnetic lows (low amplitude magnetic values) and highs (high amplitude values) are apparent on the upward continued maps. The anomalies characterised by low values of magnetic intensity range from about -77 to 0 nT and the magnetic highs range from 2 to 52 nT. The defined magnetic highs and lows as visible on the map are in real sense relative. The sharp contrast is enhanced due to sharp magnetic intensity contrast between the crystalline and the sedimentary rocks magnetic susceptibilities. The prominent high amplitude magnetic intensities noticeable on the upward continued magnetic intensity maps trend mostly in NE–SW and NW–SE directions. High amplitude magnetic values correspond to region with high magnetic mineral contents which in the study area correspond to the Pre-Cambrian to Pan-African Crystalline Basement rocks of the southwestern Nigeria. The low amplitude magnetic values trend in W–E, NNE–SSW and NW–SE. Low amplitude anomalies also characterised in the southern part of the mapped area as well as in some parts of northeast and northwest. Many of these regions coincide with areas with thin to relatively thick sedimentary cover, where the effect of the thick clastic materials of weak magnetic susceptible masks the high magnetic susceptibility originating from relatively deep basement rocks.

Figs. 3.6a - b (residual magnetic field intensity map upward continued to a height of 2000 m) show that besides the obvious long wavelength anomalies, short wavelength anomalies are essentially enhanced. The NNE-SSW trending structures provide a possible link to the Ifewara-Kalangai fault axis, while the NW-SE trends could probably be due to the separation of the South American continent from Africa to accommodate the emerging Atlantic Ocean.

Further enhancements of the short wavelength anomalies trends in the data set are achieved in the first and second vertical, total horizontal and tilt derivatives as well as analytic signal and theta angle of the upward continued magnetic intensity grid as shown in Figs. 4.1 – 4.5. Systems of negative trending anomalies of short wavelength which are rimmed by positive anomalies are clearly visible. The zero value of the second vertical derivative contour map (Fig.4.1c), which indicates the presence of a boundary, clearly defined the edges of the anomalies in the study area. The boundaries in Fig.4.1d (second vertical derivative map) clearly shows an inward extension of the Sedimentary Basin. From Fig. 4.1e (shaded relief map of the second vertical derivative), it can be seen by comparing it with Fig.3.5b (shaded relief map of the residual magnetic field intensity); the NW-SE anomalies becomes more conspicuous. Fig.4.2b (shaded relief map of the total horizontal derivative) tends to enhance the deeper structures while still retaining the shallow ones. On a regional scale, Fig. 4.5a (theta angle map) does not differentiate the geologic boundaries, but on a local scale it resolves properly the boundaries of the local anomalies.

Euler solution maps of the study area are presented in Figs. 4.6a - h. Results with tightest cluster around recognized sources are likely to give the best solutions and therefore accepted. However, obtained solutions were windowed to select the most accurate results. This was achieved by defining acceptance limit of solution depth, vertical uncertainty (%), horizontal uncertainty (%) and the offsets along the X and Y directions.

The windowed Euler deconvolution solution points coincide with regions having anomalies whose Euler depth (<100 m - >9000 m) gave useful information about the topography of the basement. Figs.4.8a and 4.8b show windowed Euler depth solutions as color coded circles, the circle's colour indicates depth range. Plotted solutions were referenced to Minna datum in Nigeria. The NE-SW structure in the northwestern part of Fig. 4.6c (Euler deconvolution solution plots for contact superimposed on the first vertical derivative map) could probably be a deep seated rift or valley given that it did not appear well on the geologic and topographic/bathymetric maps.

Werner deconvolution method was applied along profiles 1 to 10 on the filtered aeromagnetic data. The method was used to determine the position (distance along the profile) depth, dip (orientation) and intensity (susceptibility) of magnetic source bodies on the magnetic profile. A high residual cut-off was applied which is a variable required to generate few solutions of Werner deconvolution. The study area was found to be characterised by more of contact to dyke solutions. The estimated depth ranges from 1.4 to 5.0 km, the susceptibility values calculated along the profiles vary from 0.0323 to 2.8517 and the dip angle estimated from the models range from 36º to 81º (Table 4.1).

Modelling using GM-SYS forward modelling and inversion subroutine programme of Oasis Montaj was performed on three profiles (Fig. 4.9). The selection of profiles for the magnetic modelling was done taking into account the main anomalies displayed on the magnetic maps. Along each profile, the structure and type of anomaly in the area was determined. The results indicate that Ifewara fault is about 6.0 km wide and occurs at a depth of 3.2 km, while the circular structure along profile P2a-P2b occurs at a depth of 4.4 km.

5.2 Conclusion

In this research, high resolution aeromagnetic data have been used to investigate the presence of anomalies in the study area. Both qualitative (first and second vertical derivatives, total horizontal derivative, analytic signal, theta map, tilt derivative, and total horizontal derivative of tilt derivative) and quantitative (Euler and Werner deconvolutions, spectral analysis as well as forward modelling and inversion) interpretation techniques were chosen to achieve the outlined objectives of this research.

The results of the qualitative techniques yield high magnetic amplitude in the Basement Complex region and low amplitude in the Sedimentary Basin and some part of Basement Complex associated with schist. The high magnetic intensity is believed to be due to the presence of hematite and magnetite in the rocks. The direction of linear features delineated correlates with the geology of the study area. The trending patterns of the linear features are NE-SW, NW-SE, NNE-SSW and E-W.

The windowed Euler deconvolution solutions points coincide with regions having anomalies whose depths (<100 m - >9000 m) gave useful information about the topography of the basement. The estimated depth range from Werner deconvolution was from 1.4 to 5.0 km, the susceptibility values varies from 0.0323 to 2.8517 and the dip angle was found to be between 36º and 81º .

Modelling of anomalies using GM-SYS have shown that Ifewara fault is 3.2 km deep.

5.3 Recommendations

Based on the results obtained, the following are recommended:

1. Another imaging technique like gravity and seismic methods should be employed to strengthen observations made in this work.
2. Curie point depths, geothermal gradients and heat flow values should be investigated using aeromagnetic data and borehole temperature logging; this would further provide detailed information on the geothermal potential of the study area.
3. A three-dimensional geothermal model could be constructed for the study area using integrated borehole, temperature and geophysical data.

REFERENCES

Abraham, E. M., Lawal, K. M., Ekwe, A. C., Alile, O., Murana, K. A. and Lawal, A. A. (2014). Spectral analysis of aeromagnetic data for geothermal energy investigation of Ikogosi Warm Spring – Ekiti State southwestern Nigeria. *Geothermal Energy*, 2(6): 1-21.

Abubakar, Y. I. (2012). An integrated technique in delineating structures: A case study of the Kushaka schist belt northwestern Nigeria. *International Journal of Applied Science and Technology*, 2(5): 164-173.

Adepelumi, A. A., Ako, B. D., Ajayi, T. R., Olorunfemi, A. O., Awoyemi, M. O., and Falebita, D. E. (2008). Integrated geophysical mapping of the Ifewara transcurrent fault system, Nigeria. *Journal of African Earth Sciences*, 52: 161-166.

Airo, M. L. and Wennerström, M. (2010). Application of regional aeromagnetic data in targeting detailed fracture zones. *Journal of Applied Geophysics*, 71: 62-70.

Ajakaiye, D. E., Hall, D. H., Ashieka, J. A. and Udensi, E. E. (1991). Magnetic anomalies in the Nigerian continental mass based on aeromagnetic surveys. In P. Wasilewski and P. Hood (eds.), Magnetic anomalies-and sea. *Tectonophysics*, 192: 211-230.

Ajayi, T. R. (2003). Mineral resources potential of Osun State, southwestern Nigeria; A commissioned report.

Akinmosin, A. A., Omosanya, K. O., Ikhane, P. R., Mosuro, G. O. and Goodluck, I. (2013). Characterisation of bitumen seepage in eastern Dahomey basin, southwestern Nigeria. *Advances in Applied Science Research*, 3(4): 2078-2089.

Akintorinwa, O. J., Ojo, J. S., and Olorunfemi, M. O. (2010). Geophysical investigation of pavement failure in a Basement Complex terrain of southwestern Nigeria. *The Pacific Journal of Science and Technology,* 2: 649-663.

Ansari, A. H. and Alamdar, K. (2009). Reduction to the pole of magnetic anomalies using analytic signal. *World Applied Sciences Journal,* 7(4): 405-409.

Badmus, B. S., Awoyemi, M. O., Akinyemi, O. D., Saheed, G. A. and Olurin, O. T. (2013). Magnetic gradient techniques on digitized aeromagnetic data of Ibadan area, southwestern Nigeria. *Central European Journal of Geosciences,* 5(3): 387-393.

Billings, M. P. (2006). Structural Geology. New Delhi, Prentice – Hall of India Private Limited.

Billman, H. G. (1992). Offshore stratigraphy and paleontology of the Dahomey Embayment. *Proceedings of the 7th African Micropaleontology Colloquium,* Ile-Ife.

Bird, D. (1997). Primer Interpreting Magnetic Data. *American Association of Petroleum Geologist. Explorer* , 18:18-21.

Blakely, R. S. (1996). Potential theory in gravity and magnetic applications. Cambridge University Press, USA.

Bongiolo, A. B. S. and Ferreira, F. J. F. (2012). Evaluation of enhancement techniques of magnetic anomalies applied to structural interpretation of the Itaituba region, State of Par*á,* Brazil. *Revista Brasileira de Geofisica,* 30(3): 373-388.

Broome, H. J. (1990). Generation and interpretation of geophysical images with examples from the Rae Province, northwestern Canada Shield. *Geophysics,* 55: 977-997.

Burke, K. C. B., Dessauvagie, T. F. J. and Whiteman, A. J. (1971). The opening of the Gulf of Guinea and the geological history of the Benue depression and Niger Delta. *Nature, Physical Science*, 233(38): 51-55.

Coker S. L, Ejedawe, J. E. and Oshiorienua, J. A. (1983). Hydrocarbon source potentials of Cretaceous rocks of Okitipupa uplift, Nigeria. *Journal of Mining and Geology*, 22: 163-169.

Cooper, G. R. J. (2008). Euler deconvolution with improved accuracy and multiple different structural indices. *Geoscience*, 19(1): 72-76.

Cordell, L. and Grauch, V. J. (1985). Mapping basement magnetization zones from Aeromagnetic data in San Juan Basin, New Mexico, in Hinze, W. J., Ed. The Utility of regional gravity and magnetic anomaly maps. *Society of Exploration Geophysicists*, 51: 181-197.

Danbatta, U. A. (2008). A review of the evolution and tectonic framework of the schist belt of Western Nigeria, West Africa. *African Geosciences Review*, 15(2): 145-158.

Debeglia, N. and Corpel, J. (1997). Automatic 3-D Interpretation of potential Field Data using Analytic Signal Derivatives. *Geophysics*, 62: 87-96.

De Swardt, A. M. J. (1953). The geology of the country around Ilesha. *Geological Survey of Nigeria. Bulletin* No. 28.

Dobrin, M. (1976). Introduction to geophysical prospecting. McGraw – Hill Book Company (3ed). New York.

Doell, U. R. and Cox, A. (1967). Magnetization of rocks. In: Society of Exploration Geophysicsists. Mining Geophysics Volume Editorial Committee (Eds.), Mining Geophysics, 2: Theory. *Society of Exploration Geophysicsists*, Tusla, 446-453.

Ekweozor, C. M. and Nwachukwu, J. I. (1989). The origin of Tar sands of southwestern Nigeria *Nigerian Association of Petroleum Exploration Bulletin*, 4(2): 82-84.

Elueze, A. A. (1998). Geology of the Precambrian schist belt in Ilesha area. South-West, Nigeria. In P. O. Oluyide, W. C. Mbonu, A. E. O. Ogezi, I. G. Egbuniwe, A. C. Ajibade and A. C. Umeji. (Eds.) *Precambrian Geology of Nigeria*; Geological Survey of Nigeria, 231-240.

Elueze, A. A. and Nton, M. E. (2004). Organic geochemical appraisal of limestone and shales in part of eastern Dahomey Basin, southwestern Nigeria. *Journal of Mining and Geology*, 40(1): 29-40.

Enu, E. I. (1990). Nature and occurrence of tar sands in Nigeria. In: B. D. Ako and E. I. Enu (eds.), Occurrence, utilization and economic importance of tar sands in Nigeria. Mining and Geosciences Society publication on tar sands workshop. Olabisi Onabanjo University, Ago – Iwoye, 11-16.

Ganiyu, S. A., Badmus, B. S., Awoyemi, M. O., Akinyemi, O. D. and Olurin, O. T. (2013). Upward continuation and reduction to pole process on aeromagnetic data of Ibadan area, southwestern Nigeria. *Earth Science Research*, 2(1): 66-73.

Grauch, V. J. S., and Cordell, L. (1987). Limitation of determining density or magnetic boundaries from the horizontal gradient of gravity or pseudogravity data. *Geophysics*, 52: 118-121.

Grauch, V. J. S., Hudson, M. R. and Minor, S. A. (2001). Case History: Aeromagnetic expression of faults that offset basin fill, Albuquerque basin. *New Mexico Geophysics,* 66(3): 707-720.

Goussev, S. A. and Pierce J. W. (2000). Gravity and Magnetic Exploration Lexicon. Geophysical Exploration and Development, Calgary, Alberta, Canada.

Hansen, R. O. and Simmonds, M. (1993). Multiple-source Werner deconvolution. *Geophysics,* 58(12): 1792-1800.

Hartman, R. R., Teskey, D. J. and Friedberg, J. L. (1971). A system for rapid digital aeromagnetic interpretation. *Geophysics,* 36(5): 891-918.

Hobbs, W. H. (1904). Lineaments of the Atlantic border region. *Geological Society of America Bulletin,* 15: 483-506.

Hood, P. and McClure, D. J. (1965). Gradient measurements in ground magnetic prospecting. *Geophysics*, 30(3): 403-410.

Hsu, K. S., Coppens, D. and Shyu, C. T. (2002). Depth to magnetic source using the generalized analytical signal. *Geophysics*, 63(6): 1947-1957.

Idowu, J. O., Ajiboye, S. A., Ilesanmi, M. A.and Tanimola, A. (1993). Origin and significance of organic matter of Oshosun Formation, southwestern Dahomey Basin, Nigeria. *Journal of Mining and Geology*, 29: 9-17.

Johnson, W. W. (1969). The least-square method of interpreting magnetic anomalies caused by Two-dimensional structures. *Geophysics*, 34: 65-74.

Jones, H.A. and Hockey, R.D. (1964). The geology of part of southwestern Nigeria. *Geological Survey of Nigeria Bulletin*, 31: 87.

Keating, P., and Pilkington, M. (2004). Euler deconvolution of the analytic signal and its application to magnetic interpretation. *Geophysical Prospecting*, 52(3): 165-182.

Kilty, K. T. (1983): Werner deconvolution of profile potential field data. *Geophysics*, 48(2), 234-237.

Kingston, D. R., Dishroon, C. P. and Williams, P. A. (1983). Global basin classification system. *American Association of Petroleum Geologist. Bulletin*, 67: 2175-2193.

Klemme, H. D. (1975). Geothermal gradient, heat flow and hydrocarbon recovery. In: A.G. Fischer and S. Judson (Eds.). *Petroleum and Global Tectonics*. Princeton University Press, 251-304.

Kogbe, C. A. (1985). Landsat imagery interpretation map of curve-linear structures in north-central Nigeria. *Journal of African Earth Sciences*, (3): 269-270.

Kolawole, F., and Anifowose, A. Y. B. (2011). Remote sensing analysis of a dextral discontinuity along Ifewara-Zungeru area, Nigeria, West Africa. *Indian Journal of Science and Technology*, 4(1): 46-51.

Kowalik, W. S. and Glen, W. (1987). Image processing of aeromagnetic data and integration with landsat images for improved structural interpretation. *Geophysics*, 52: 875–884.

Ku, C. C., Telford, W. M. and Lim, S. H. (1971). The use of linear filtering in gravity problems. *Geophysics*, 36: 1174-1203.

Li, L. (2013). Improved edge detection tools in the interpretation of potential field data. *Exploration Geophysics*, 44: 128-132.

Lipponen, A. and Airo, M. L., (2006). Linking regional-scale lineaments to local-scale fracturing and groundwater inflow into Päijänne water conveyance tunnel, Finland. *Near Surface Geophysics*, 4: 97-111.

Marquardt, D. W. (1963). An algorithm for least-squares estimation of nonlinear parameters. *Journal of the Society for Industrial and Applied Mathematics*, 11(2): 431-441.

Matzner, R. A. (2001). Dictionary of Geophysics, Astrophysics and Astronomy (A volume in the Comprehensive Dictionary of Physics). Boca Raton, Florida, CRC press.

Merrill, R. T., McElhinny, M. W. and McFadden, P. I. (1996). The magnetic field of the earth: Paleomagnetism, the core and the deep mantle. San Diego, Academic Press.

Milligan, P. R., and Gunn, P. J. (1997). Enhancement and presentation of airborne geophysical data. *AGSO Journal of Australian Geology and Geophysics*, 17(2): 63-75.

Mohammad, A. (2009). Aeromagnetic data interpretation to locate buried faults in Yazd Province, Iran. *World Applied Sciences Journal*, 6 (10): 1429-1432.

Mpanda, S. (1997). Geological development of East African coastal basin of Tanzania (Doctoral dissertation, Acta Universitatis Stockholmiensis), Sweeden.

Mushayandebvu, M. F., Driel, P. V., Reid, A. B. and Fairhead, J. D. (2001). Magnetic source parameters of two-dimensional structures using extended Euler deconvolution. *Geophysics*, 66: 814-823.

Nabighian, M. N. (1972). The analytic signal of two-dimensional magnetic bodies with polygonal cross-section. Its properties and use for automated anomaly interpretation. *Geophysics*, 37: 507-517.

Nabighian, M. N. (1984): Towards the three-dimensional automatic interpretation of potential field data via generalised Hilbert transforms: Fundamental Relations. *Geophysics*, 53: 957-966.

Nelson, J. B. (1988). Calculation of the magnetic gradient tensor from total field gradient measurements and its application to geophysical interpretation. *Geophysics*, 53: 957- 966.

NGSA. (2008). Geology and mineral resources of southwest zone Nigeria. Regional geology and minerals series. Publication of Ministry of Mines and Steel Development.

NGSA. (2010). Application and results of airborne data in Nigeria. Elizabethan Publishing Company, Lagos.

Nton, M. E. (2001). Sedimentological and geochemical studies of rock units in the eastern Dahomey Basin, southwestern Nigeria. Unpublished Ph. D. thesis. Geology Department, University of Ibadan.

Nton, M. E., Eze, F. P. and Elueze, A. A. (2006). Aspects of source rock evaluation and diagenetic history of the Akinbo Shale eastern Dahomey basin, south-western Nigeria. *Nigerian Association of Petroleum Geologists Bulletin*, 19(1): 35-49.

Nwankwo, L. I., Olasehinde, P. I. and Akoshile, C .O. (2011). Heat flow anomalies from spectral analysis of airborne magnetic data of Nupe basin, Nigeria. *Asian Journal of Earth Sciences*, 4: 20-28.

Ogbe, F. G. A. (1972). Stratigraphy of strata exposed in the Ewekoro quarry, Western Nigeria. In: T. F. J. Dessauvagie and Whiteman (eds.) *African Geology*. University Press, Nigeria, 305-322.

Ojo, O. (2007). The climate of West Africa. London, Heinemann Educational Books Ltd.

Okosun, E. A. (1998). Review of the Early Tertiary stratigraphy of southwestern Nigeria. *Journal of Mining and Geology*, 34(1): 27-35.

Oladunjoye, M. A., Olayinka, A. I., Alaba, M. and Adabanija, M. A. (2016). Interpretatin of high resolution aeromagnetic data for lineaments study and occurrence of Banded Iron Formation in Ogbomoso area, southwestern Nigeria. *Journal of African Earth Sciences*, 114: 43-53.

Olarewaju, V. O. (1988). Rare earth elements in the charnokitic and associated granitic rocks of Ado – Ekiti area, southwestern Nigeria. In Oluyide, P. O., W. C. Mbonu, A. E. O. Ogezi, I. G. Egbuniwe, A. C. Ajibade and A. C. Umeji(eds.). *Precambrian Geology of Nigeria*; Geological Survey of Nigeria, 231-240.

O'Leary, D. W., Friedman, J. D. and Pohn, H. A. (1976). Lineament, linear and lineation: some proposed new standards for old terms. *Geological Society of America Bulletin*, 87: 1463-1469.

Omatsola, M. and Adegoke, O. S. (1981). Tectonic evolution and Cretaceous stratigraphy of the Dahomey Basin. *Journal of Mining and Geology*, 18 (1): 130-137.

Onyedim, G. C. (2007). Enhancement of fault anomalies by application of steerable filters: Application to aeromagnetic map of part of Ifewara fault zone, southwestern Nigeria. *Journal of Applied Sciences*, 7(2): 214-219.

Oppenhein, A. V. and Schafer, R. W. (1975). Digital Signal Processing. Prentice-Hill International Incorporation, New Jersey.

Osinowo, O. O. and Olayinka, A. I. (2013). Aeromagnetic mapping of basement topography around the Ijebu – Ode geological transition zone, southwestern Nigeria. *Acta Geodesy and Geophysics*, 48: 451-470.

Osinowo, O. O., Akanji, A. O., and Olayinka, A. I. (2014). Application of high resolution aeromagnetic data for basement topography mapping of Siluko and environs, southwestern Nigeria. *Journal of African Earth Sciences*, 99: 637-651.

Oyawoye, M. O. (1972). The basement complex of Nigeria. In Dessanvagie, T. F. J. and Whiteman, A. J. (eds.): *African Geology*. Geology Department. University of Ibadan, 67-99

Papoulis, A. (1962). The Fourier integral and its applications. McGraw Hill Book Company.

Pedersen, L. B. (1989). Relations between horizontal and vertical gradients of potential fields. *Geophysics*, 54: 662-663.

Rahman, M. A. (1988). Recent advances in the study of the basement complex of Nigeria. In Oluyide, P. O., W. C. Mbonu, A. E. O. Ogezi, I. G. Egbuniwe, A. C. Ajibade and A. C. Umeji(eds.). *Precambrian Geology of Nigeria*; Geological Survey of Nigeria, Kaduna, 11-43.

Rasmussen, R. and Pedersen, L. B. (1979). End Corrections in Potential Field Modelling, *Geophysics Prospecting*, 27: 749-760.

Ravart, D. (1996). Analysis of the Euler method and its applicability on environmental magnetic investigations. *Journal of Environmental and Engineering Geophysics*, 1: 229-238.

Reeves, A., (1990). Olympic Dam Copper-Uranium Gold-Silver Deposit. In: F. E. Hughes (Ed.) Geology of the Mineral Deposits of Australia and Papua New Guinea. *The Australasian Institute of Mining and Metallurgy*, 1009-1035.

Reid, A. B., Allsop, J. M., Granser, H., Millett, A. J. and Somerton, I. W. (1990). Magnetic interpretation in three dimensions using Euler deconvolution. *Geophysics*, 55:80 – 91.

Reid, A. B. (1995). Euler deconvolution: Past, present and future – a review. 65th SEG meeting, Houston, USA, Expanded Abstract, 272-273.

Roest, W. R., Verhoef, J. and Pikington, M. (1992). Magnetic interpretation using the 3-D analytic signal. *Geophysics*, 57: 116-125.

Sabins, F. F. Jr. (1986). Remote sensing principles and interpretation. 2nd edition Freeman, New-York, 99.

Samson, D. T. (1982). EULDPH – a new technique for computer-assisted depth estimates from magnetic data. *Geophysics*, 47: 31-37.

Samuel, O. A. (2011). The geology, stream sediment, geochemical survey and groundwater quality evaluation of Okemesi area, south-western Nigeria. *International Journal of Geology, Earth and Environmental Sciences*, 1(1): 73-97.

Sharma, K. K., (1998). Geological evolution and crustal growth of the Bundelkh, and Carton and Its Relict in the Surrounding Regions, North Indian Shield. *The Indian Precambrian*. Scientific Publishers, Jodhpur, India, 33-43.

Sharma, P. V. (2002). Environmental and engineering geophysics. Cambridge University Press, United Kingdom.

Skeels, D. C. (1967). What is residual gravity? *Geophysics*, 32: 872-876.

Storey, B. C. (1995). The role of mantle plumes in continental breakup: case history from Gonwanaland. *Nature*, 377: 301-308.

Talwani, M., and Heirtzler, J. R. (1964). Computation of magnetic anomalies caused by two-dimensional structures of arbitrary shape: Computers in the Mineral Industries, G.A. Parks, ed., School of Earth Sciences: Stanford University, 464-480.

Talwani, M., Worzel, J. L. and Landisman, M., (1959). Rapid gravity computations for two-dimensional bodies with applications to the mendocino submarine fracture zones. *Geophysics Research*, 64: 49-59.

Tarlowski, C.,Gunn, P. J. and Mackey, T. (1997). Enhancements of the magnetic map of Australia. *AGSO Journal of Australian Geology and Geophysics*, 17(2): 77-82.

Telford, W. M., Geldert, L. P. and Sheriff, R. E. (1990). Applied Geophysics. Cambridge University Press.

Thompson, D. T. (1982). EULDPH—a new technique for making computer-assisted depth estimates from magnetic data. *Geophysics*, 47:31-37

Tom, P., Gerry, C. and Rowland, F. (2009). GM-SYS Profile modeling. Gravity and magnetic modeling software for Oasis Montaj^{Tm}, User Guide, Version 4.1., Geosoft Inc. Toronto, ON Canada M5J 1A7.

Verduzco, B., Fairhead, J.D., Mackenzie, C. and Green, C. M. (2004). New insights into magnetic derivatives for structural mapping. *The Leading Edge*: 116-119.

Webring, M. (1985). SAKI: A FORTRAN Program for generalized inversion of gravity and magnetic profiles. *United States Geological Survey Open File Report*, 85-122.

Werner, S. (1953). Interpretation of magnetic anomalies at sheet-like bodies, Sveriges Geologiska Undersok, Ser., 43: 6-13.

Whiteman, A.J. (1982). Nigeria: Its petroleum geology, resources and potential. Graham and Trottan London, p 394.

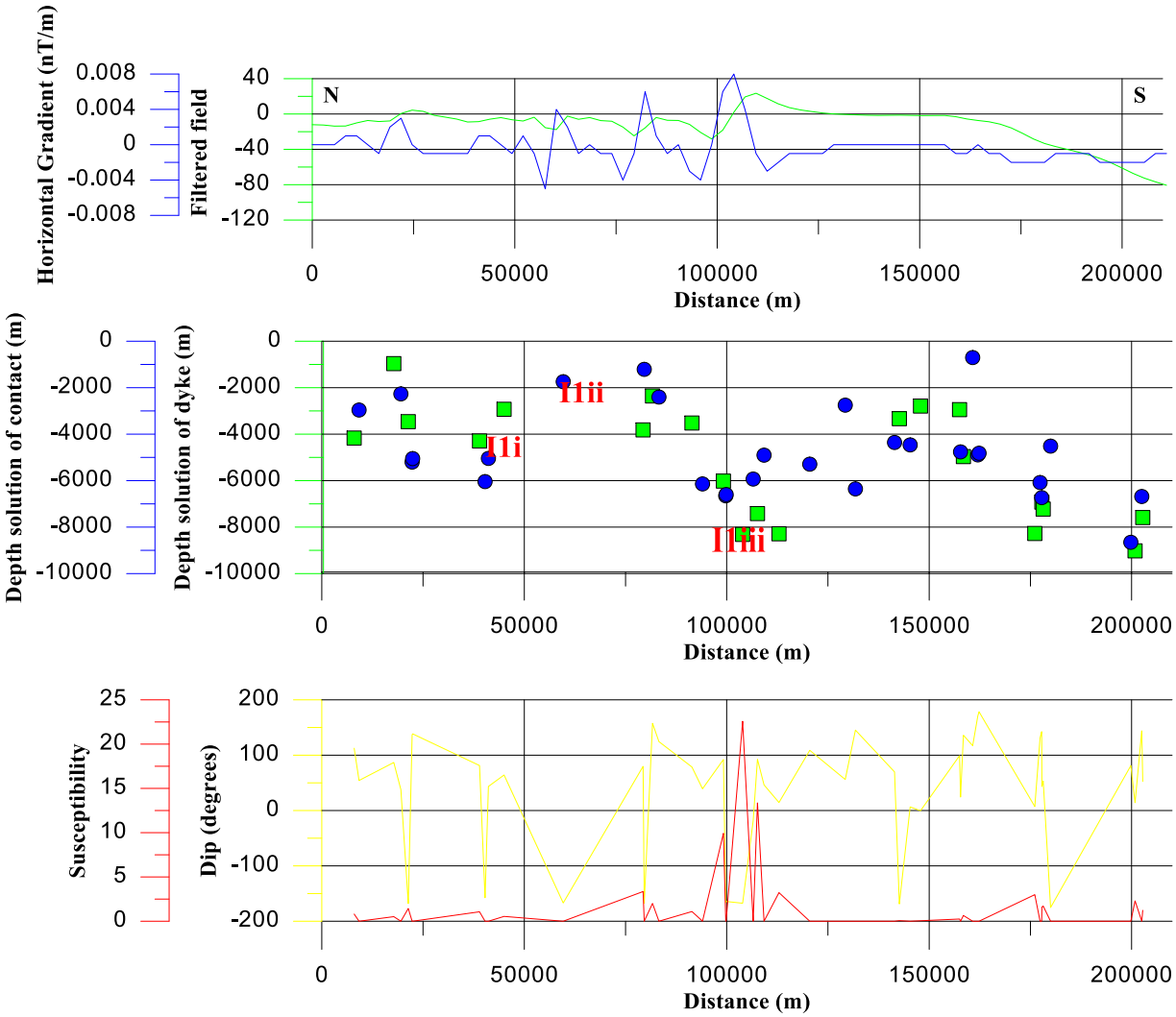
Wijn, S. C., Perez, C. and Kowalczyk, P. (2005). Theta map: Edge detection in magnetic data. *Geophysics*, 70 (4): L39-L43.

Won, I. J. and Bevis, M., (1987). Computing the gravitational magnetic anomalies due to a polygon: Algorithm and FORTRAN subroutines. *Geophysics,* 52(2): 232-238.

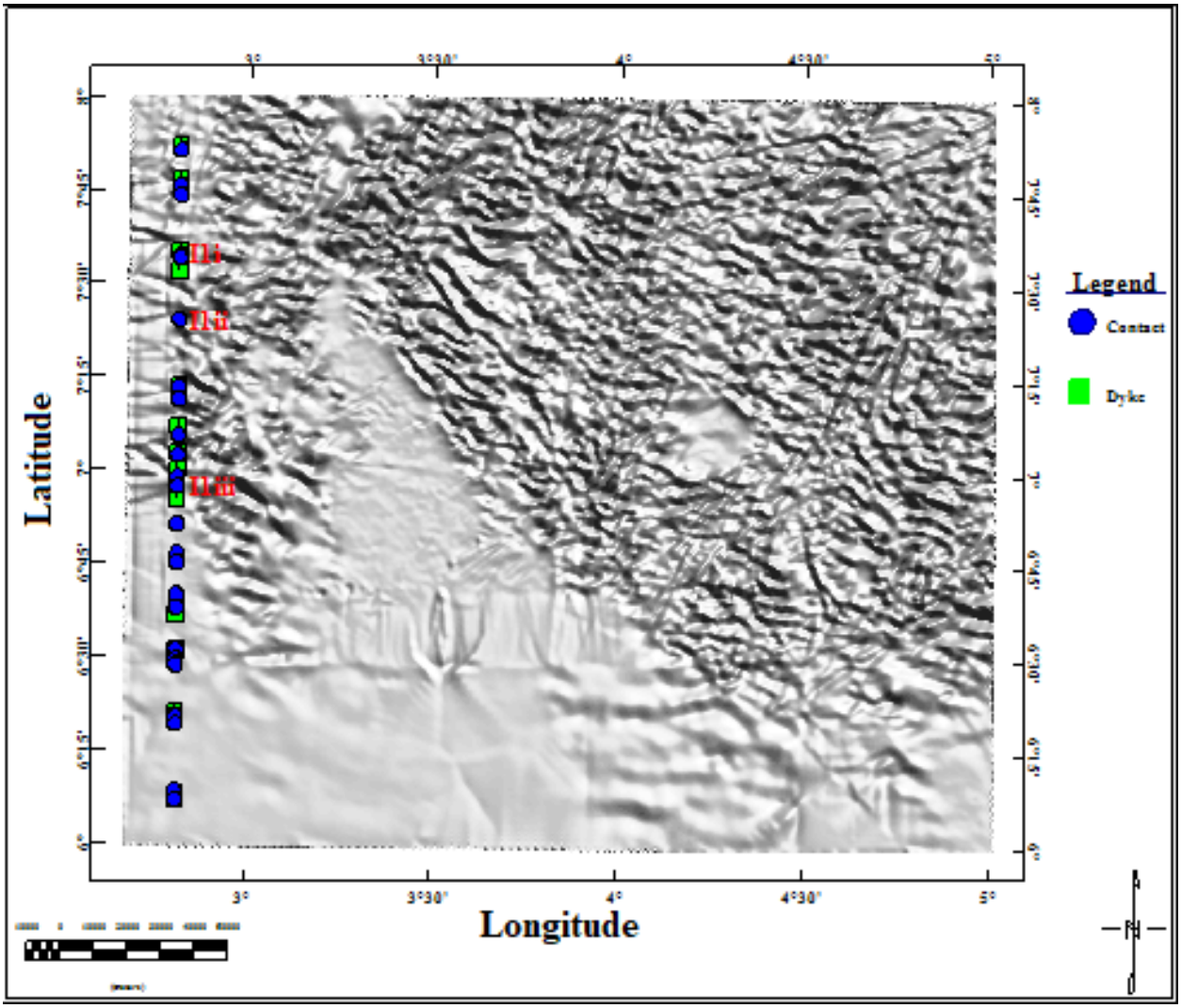
Wright, J.B. (1976). Fracture systems in Nigeria and initiation of fracture zones in the South-Atlantic. *Tectonophysics*, 34: T43-T47.

APPENDIX A

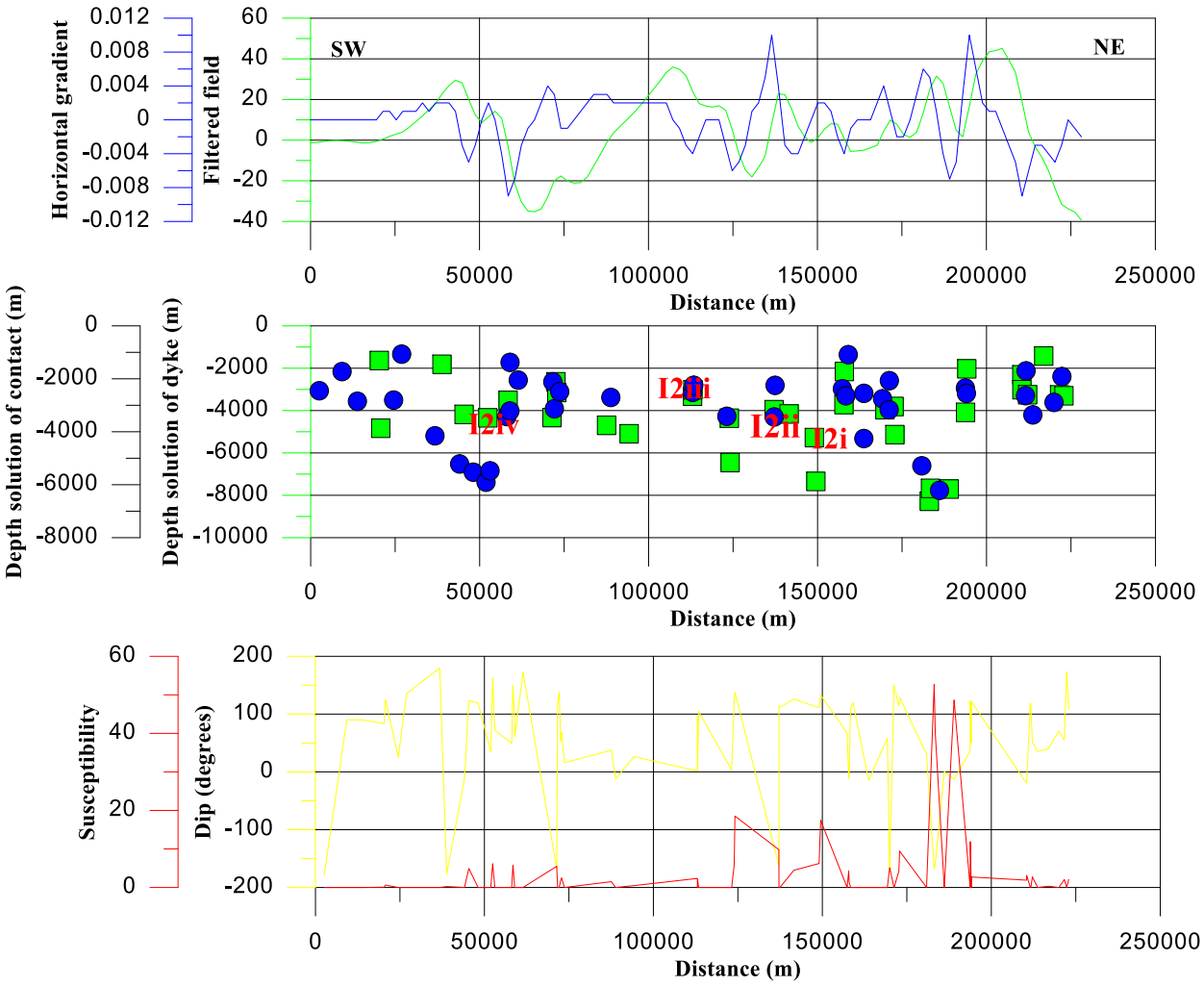
WERNER DECONVOLUTION SOLUTIONS AND POSTS FOR THE TEN PROFILES ON SECOND VERTICAL DERIVATIVE MAP



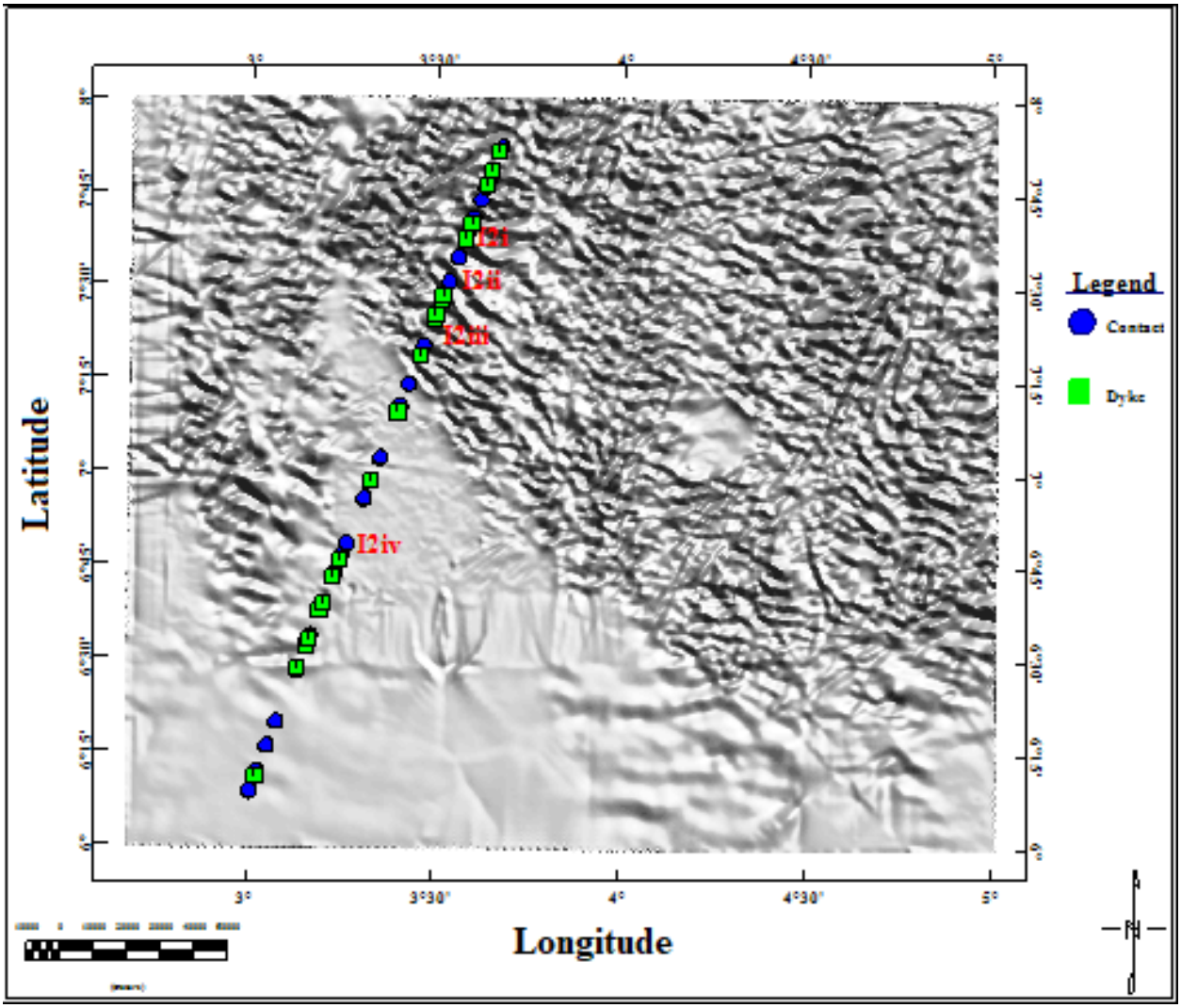
PLOT A1 (a): Werner plots for profile P_{1A} P_{1B}.



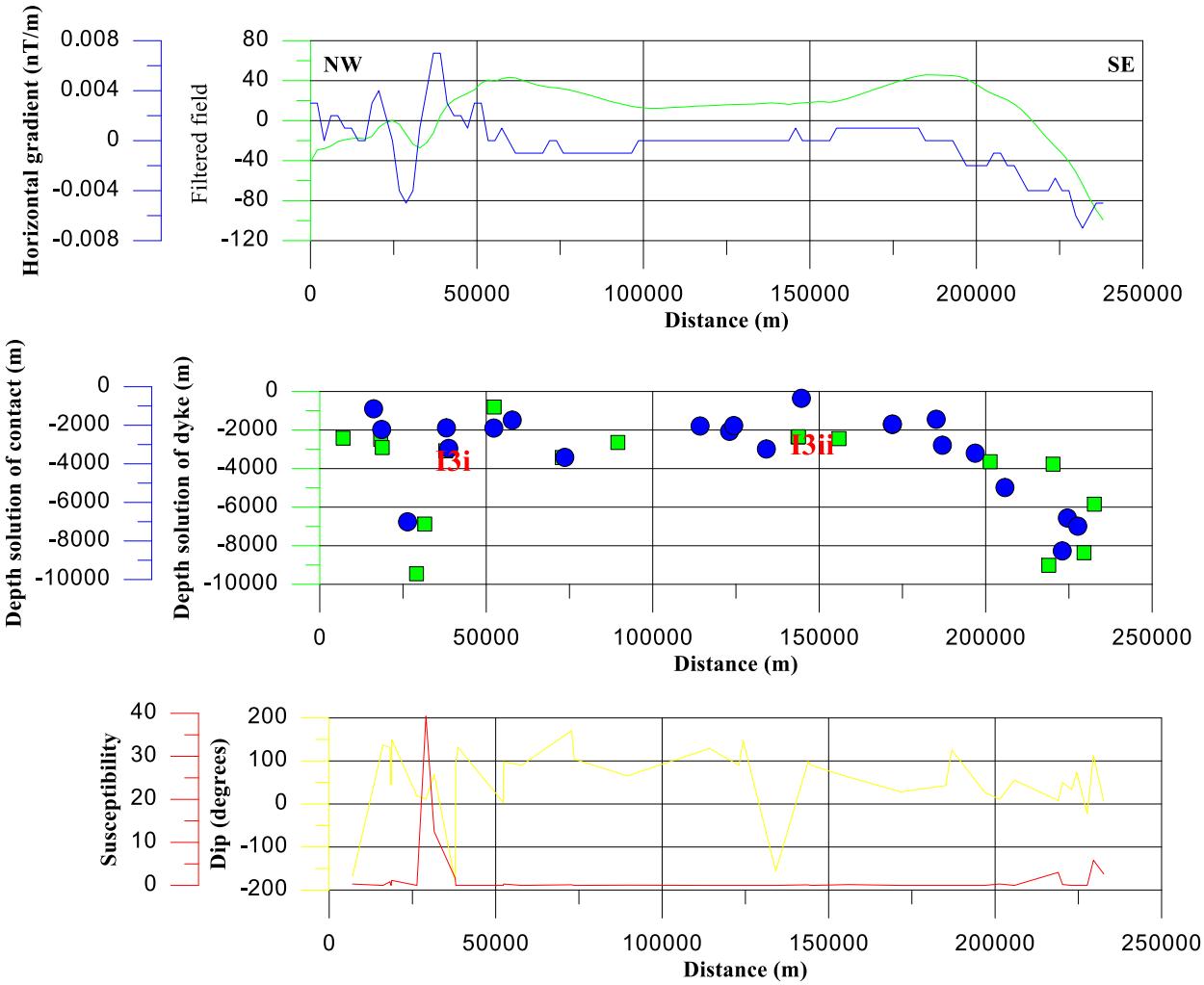
PLOT A1 (b): Werner post on second vertical derivative map for profile P_{1A} P_{1B}.



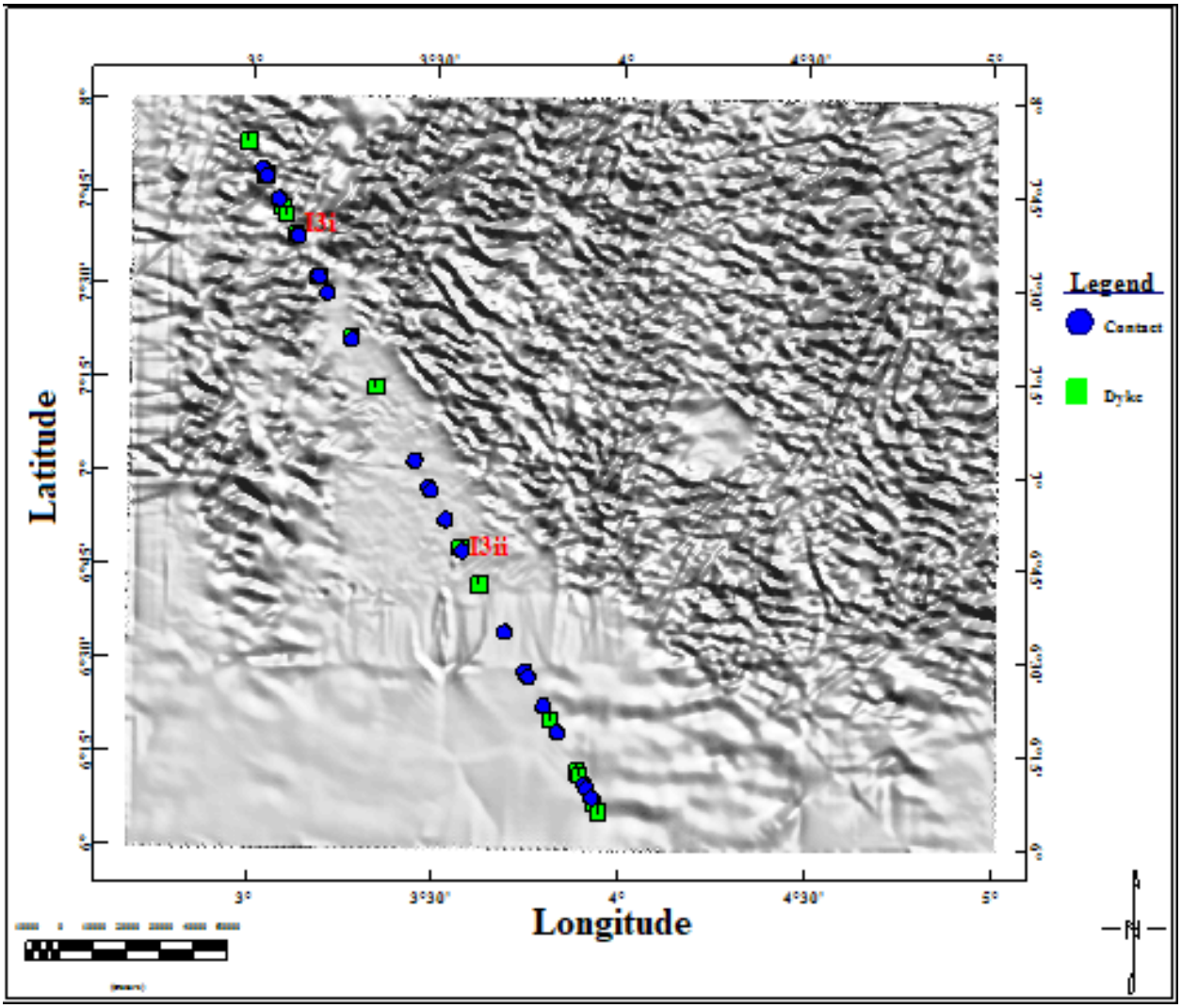
PLOT A2 (a): Werner plots for profile P_{2A} P_{2B}.



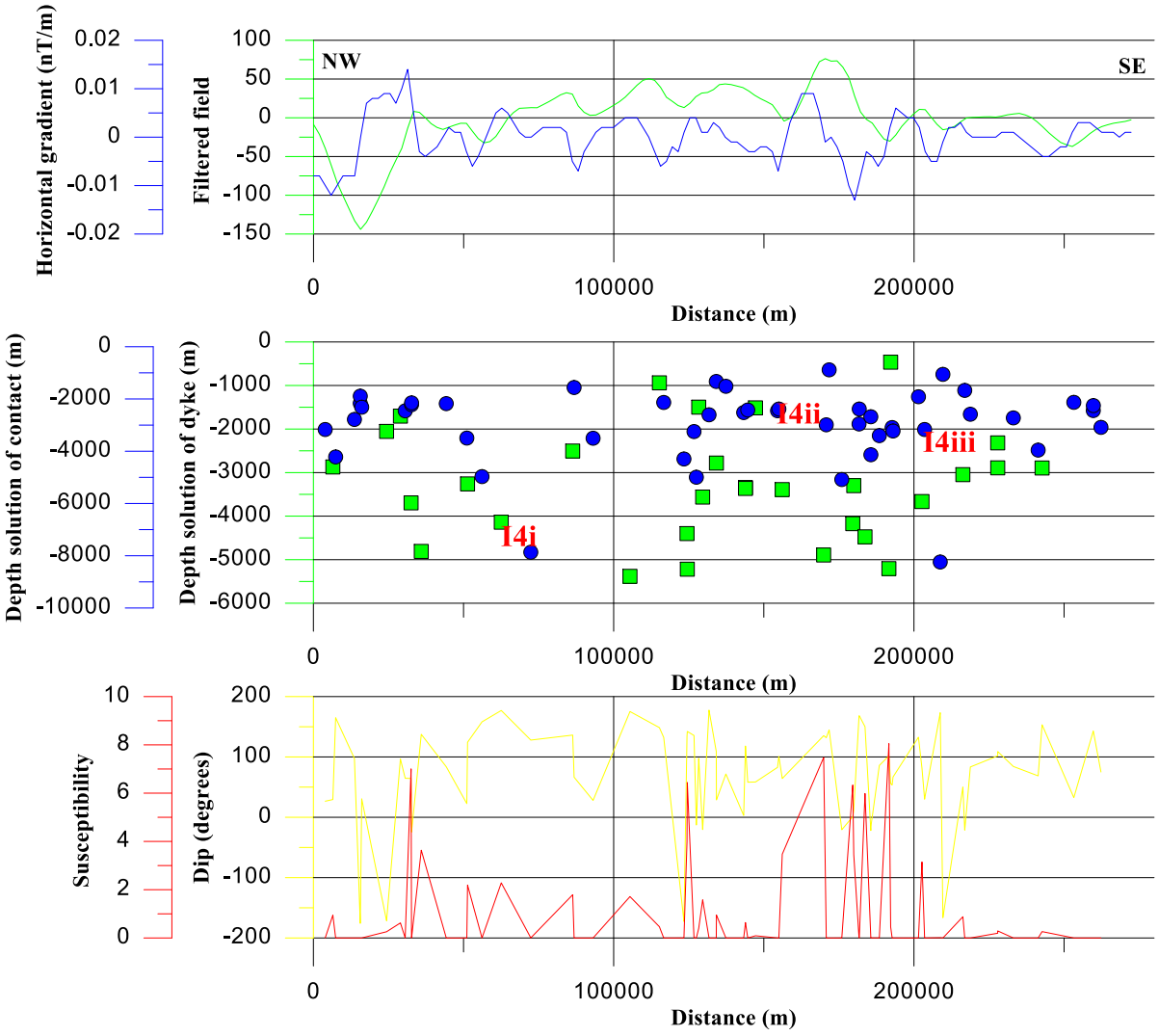
PLOT A2 (b): Werner post on second vertical derivative map for profile P_{2A} P_{2B}.



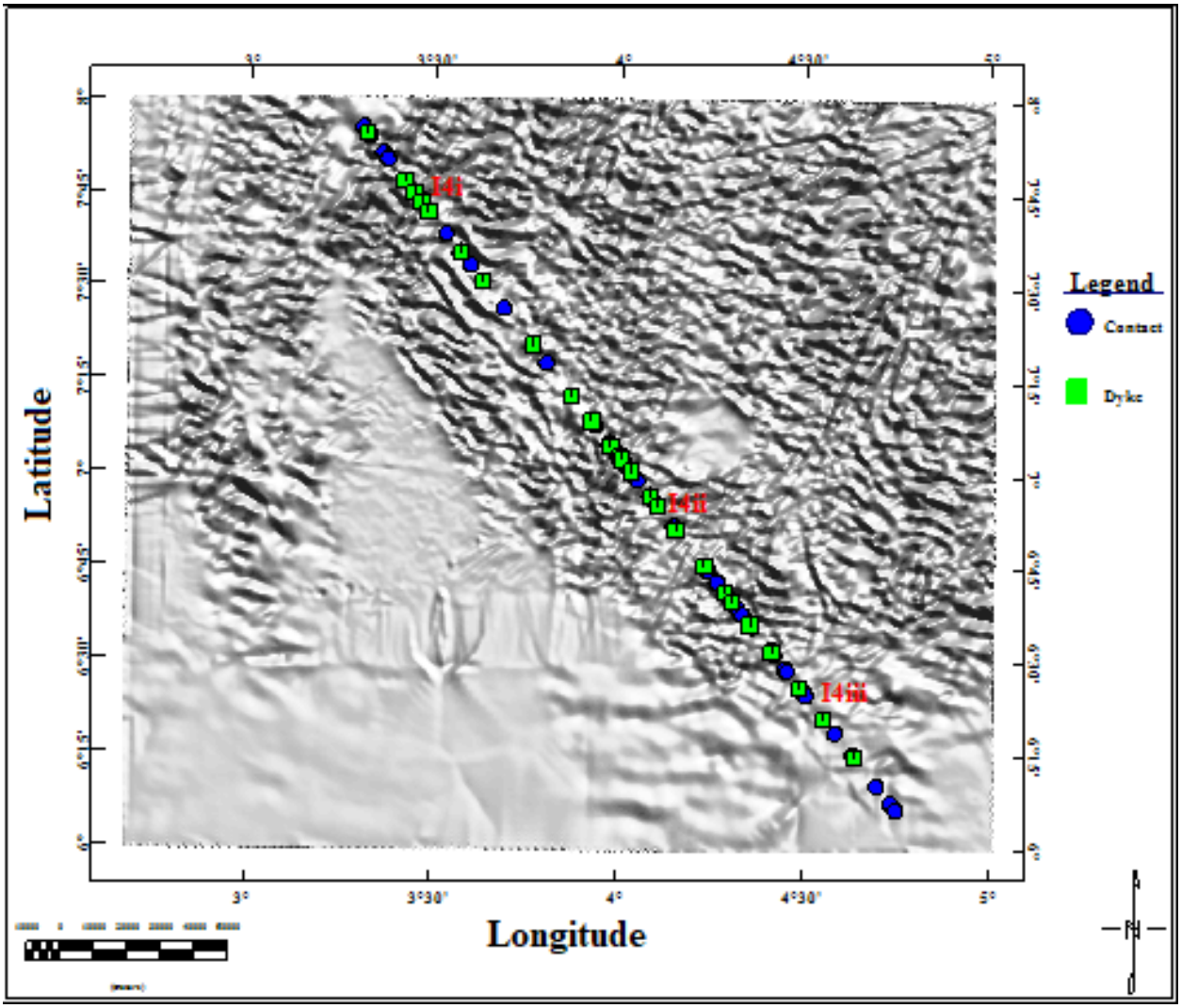
PLOT A3 (a): Werner plots for profile P_{3A} P_{3B}.



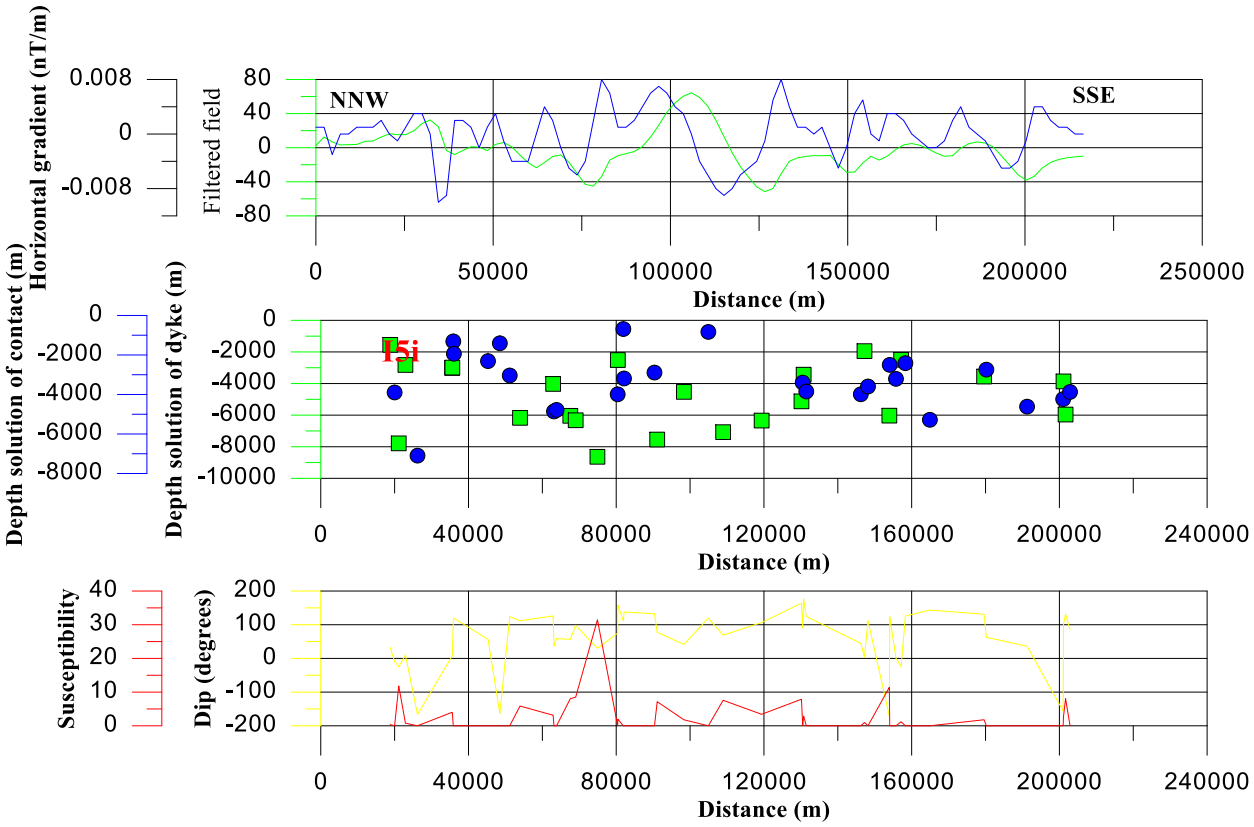
PLOT A3 (b): Werner post on second vertical derivative map for profile P_{3A} P_{3B}.



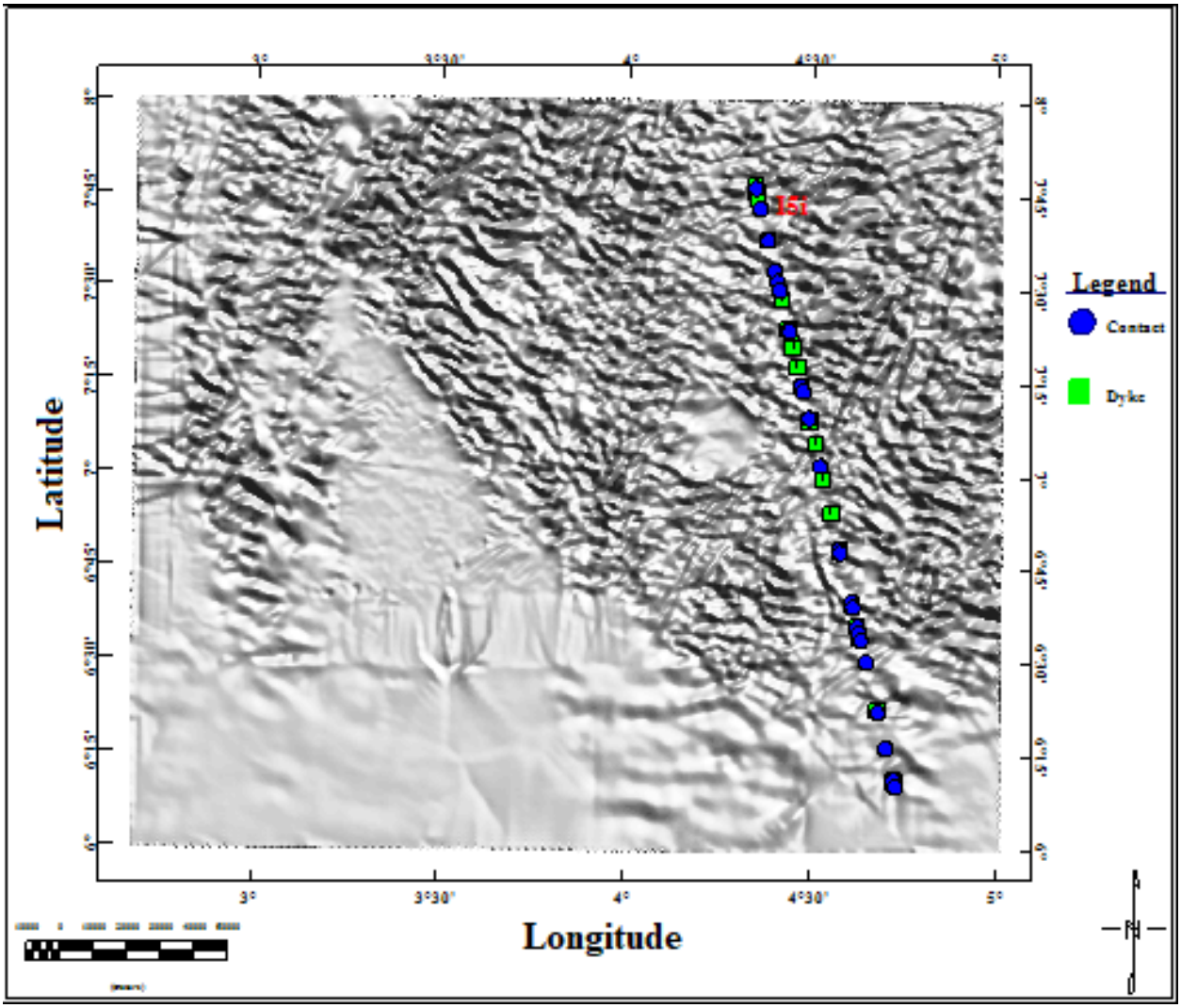
PLOT A4 (a): Werner plots for profile P_{4A} P_{4B}.



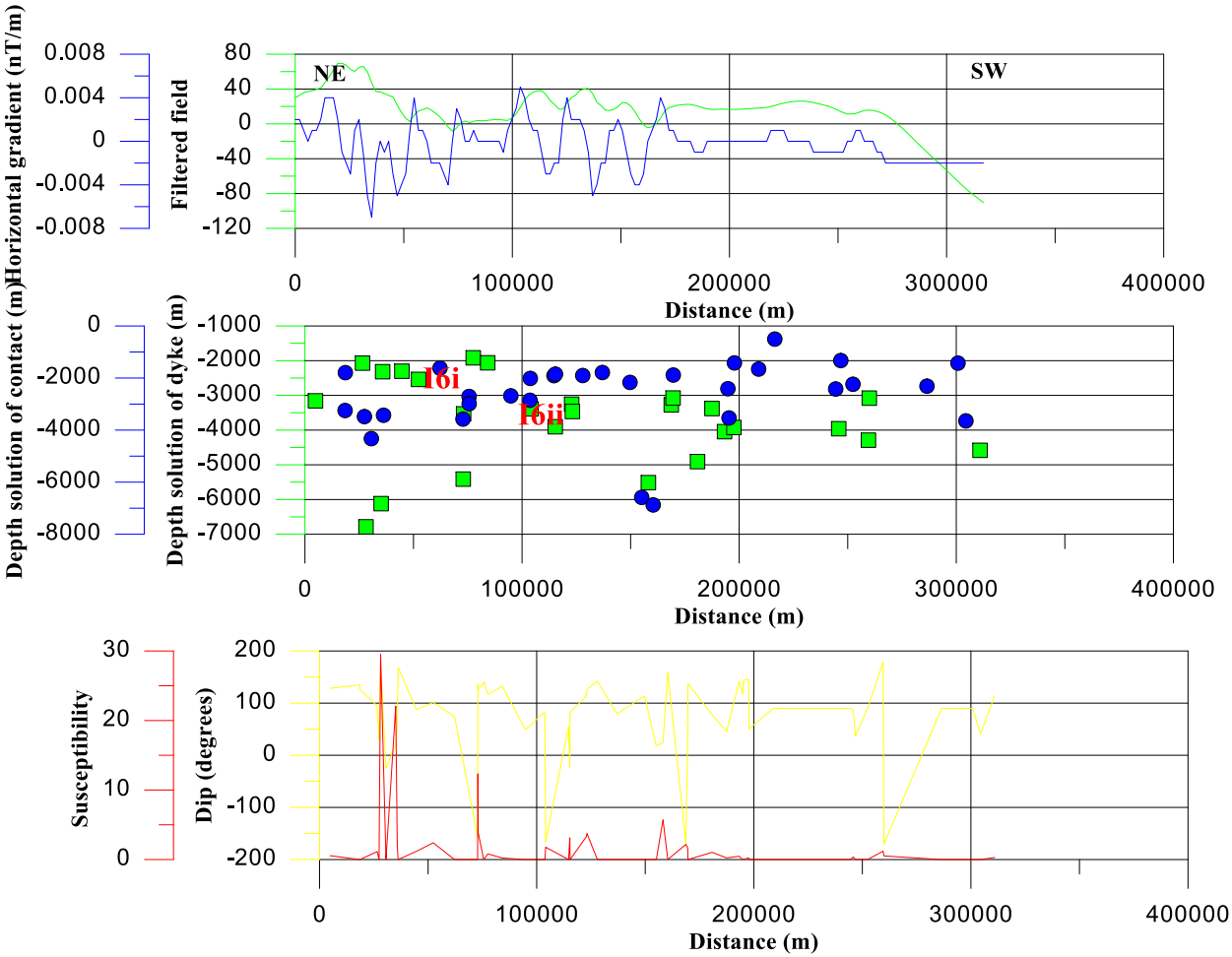
PLOT A4 (b): Werner post on second vertical derivative map for profile P_{4A} P_{4B}.



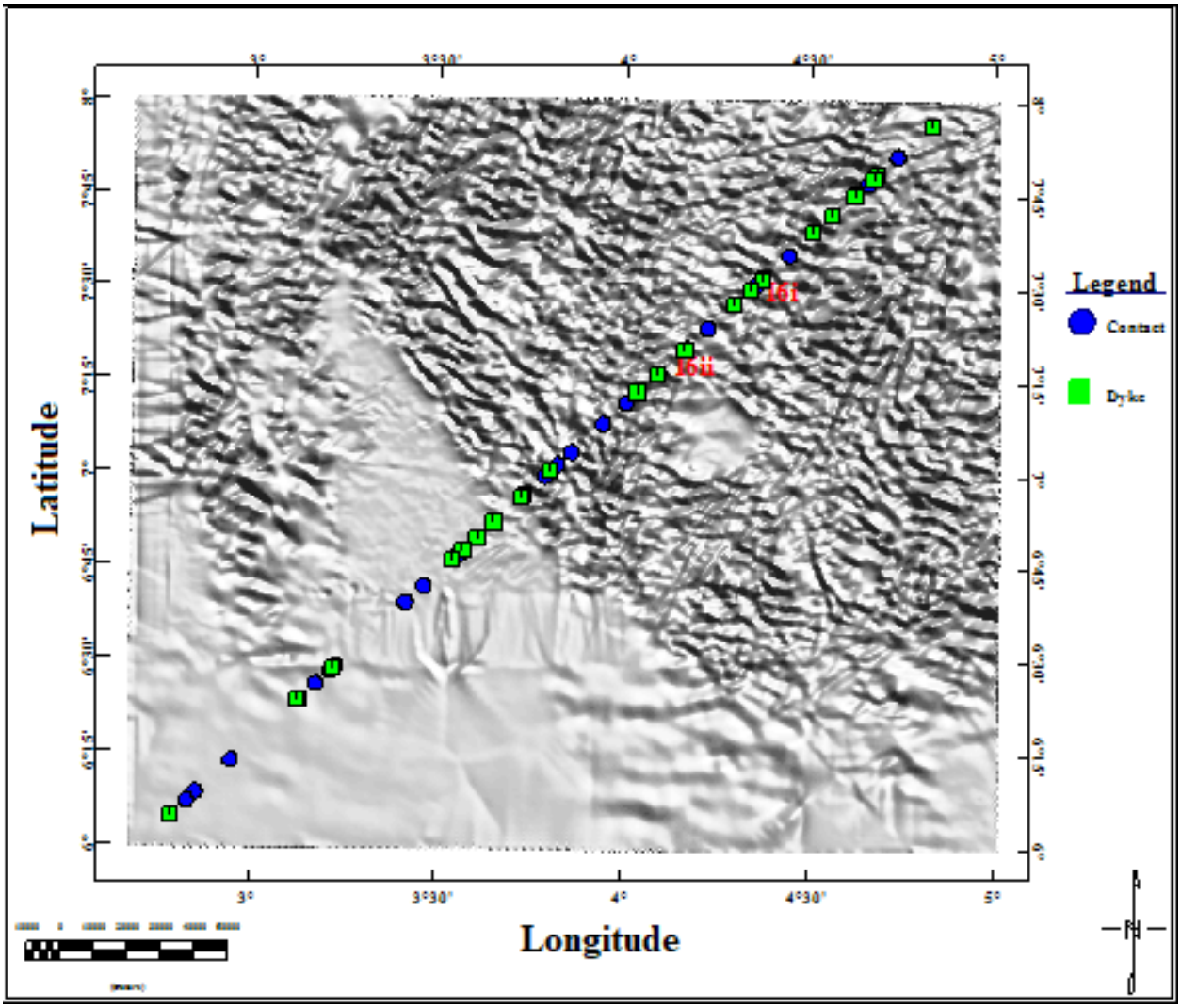
PLOT A5 (a): Werner plots for profile P_{5A} P_{5B}.



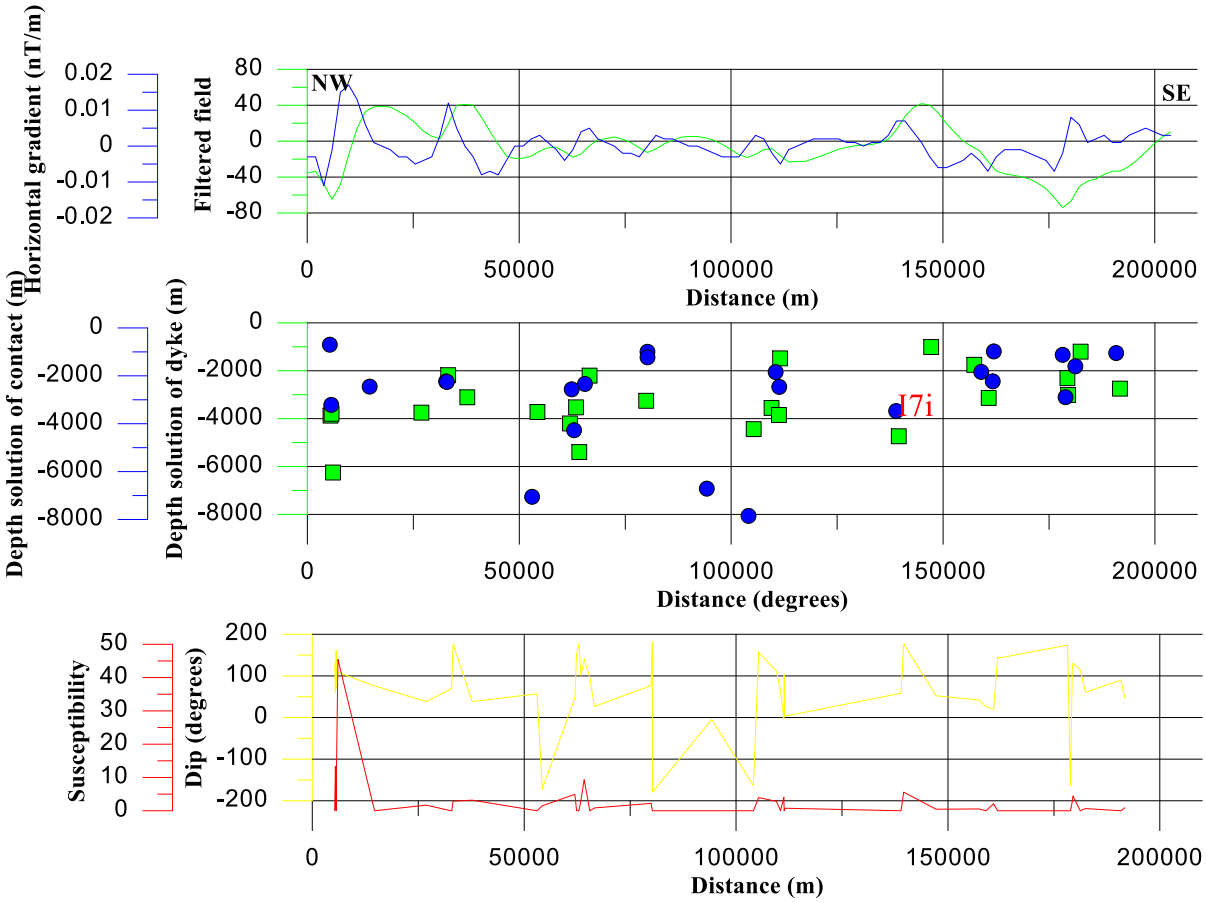
PLOT A5 (b): Werner post on second vertical derivative map for profile P_{5A} P_{5B}.



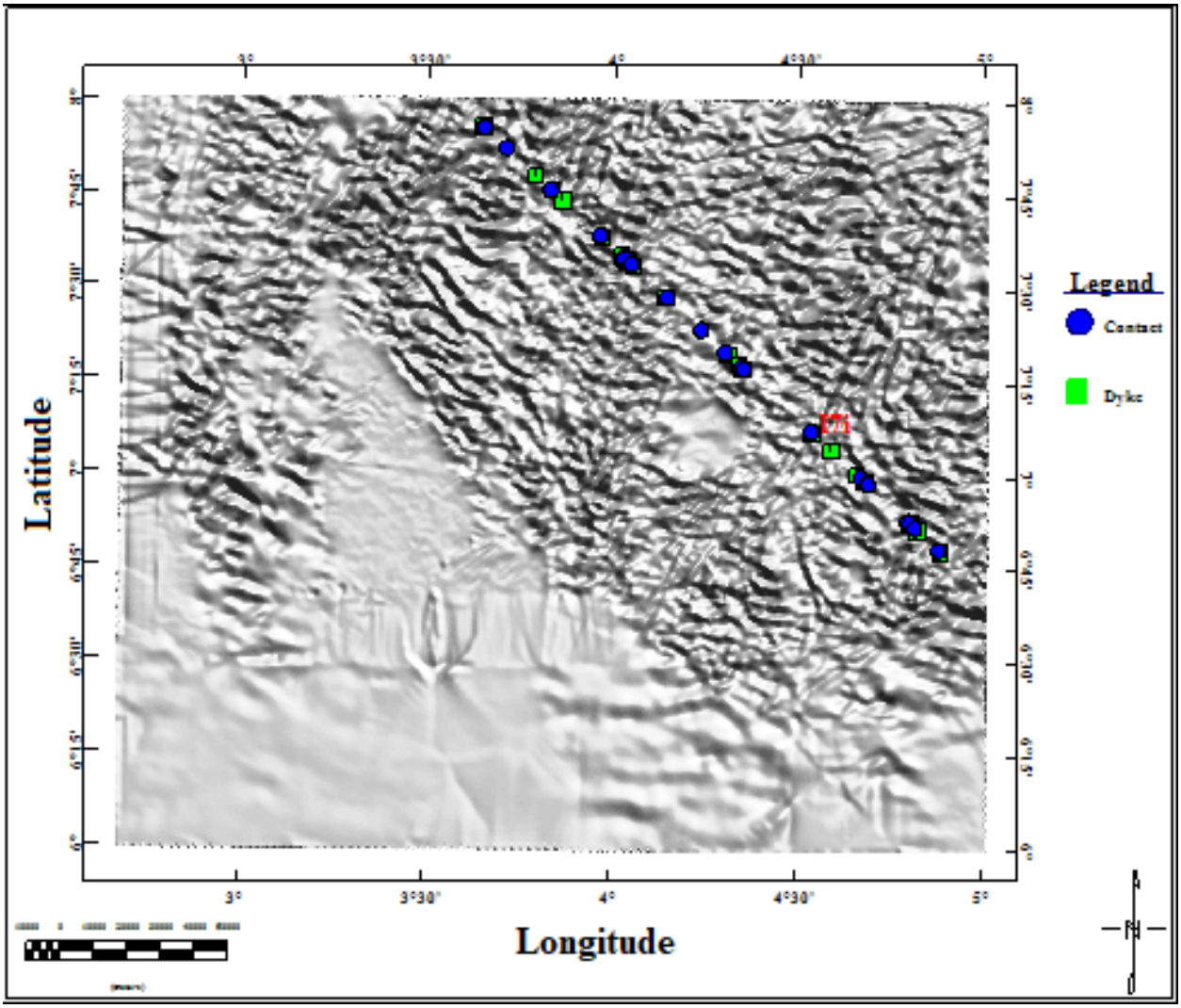
PLOT A6 (a): Werner plots for profile P_{6A} P_{6B}.



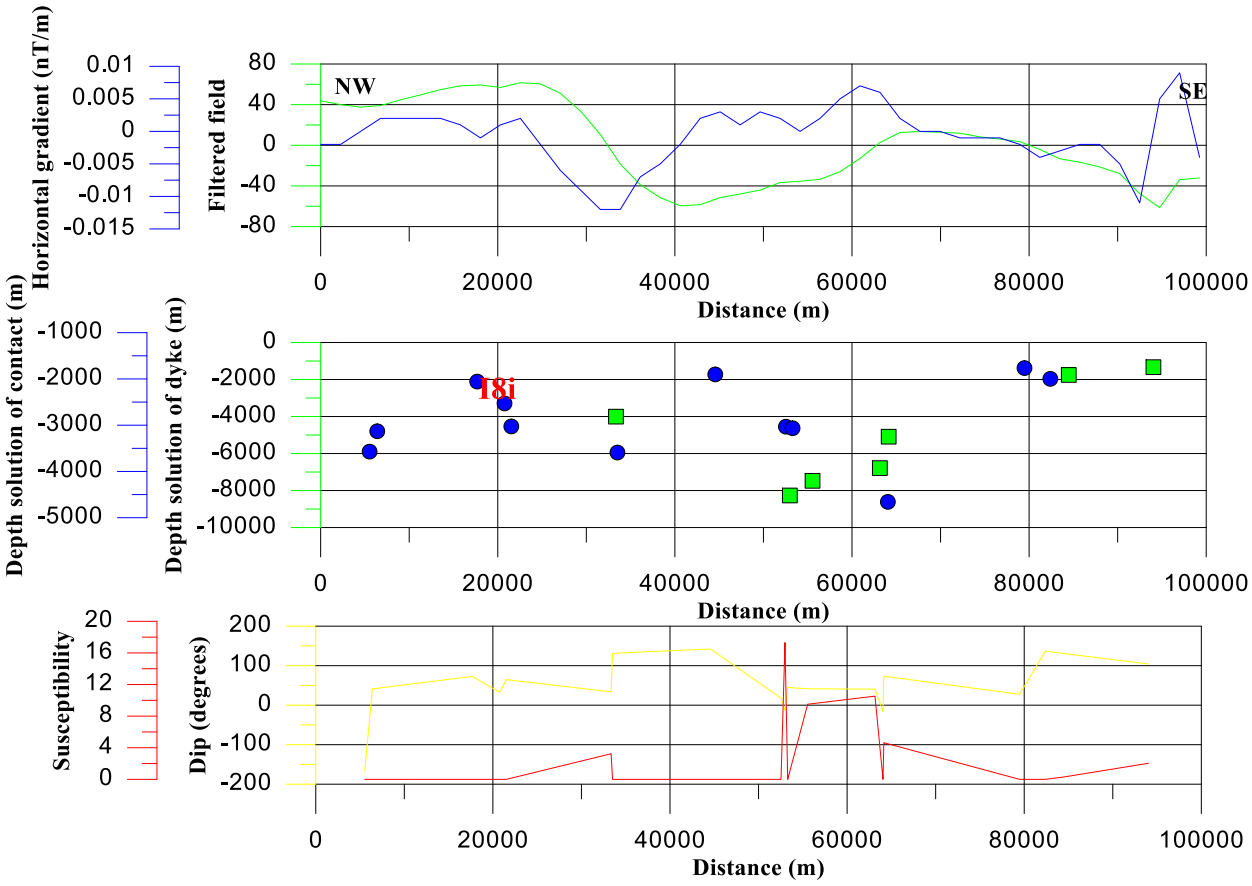
PLOT A6 (b): Werner post on second vertical derivative map for profile P_{6A} P_{6B}.



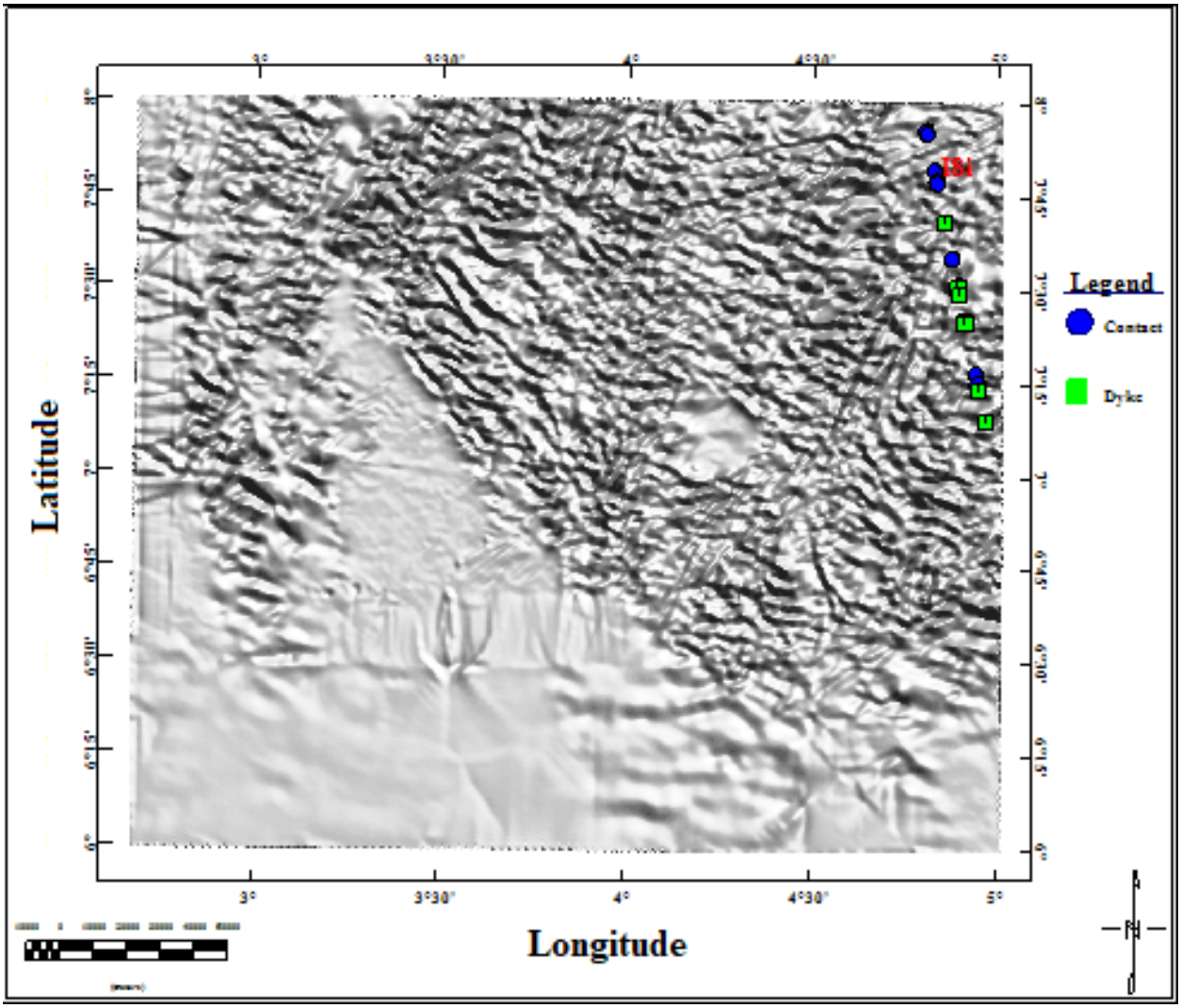
PLOT A7 (a): Werner plots for profile P_{7A} P_{7B}.



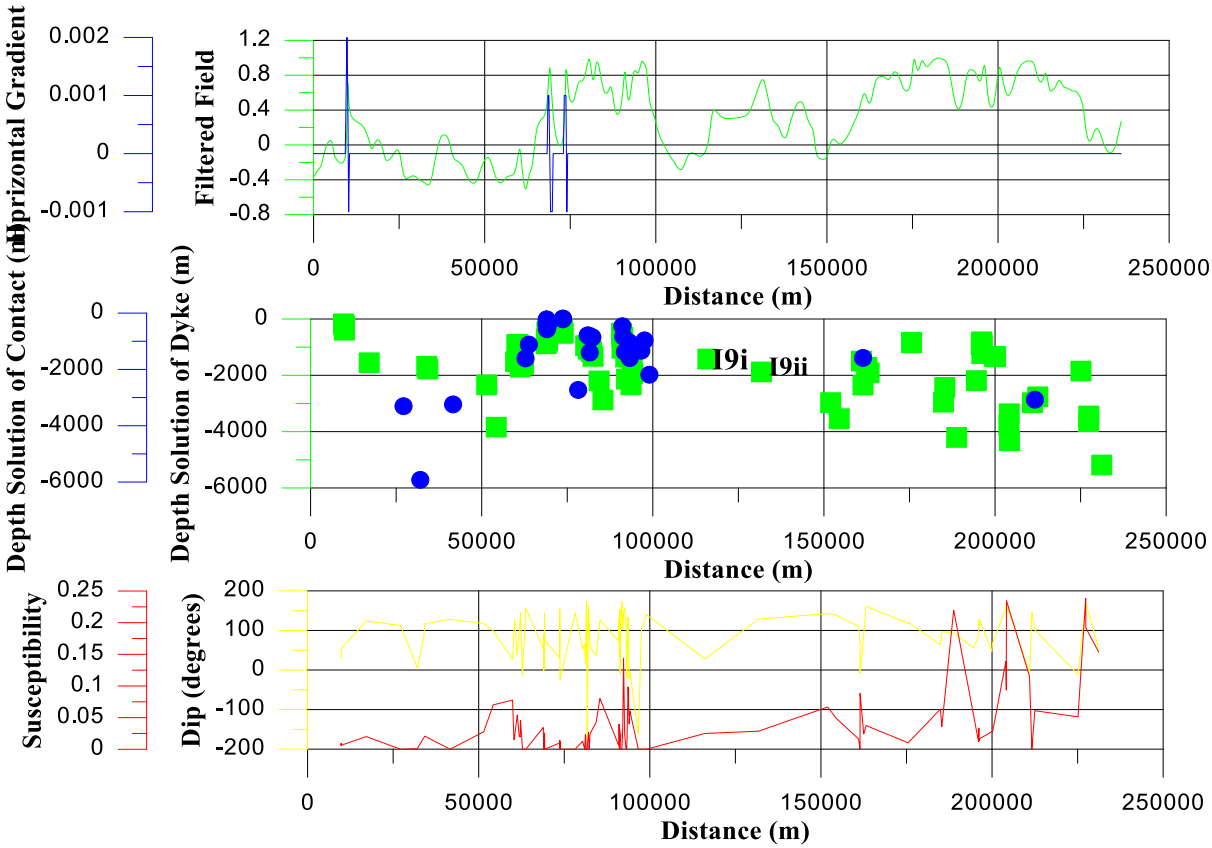
PLOT A7 (b): Werner post on second vertical derivative map for profile P_{7A} P_{7B}.



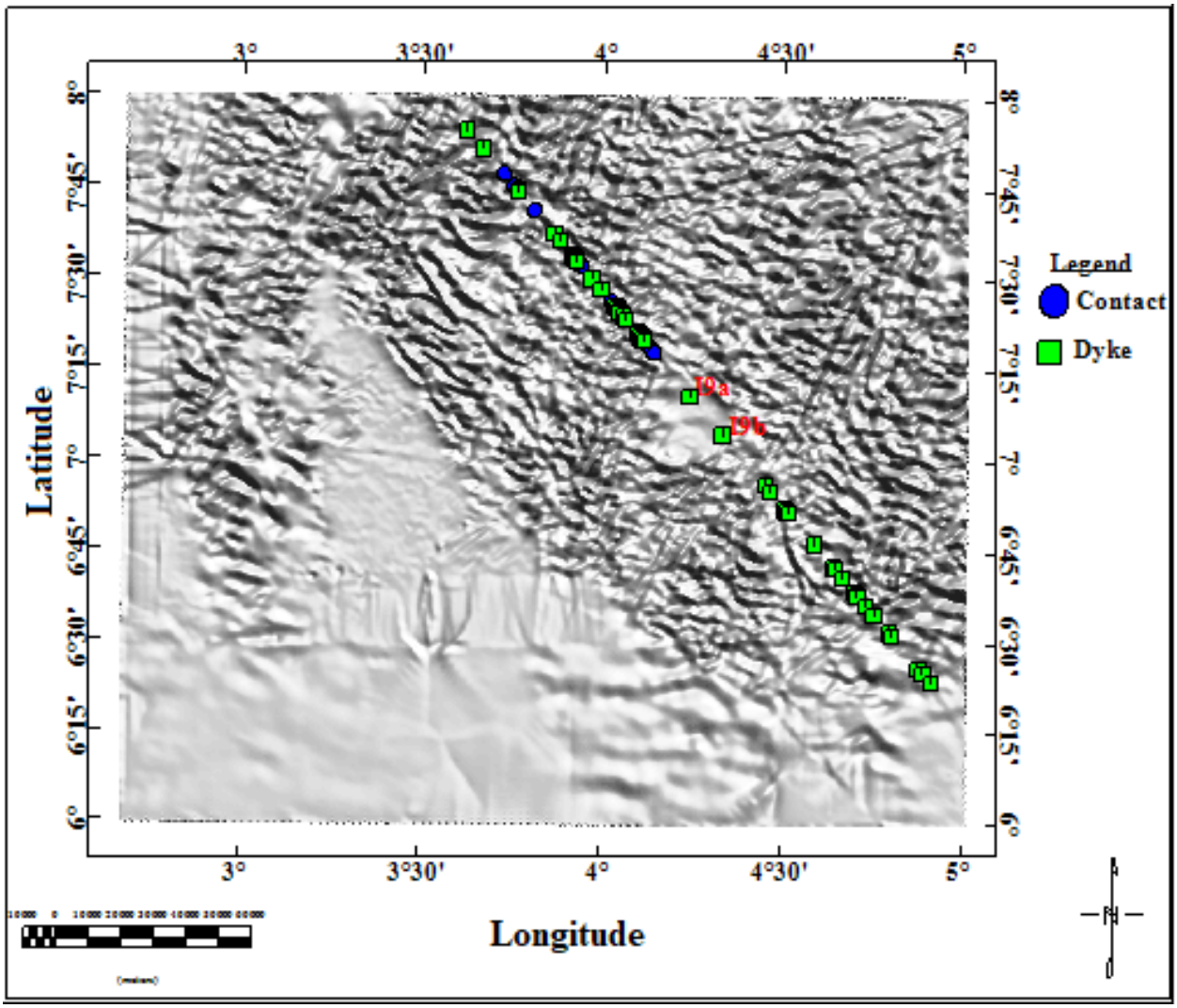
PLOT A8 (a): Werner plots for profile P_{8A} P_{8B}.



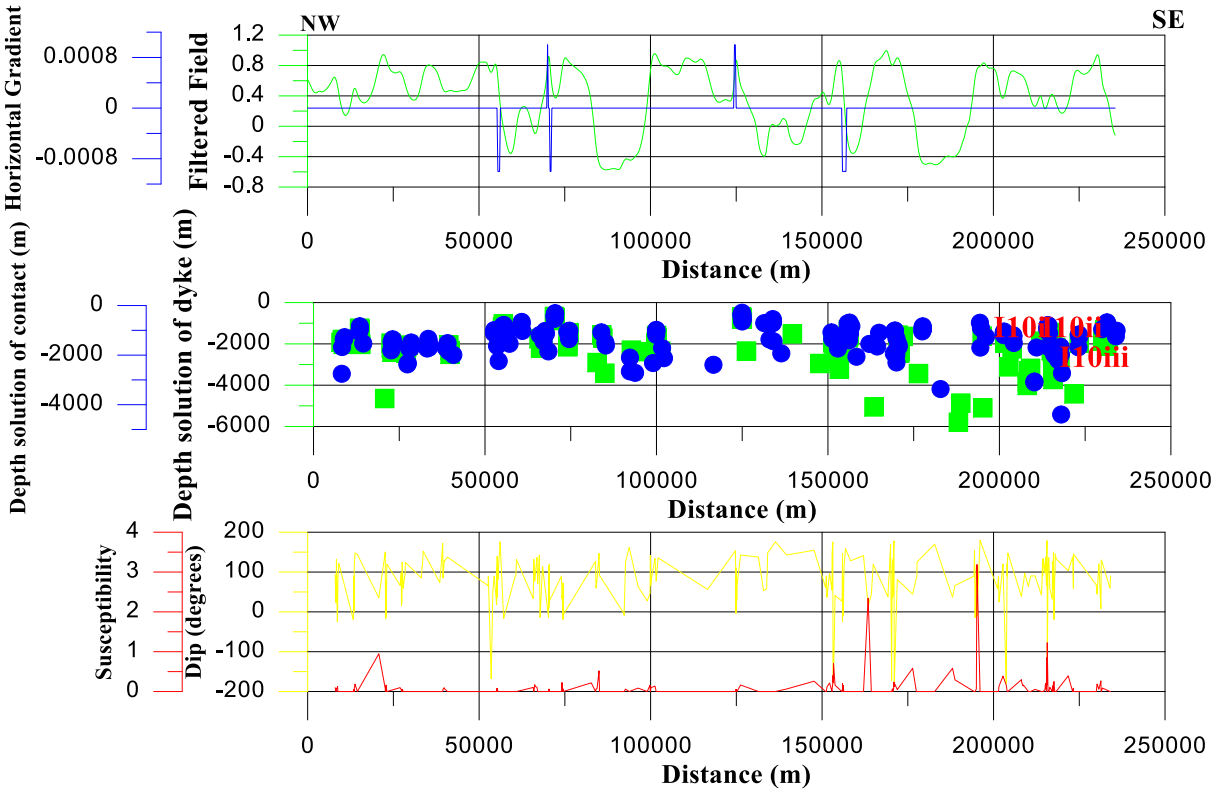
PLOT A8 (b): Werner post on second vertical derivative map for profile P_{8A} P_{8B}.



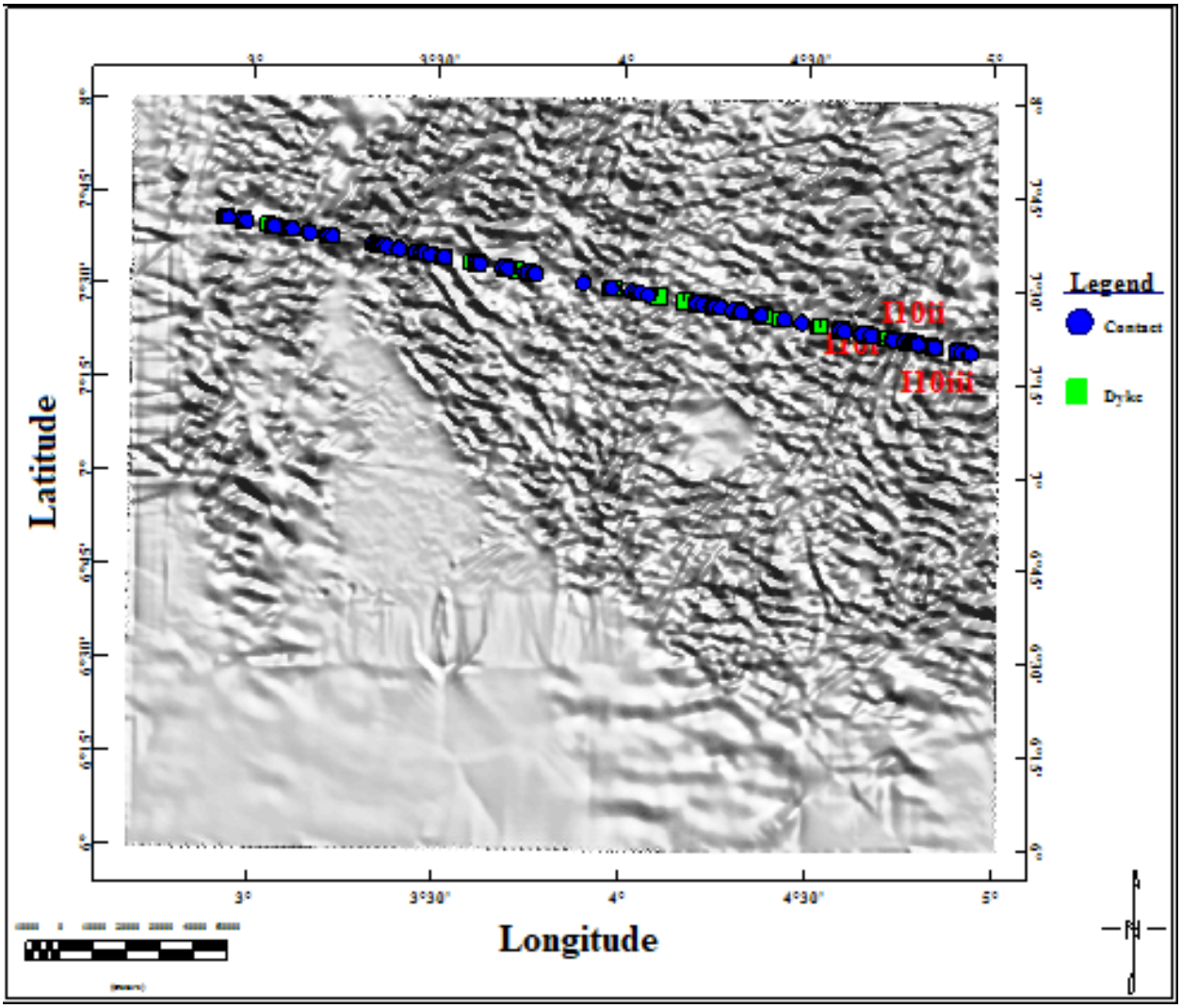
PLOT A9 (a): Werner plots for profile P_{9A} P_{9B}.



PLOT A9 (b): Werner post on second vertical derivative map for profile P_{9A} P_{9B}.



PLOT A10 (a): Werner plots for profile P_{10A} P_{10B}.



PLOT A10 (b): Werner post on second vertical derivative map for profile P_{10A} P_{10B}.